

## Self-healing Thermal Interface Materials

Zhong, N.

**DOI**

[10.4233/uuid:0e828acb-5ade-4de2-b5a6-e5ae38d2aa9c](https://doi.org/10.4233/uuid:0e828acb-5ade-4de2-b5a6-e5ae38d2aa9c)

**Publication date**

2020

**Document Version**

Final published version

**Citation (APA)**

Zhong, N. (2020). *Self-healing Thermal Interface Materials*. [Dissertation (TU Delft), Delft University of Technology]. <https://doi.org/10.4233/uuid:0e828acb-5ade-4de2-b5a6-e5ae38d2aa9c>

**Important note**

To cite this publication, please use the final published version (if applicable).  
Please check the document version above.

**Copyright**

Other than for strictly personal use, it is not permitted to download, forward or distribute the text or part of it, without the consent of the author(s) and/or copyright holder(s), unless the work is under an open content license such as Creative Commons.

**Takedown policy**

Please contact us and provide details if you believe this document breaches copyrights.  
We will remove access to the work immediately and investigate your claim.

# **Self-healing Thermal Interface Materials**

Dissertation

for the purpose of obtaining the degree of doctor  
at Delft University of Technology

by the authority of the Rector Magnificus Prof. dr. ir. T.H.J.J. van der Hagen  
chair of the Board for Doctorates  
to be defended publicly on  
Thursday 17 September 2020 at 15:00 o'clock

By

**Nan ZHONG**

Master of Material Science and Engineering, Tsinghua University, China  
born in Chongqing, China

This dissertation has been approved by the promotor.

Composition of the doctoral committee:

Rector Magnificus,

Chairperson

Prof. dr. ir. S. van der Zwaag  
Dr. S.J. Garcia Espallargas

Delft University of Technology, promotor  
Delft University of Technology, promotor

Independent members:

Prof.dr.ir. J.H.B. Sprakel  
Prof.dr. G.Q. Zhang  
Prof.dr.ir. K.M.B. Jansen  
Prof.dr.ir. R. Benedictus  
Prof.dr. S.J. Picken

Wageningen University & Research  
Delft University of Technology  
Delft University of Technology  
Delft University of Technology  
Delft University of Technology

The research carried out in this thesis is funded by the Dutch National IOP program on self-healing materials under project number IOP-SHM 012016.



Netherlands Enterprise Agency



Keywords: Thermal interface materials, Functional composites, Reliability, Disulfide

Printed by Ipskamp Printing, Enschede.

ISBN: 978-94-028-2155-0

Copyright ©2020 by Nan ZHONG

Cover by Nan ZHONG

An electronic version of this dissertation is available at <http://repository.tudelft.nl/>

All rights reserved

Author email: zhongn06@gmail.com

---

# Contents

---

## Chapter 1 Introduction

1.1 Self-healing materials .....	2
1.2 Thermal interface material .....	3
1.3 Challenges and future prospects .....	4
1.4 Scope and thesis outline .....	4
References.....	6

## Chapter 2 Self-repair of structural and functional composites via intrinsically self-healing polymer matrices: A review

2.1 Introduction.....	10
2.2 Intrinsically self-healing matrix polymers .....	12
2.2.1 Heat triggered self-healing .....	13
2.2.2 Photochemical triggered self-healing.....	15
2.2.3 Electrically triggered self-healing.....	16
2.2.4 Moisture triggered self-healing.....	17
2.3 Structural composites containing an intrinsically self-healing polymer matrix .....	17
2.3.1 Stiffness recovery .....	17
2.3.2 Strength recovery .....	21
2.4 Functional composites containing an intrinsically self-healing polymer matrix .....	23
2.4.1 Electrically conductive polymer composites.....	24
2.4.2 Electromagnetic polymer composites.....	26
2.4.3 Electromechanical polymer composites .....	27
2.4.4 Magnetic polymer composites.....	30
2.4.5 Thermally conductive polymer composites .....	31
2.5 Conclusion .....	34
References.....	35

**Chapter 3 Numerical simulation of the thermal conductivity and mechanical properties of thermal interface materials with micro- or macro- damages**

3.1 Introduction ..... 46

3.2 Numerical method..... 48

    3.2.1 The effect of micro damage at particle–matrix interfaces on thermal conductivity..... 49

    3.2.2 The effect of micro damage at particle–matrix interfaces on stiffness .... 50

    3.2.3 The effect of macro–damage at the TIM–heat source interface on the thermal conductivity and interfacial thermal stresses ..... 51

3.3 Results and discussion..... 52

    3.3.1 The effect of micro damage at particle–matrix interfaces on thermal conductivity and Young’s modulus ..... 52

    3.3.2 The effect of macro damage at TIM–heat source interface on thermal conductivity and interfacial thermal stress..... 56

3.4 Conclusion..... 60

References ..... 62

**Chapter 4 On the role of disulfide bond concentration and irreversible crosslink density on mechanical properties and crack healing efficiencies of organic–inorganic dual network polymers**

4.1 Introduction ..... 66

4.2 Experimental..... 67

    4.2.1 Materials ..... 67

    4.2.2 Polymer preparation ..... 69

    4.2.3 Characterization methods ..... 69

4.3 Results ..... 74

    4.3.1 Without catalyst..... 74

    4.3.2 With catalyst..... 77

4.4 Discussion ..... 80

    4.4.1 Curing mechanism ..... 80

    4.4.2 Healing mechanism..... 84

    4.4.3 The effect of disulfide bond concentration versus irreversible crosslink density on the healing of polymers..... 85

4.5 Conclusion..... 86

References ..... 87

**Chapter 5 The effect of filler parameters on the healing of thermal conductivity and mechanical properties of a thermal interface material based on a self-healable organic-inorganic polymer matrix**

5.1 Introduction.....	92
5.2 Experimental.....	93
5.2.1 Material preparation.....	93
5.2.2 Mechanical healing test.....	94
5.2.3 Thermal conductivity restoration test.....	95
5.3 Results and discussion.....	96
5.3.1 The effect of PVC on mechanical properties and healing efficiency.....	96
5.3.2 The effect of particle size on mechanical healing.....	98
5.3.3 The effect of particle size on thermal conduction and healing efficiency.....	99
5.4 Conclusion.....	102
References.....	103

**Chapter 6 Thermal cycling test of self-healing TIMs**

6.1 Introduction.....	106
6.2 Experimental.....	107
6.2.1 Material preparation.....	107
6.2.2 Thermal cycling test protocols.....	109
6.3 Results and discussion.....	115
6.3.1 Drop-off test.....	115
6.3.2 Adhesion decay test.....	116
6.4 Conclusion.....	120
References.....	122

**Chapter 7 Laser Speckle Imaging observation of collective molecular motion during curing and adhesive bond formation of a sol-gel hybrid polymer**

7.1 Introduction.....	126
7.2 Experimental.....	127
7.2.1 Material preparation.....	127
7.2.2 LSI test geometry.....	129
7.2.3 LSI principle, data acquisition and data processing.....	131

7.2.4 Rheology measurement .....	133
7.2.5 Adhesion strength measurement.....	133
7.3 Results and discussion.....	133
7.3.1 The polymer curing process.....	133
7.3.2 The adhesive bonding process.....	138
7.4 Conclusion.....	142
References .....	144
Appendix .....	146
<b>Summary .....</b>	<b>147</b>
<b>Samenvatting.....</b>	<b>151</b>
<b>Acknowledgements .....</b>	<b>155</b>
<b>Publications .....</b>	<b>157</b>
<b>Curriculum Vitae .....</b>	<b>159</b>

# Chapter 1

---

**Introduction**

---



## 1.1 Self-healing materials

1

Over the past few decades, self-healing materials, which are inspired by nature and are capable of repairing structural or functional damage automatically leading to potential extension of service lifetime or increasing reliability of a product, have drawn more and more attention of academic and industrial researchers [1-4].

At the pioneering start of the field of self-healing materials, the self-healing ability was created by the introduction of microcapsules or vascular networks containing a mobile 'healing agent', which can rebuild or reinforce the polymer structure, into an otherwise non-self-healing polymer [5-7]. This approach of localized supply of a discrete liquid-like healing agent was later applied to other materials such as concrete[8], asphalt[9] and high temperature ceramics[10] and is generically classified as 'extrinsic self-healing'. Apart from issues with encapsulation and the limited shelf-life of the healing agent, a major disadvantage of this approach is that very limited times (mostly only one time) of healing events can occur at a particular damage site due to local exhaustion of healing agent. Some attempts have been made to introduce multi-times healing ability into extrinsic self-healing systems, such as compartmented fibers approach and so on[11-13]. However the intrinsic limitation of a restricted number of healing events per damage site remains.

An alternative approach to create self-healing polymers is the 'intrinsic self-healing' concept, which relies on the presence of special moieties in the polymer backbone that have an in-build tendency to chemically rebond once. In the case of intrinsic self-healing polymers, the reversible moieties can be reversible supramolecular interaction or reversible covalent bonds, such as hydrogen bonding,  $\pi$ - $\pi$  stacking, disulfide bonds, etc. [14-20]. In those intrinsic self-healing systems, local damage restoration can theoretically be infinitely repeated due to the reversible nature of the bonds formation. This is a significant advantage comparing to extrinsic self-healing materials. Intrinsic self-healing is usually triggered by an external stimulus such as heat, UV light, electric current or moisture [21-28]. Therefore intrinsic self-healing materials can be designed and applied based on the application condition and the type of stimulus.

## 1.2 Thermal interface material

Nowadays with the rapid development of electronic industry, electronic devices such as integrated circuit (IC) chips and solid state lighting (SSL) components are becoming more and more powerful but also require more electrical power. Consequently, there is more and more heat generated when they are in operation. If the heat cannot be released in time, the temperature rise will influence the normal operation and even lead to premature device failure. Usually relatively large metallic heat sinks are used to dissipate the heat produced. However direct bonding of electronic devices to metallic heat sinks is impossible from an electronic and in particular a heat management perspective. In order to reduce this contact thermal resistance and enhance heat dissipation, thermal interface materials (TIMs) are applied to fill in the air gap between heat sink and electronic device[29].

There are generally three types of thermal interface material: metallic TIMs, carbon-based TIMs and polymer-based TIMs. Metallic TIMs are often made of solder alloys or low melting metals such as Indium or Gallium [30-34]. The significant advantage of metallic TIMs is their intrinsic high thermal conductivity (usually higher than 20 W/m·K) However the relatively high mismatch in the coefficient of thermal expansion (CTE) between the metallic TIMs and the other components is one of the major disadvantages. Metallic TIMs will also be easily degraded due to oxidation reactions at elevated temperatures. Besides, some metallic TIMs enter a (partial) liquid state during operation, which brings a high potential risk of short circuiting to the system. In carbon-based TIMs, carbon fibers, carbon nanotubes or graphite flakes are aligned along the heat flow direction to provide anisotropic high thermal conduction [35-37]. However the orientated structure will be irreversibly destroyed under higher pressures, which limits the application of carbon-based TIMs. Meanwhile the wetting between carbon-based TIMs and contacted surfaces are usually very poor, which leads to a relatively high contact thermal resistance comparing to other TIMs. Polymer-based TIMs usually consist of thermally conductive fillers, such as metal powders or ceramic ( $\text{Al}_2\text{O}_3$ ,  $\text{AlN}$ ,  $\text{Si}_3\text{N}_4$ ,  $\text{ZnO}$ ,  $\text{BN}$ , etc.) particles, and a polymeric matrix to bind the filler particles together and to provide some overall mechanical flexibility [38-42]. In order to achieve high thermal conductivity, the volume fraction of thermally conductive fillers can be as high as 70% and even more. Currently, polymer-based TIMs are most widely used in electronic industry as they are chemically stable, easy to apply and relatively cheap. All this results in a wide abundance of polymer-based TIMs tailored to particular applications.

### **1.3 Challenges and future prospects**

The overheating issue as a result of degradation or non-functioning of TIMs has become one of the major reasons for premature device failure in electronic systems. In order to improve the service lifetime and reliability of polymer-based TIMs it is promising to introduce the (intrinsic) self-healing concept into polymer-based TIMs. While the topic of autonomous healing of delamination damage in TIMs seems very promising, as the damage itself leads to a temperature rise and the temperature rise leads to the required increased local molecular mobility) at the start of this PhD project only very few attempts had been made to develop self-healing TIMs [43]. As the (ceramic or metallic) filler particles are non-self-healing, the healing functionality has to come from the polymer matrix. It is a big challenge is to ensure enough structural and functional healing ability provided by the relatively small amount of self-healing polymer matrix. In addition, the relationship between structural recovery (i.e. restoration of the bond strength at the delaminated area) and functional recovery (i.e. the thermal conductions) is yet to be revealed. Another challenge is the detection and observation of the actual interfacial healing process, which plays an essential role in validating self-healing effect in polymer-based TIMs.

### **1.4 Scope and thesis outline**

This thesis aims to contribute to the introduction of the self-healing concept into polymer-based TIMs. As such, each chapter targets one of the scientific issues identified above.

Chapter 2 gives a detailed overview of a variety of approaches to intrinsic structural and functional healing in polymer systems that have been reported in the literature in recent years. Unlike other reviews on self-healing polymers this literature study aims to address the question whether the crucial factors for successful functional healing are similar to those for structural healing.

Chapter 3 applies numerical simulations using COMSOL Multiphysics to investigate the effect of micro damage at particle-matrix interfaces and macro delamination at a TIM-heat source interface on the thermal conductivity and mechanical properties of TIMs. These simulations not only can help to understand the damage sensitivity of current thermal interface materials but also guide the further development of self-healing TIMs.

In Chapter 4, the development of healable organic–inorganic dual network polymers based on disulfide chemistry, which could serve as the polymer matrix in TIMs and other types of composites, is described. By tuning the reversible bond (disulfide bond) concentration and the irreversible crosslink density in the polymer structure, the coupled effects of both on mechanical properties and crack healing efficiency are studied.

In Chapter 5, a novel TIM system based on the healable organic–inorganic dual network polymers developed in chapter 4 filled with spherical glass beads is presented. The effect of particle volume concentration (PVC) and particle size on tensile strength and thermal conductivity healing behavior is investigated.

Chapter 6 presents some thermal cycling tests performed to investigate the long-term reliability of two self-healing TIMs and one commercial non-healing reference TIM. The purpose of this study is to get a first impression whether the self-healing concept works or not in thermal interface materials.

Chapter 7 first explores the potential application of a recently developed optical material characterization technique, Laser Speckle Imaging (LSI) to monitor the adhesion process of a self-healing polymer to a glass substrate by monitoring the dynamics of interfacial healing (i.e. re-bonding). Prior to these measurements and in order to demonstrate the potential of the technique for the polymer system at hand, the molecular dynamics of the curing process in the sol–gel hybrid polymer has been measured and linked to the results of conventional rheology measurements.

## References

1. Wool RP. Self-healing materials: a review. *Soft Matter*. 2008;4(3):400-418.
2. Wu DY, Meure S, Solomon D. Self-healing polymeric materials: a review of recent developments. *Progress in Polymer Science*. 2008;33(5):479-522.
3. Van Der Zwaag S. An Introduction to Material Design Principles: Damage Prevention versus Damage Management. In: Van Der Zwaag S, editor. *Self-Healing Materials an Alternative Approach to 20 Centuries of Materials Science* 2007.
4. Zhong N, Post W. Self-repair of structural and functional composites with intrinsically self-healing polymer matrices: A review. *Composites Part A: Applied Science and Manufacturing*. 2015;69:226-239.
5. Toohey KS, Sottos NR, Lewis JA, Moore JS, White SR. Self-healing materials with microvascular networks. *Nat Mater*. 2007;6(8):581-585.
6. White SR, Sottos NR, Geubelle PH, Moore JS, Kessler MR, Sriram SR, et al. Autonomic healing of polymer composites. *Nature*. 2001;409(6822):794-797.
7. Mcilroy DA, Blaiszik BJ, Caruso MM, White SR, Moore JS, Sottos NR. Microencapsulation of a Reactive Liquid-Phase Amine for Self-Healing Epoxy Composites. *Macromolecules*. 2010;43(4):1855-1859.
8. Jonkers HM. Bacteria-based self-healing concrete. *Heron*. 2011;56(1-2):p.1-12.
9. Tabakovic A, Post W, Cantero D, Copuroglu O, Garcia SJ, Schlangen E. The reinforcement and healing of asphalt mastic mixtures by rejuvenator encapsulation in alginate compartmented fibres. *Smart Material Structures*. 2016;25(8):084003.
10. Li S, Xiao L, Song GM, Wu X, van der Zwaag S. Oxidation and Crack Healing Behavior of a Fine-Grained Cr2AlC Ceramic. *Journal of the American Ceramic Society*. 2013;96(3):892-899.
11. Post W, Jeoffroy E, García SJ, van der Zwaag S. Self-healing glass fiber reinforced polymer composites based on montmorillonite reinforced compartmented alginate fibers. *Polymer Composites*. 2017.
12. Mookhoek SD, Fischer HR, van der Zwaag S. Alginate fibres containing discrete liquid filled vacuoles for controlled delivery of healing agents in fibre reinforced composites. *Composites Part A*. 2012;43(12):2176-2182.
13. Mookhoek SD, Fischer HR, van der Zwaag S. A numerical study into the effects of elongated capsules on the healing efficiency of liquid-based systems. *Computational Materials Science*. 2009;47(2):0-511.
14. Cordier P, Tournilhac F, Soulie-Ziakovic C, Leibler L. Self-healing and thermoreversible rubber from supramolecular assembly. *Nature*. 2008;451(7181):977-980.
15. Burattini S, Colquhoun HM, Greenland BW, Hayes W. A novel self-healing supramolecular polymer system. *Faraday Discussions*. 2009;143:251-264.
16. Cao J, Meng L, Zheng S, Li Z, Jiang J, Lv X. Self-healing supramolecular hydrogels fabricated by cucurbit[8]uril-enhanced  $\pi$ - $\pi$  interaction. *International Journal of Polymeric Materials and Polymeric Biomaterials*. 2016;65(10):537-542.
17. Burattini S, Colquhoun HM, Fox JD, Friedmann D, Greenland BW, Harris PJF. A self-repairing, supramolecular polymer system: healability as a consequence of donor-acceptor  $\pi$ - $\pi$  stacking interactions. *Chemical Communications*. 2009(44):6717-6719.

18. Canadell J, Goossens H, Klumperman B. Self-Healing Materials Based on Disulfide Links. *Macromolecules*. 2011;44(8):2536-2541.
19. Pepels M, Pilot I, Klumperman B, Goossens H. Self-healing systems based on disulfide-thiol exchange reactions. *Polymer Chemistry*. 2013;4(18):4955-4965.
20. Lafont U, Van Zeijl H, Van Der Zwaag S. Influence of cross-linkers on the cohesive and adhesive self-healing ability of polysulfide-based thermosets. *ACS Applied Materials and Interfaces*. 2012;4(11):6280-6288.
21. Kavitha AA, Singha NK. "Click Chemistry" in Tailor-Made Polymethacrylates Bearing Reactive Furfuryl Functionality: A New Class of Self-Healing Polymeric Material. *ACS Applied Materials & Interfaces*. 2009;1(7):1427-1436.
22. Tian Q, Rong MZ, Zhang MQ, Yuan YC. Synthesis and characterization of epoxy with improved thermal remendability based on Diels-Alder reaction. *Polymer International*. 2010;59(10):1339-1345.
23. Bai N, Saito K, Simon GP. Synthesis of a diamine cross-linker containing Diels-Alder adducts to produce self-healing thermosetting epoxy polymer from a widely used epoxy monomer. *Polymer Chemistry*. 2013;4(3):724-730.
24. Chung C-M, Roh Y-S, Cho S-Y, Kim J-G. Crack Healing in Polymeric Materials via Photochemical [2+2] Cycloaddition. *Chemistry of Materials*. 2004;16(21):3982-3984.
25. Ling J, Rong MZ, Zhang MQ. Coumarin imparts repeated photochemical remendability to polyurethane. *Journal of Materials Chemistry*. 2011;21(45):18373-18380.
26. Amamoto Y, Kamada J, Otsuka H, Takahara A, Matyjaszewski K. Repeatable Photoinduced Self-Healing of Covalently Cross-Linked Polymers through Reshuffling of Trithiocarbonate Units. *Angewandte Chemie*. 2011;123(7):1698-1701.
27. Chuo T-W, Wei T-C, Liu Y-L. Electrically driven self-healing polymers based on reversible guest-host complexation of  $\beta$ -cyclodextrin and ferrocene. *Journal of Polymer Science Part A: Polymer Chemistry*. 2013;51(16):3395-3403.
28. Zhang Z, Hu Y, Liu Z, Guo T. Synthesis and evaluation of a moisture-promoted healing copolymer. *Polymer*. 2012;53(14):2979-2990.
29. Prasher R. Thermal Interface Materials: Historical Perspective, Status, and Future Directions. *Proceedings of the IEEE*. 2006;94(8):1571-1586.
30. Roy CK, Bhavnani S, Hamilton MC, Johnson RW, Knight RW, Harris DK. Durability of Low Melt Alloys as Thermal Interface Materials. *Journal of Electronic Packaging*. 2016;138(1):010913.010911-010913.010917.
31. Roy CK, Bhavnani S, Hamilton MC, Johnson RW, Knight RW, Harris DK. Accelerated aging and thermal cycling of low melting temperature alloys as wet thermal interface materials. *Microelectronics Reliability*. 2015;55(12PT.B):2698-2704.
32. Gao Y, Liu J. Gallium-based thermal interface material with high compliance and wettability. *Applied Physics A*. 2012;107(3):p.701-708.
33. Touzelbaev M, Khan M, Master R, Diep J, Keok K-H, editors. Indium Thermal Interface Material Development for Microprocessors. *Semiconductor Thermal Measurement & Management Symposium*; 2009.
34. Dutta I, Raj R, Kumar P, Chen T, Nagaraj CM, Liu J, et al. . Liquid Phase Sintered Solders with Indium as Minority Phase for Next Generation Thermal Interface Material Applications. *Journal of Electronic Materials*. 2009;38(12):p.2735-2745.

35. Memon MO, Haillot S, Lafdi K. Carbon nanofiber based buckypaper used as a thermal interface material. *Carbon*. 2011;49(12):3820-3828.
36. Lee YT, Shanmugan S, Mutharasu D. Thermal resistance of CNTs-based thermal interface material for high power solid state device packages. *Applied Physics A*. 2014;114(4):1145-1152.
37. Chung DDL. Carbon materials for structural self-sensing, electromagnetic shielding and thermal interfacing. *Carbon*. 2012;50(9):3342-3353.
38. Koning P, Prstic S, Shipley J, Prasher RS. Thermal Resistance of Particle Laden Polymeric Thermal Interface Materials. *Journal of Heat Transfer*. 2003;125(6):1170-1177.
39. Anithambigai P, Shanmugan S, Mutharasu D, Ibrahim K, editors. Heat transfer in high-power LED with thermally conductive particle-filled epoxy composite as thermal interface material for system-level analysis. *Quality Electronic Design*; 2013.
40. Wen MJ, Subramani S, Devarajan M, Sulaiman F. Effect of ethyl cellulose on thermal resistivity of thixotropic ZnO nano-particle paste for thermal interface material in light emitting diode application. *Materials Science in Semiconductor Processing*. 2017;58:61-67.
41. Goyal V, Balandin AA. Thermal properties of the hybrid graphene-metal nano-micro-composites: Applications in thermal interface materials. *Applied Physics Letters*. 2012;100(7):p.073113.073111-073113.073114.
42. Chen J, Huang X, Sun B, Wang Y, Zhu Y, Jiang P. Vertically Aligned and Interconnected Boron Nitride Nanosheets for Advanced Flexible Nanocomposite Thermal Interface Materials. *Acs Applied Materials & Interfaces*. 2017;9(36):30909-30917.
43. Lafont U, Moreno-Belle C, van Zeijl H, van der Zwaag S. Self-healing thermally conductive adhesives. *Journal of Intelligent Material Systems and Structures*. 2014;25(1):67-74.

# Chapter 2

---

## **Self-repair of structural and functional composites via intrinsically self-healing polymer matrices: A review**

---

**This chapter has been published as:**

**Zhong N, Post W**

*Self-repair of structural and functional composites with intrinsically self-healing polymer matrices: A review*

Composites Part A: Applied Science and Manufacturing. 2015;69:226-239.



## 2.1 Introduction

Over the last decades the amount of studies reporting on polymer composite functionality and mechanical properties has grown significantly. Polymer composites showing for example thermal and electrical properties can be found in daily life in communication, lightning and aerospace applications [1, 2]. Although the field of multifunctional polymer composites is increasing rapidly, researchers are far away from reaching the diversity in functionalities that nature has established in its composites over the past millions of years. Wood is one of nature's finest examples of a multifunctional fibrous composite material. This well-known material consists of parallel hollow tubular cells reinforced by spirally wound cellulosic fibrils embedded in a hemicellulose and lignin matrix. The helix angle of the spiral fibrils is responsible for a variety of mechanical properties such as wood stiffness and toughness, whereas the hollow tubular cells are capable of transporting nutrients from the soil to the top parts of a tree [3]. A second example of nature's engineering capabilities can be found in bones which deliver optimal mechanical properties due to a smart combination of material selection and material shaping [4].

Besides a variety of mechanical and functional properties, wood and bone possess the capability to self-repair damage that is inflicted to their components. Since both structural and functional polymer composites show a drop in performance when subjected to a certain cyclic or impact loading due to the formation of cracks or delamination, a bio-inspired system that autonomously restores the material properties is considered tremendously valuable. Therefore, in the past two decades, the self-healing capacity has inspired many researchers to design polymer composites that are capable of healing damage rather than preventing it [5, 6]. This field was pioneered by Dry who included hollow glass fibers containing liquid adhesive in a concrete matrix. The liquid agent is released upon local fracture, wets the crack surface and crosslinks thereby partially restoring the load bearing capacity [7, 8]. White et al. showed the recovery of tensile strength of an epoxy material by embedding polymeric microcapsules filled with crosslinkable liquid oligomer into the polymer matrix with dispersed Grubbs catalyst [9]. However, since it is quite challenging to obtain a uniform distribution of healing agent using particulate containers, Bond et al. developed a self-healing fiber reinforced composite by introducing glass fibers filled with healing agent. The resulting composite was capable of restoring a significant amount of its original flexural strength [10].

At the pioneering start of the field of self-healing composites, the employed healing strategies are extrinsic (i.e. are due to the inclusion of discrete entities containing the healing agents in an otherwise non-self-healing surroundings) and therefore only a single healing event can occur at the same damaged site. In more recent years, the intrinsically self-healing route (i.e. the architecture of the polymer is such that local damage can be restored upon a mild proper trigger by the reformation of reversible chemical bonds) was shown as a conceptually more attractive alternative. The concept of intrinsic healing can theoretically lead to infinite amount of healing cycles as no external healing agents are required. The healing process depends on the ability of the matrix to acquire local mobility upon the stimulation of an external stimulus, such as temperature, light induction, electrical current and moisture exposure. Therefore, in contrast with their extrinsic counterparts, intrinsic healing materials are not fully autonomous. Still, the implementation of intrinsic healing in polymer composites is considered as a next step in development of materials that are designed to mend damage rather than preventing it [6, 11, 12].

The majority of studies that cover the intrinsic healing of polymer composites reported on the healing of structural properties (i.e. properties related to load bearing behavior, such as stiffness, strength and failure strain), whereas the field of general self-healing polymer functionality (including healing of non-mechanical properties such as thermal conduction, electrical conduction and magnetic shielding etc.) is emerging only in the last couple of years. However, damage (upon fatigue or impact loading) in either the polymer matrix (cracks) or at the matrix-filler interface (delamination) is responsible for a decrease in the properties of both structural and functional polymer composites, because the filler material is no longer capable of transferring its specific properties towards the matrix material. Therefore healing strategies in both types of composites can be similar and will be most effective in the form of a polymer matrix capable of restoring either itself or the matrix-filler interface. For this reason the development of polymer matrices that can intrinsically heal themselves or restore the adhesive properties at the composite interface is considered to be a major challenge within the field of self-healing polymers. This review aims to give an overview of the progress that is made on intrinsic matrix healing of both structural and functional properties in polymer composites. Firstly, the current developments in intrinsic polymer matrix healing are discussed, grouped by the triggering mechanism for the healing process. Secondly, the general concepts and influence of filler materials on structural composite properties (stiffness, strength) and their healing capabilities is covered. Finally, a similar approach is used

to analyze the self-healing potential of functional (electrical, electromagnetic, electromechanical, magnetic and thermal) polymer based composites.

## 2.2 Intrinsically self-healing matrix polymers

2

In structural and functional composites, polymers, such as polyester, polyimide, polyurethane, epoxy or silicone rubber, are used as matrix because of their ability to bind and preserve the location of the filling material, their low density, chemical inertness, low cost and versatility in fabrication methods. Traditionally polymer based composite systems were composed such that a maximum resistance to local mechanical, thermo-mechanical or chemo-mechanical degradation is obtained. Very often the optimization focused on creating a lasting chemo-mechanical bond between the polymer matrix and the filling agent. In this conventional optimization damage, virtually always starting in the polymer matrix or at the matrix-particle interface, was treated as an irrecoverable event. However, with the advent of intrinsically self-healing polymers, i.e. polymers which can restore mechanical bonding with itself or a different material due to reformation of chemical bonds under the appropriate stimulus (see Figure 2.1 and Figure 2.2), the design concepts for composites have changed significantly and irreversibly. Below, we describe the range of self-healing polymers and group them according to the trigger they need to heal cracks and interfacial delamination.

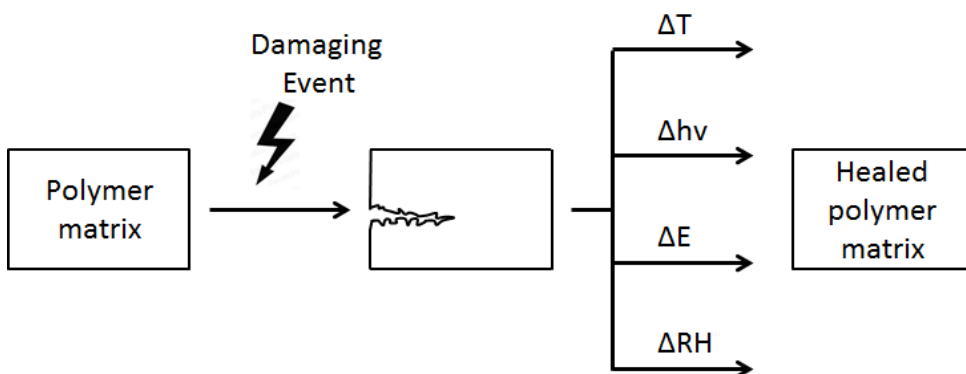


**Figure 2.1** Schematic representation of intrinsic self-sealing by external stimuli; thermal, photochemical, electrical and moisture activation.

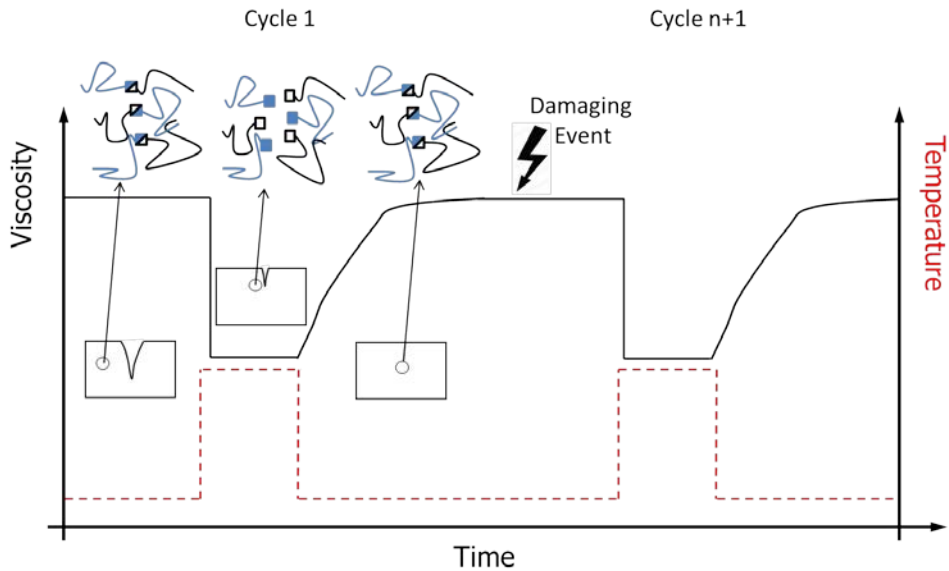


**Figure 2.2** General concept of matrix healing using intrinsic healing concepts. Figure shows a sudden drop in viscosity upon heating linked to local temporary network mobility necessary for flow and damage repair. Upon cooling the local properties (e.g. viscosity) are restored to initial values so the material can be further used. Figure also shows the multiple healing events possible with intrinsic healing concepts [6].

### 2.2.1 Heat triggered self-healing

Intrinsic self-healing polymers based on heat triggered reversible reactions have been studied extensively. Among them, the Diels-Alder/retro-Diels-Alder reaction (DA/rDA) has received the most attention. The Diels-Alder reaction is a reversible reaction that takes place between a conjugated diene and a substituted alkene, usually termed the dienophile to form a substituted cyclohexene system. DA/rDA reaction can be used as healing mechanism in multiple polymer systems (e.g. polyamide, polyethylene and epoxies) and can be used to heal both the matrix and the matrix-filler interface. The latter one is schematically depicted in Figure 2.3. The healing temperature ranges from 100°C to 150°C and the healing times were reported in the range of 10min to 2h [13-21].

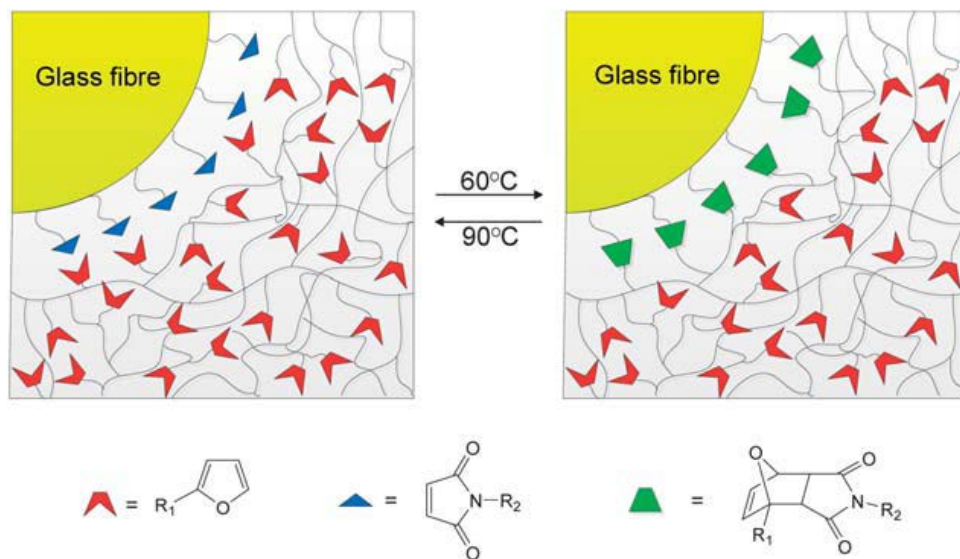


**Figure 2.3** Self-healing of composite strength via a reversible Diels-Alder reaction at the fiber-matrix interface. Glass fibers are functionalized with maleimide functionalized groups (blue figures) and placed in a furan group (red figures) containing polymer network. The resulting composite is capable of thermoreversible interface healing resulting in restoration of stress transfer between fibers and matrix [22, 23].

A second type of thermally activated self-healing was introduced by Canadell et al. who used remendable disulfide chemistry in a covalently cross-linked rubber [24]. In their work, an epoxy resin containing disulfide groups was cross-linked with a tetrafunctional thiol in a base-catalyzed addition reaction. Upon fracture, the mechanical properties of this material can be fully restored by re-contacting the fractured surfaces while heating at 60°C for 1h. A more recent study showed that the dominant healing mechanism is based on the thiol-disulfide exchange and that reaction is highly pH dependent [25]. An advantage of using disulfide chemistry as self-healing mechanism is that healing can be achieved at moderate temperatures, while keeping a reasonable level of bond strength.

Another example of self-healing by a thermal stimulus is the radical exchange reaction of alkoxyamine units that can be used to prepare a thermodynamic polymer cross-linking system [26, 27]. Based on this mechanism, Yuan et al. developed self-healing polystyrene with alkoxyamine side chains which function as cross-linker. In

this system, fission and radical recombination of C-ON bonds takes place among alkoxyamine moieties when a thermal stimulus is applied. The healing efficiency of this system reaches values of 75.9% by heating upon 130°C for 2.5 hours [28].

Besides the aforementioned thermally triggered covalent self-healing systems, matrices can use supramolecular interactions, such as hydrogen bonding and  $\pi$ - $\pi$  interactions, as a mechanism for intrinsic healing. In healing systems based on hydrogen bonding, mending will occur already at room temperature when the functional groups are brought into effective contact with each other. However, the healing efficiency decreases with increasing waiting time between the damage event and mending because the free hydrogen bonds can rearrange and associate with one another at the fractured surface instead of those on the other side of the crack. Moreover, the elevation of the healing temperature can increase the molecular dynamics and accelerate the equilibrium, thereby decreasing the healing time [29-35].

A second system capable of supramolecular healing is based on  $\pi$ -electron-poor receptors and  $\pi$ -electron-rich pyrenyl end-groups. Here, the healing mechanism involves two steps. The first step is the disruption of the intermolecular  $\pi$ - $\pi$  stacking cross-links upon an increased temperature. The second step is the rearrangement of chains and reformation of  $\pi$ - $\pi$  stacking cross-links occurs when the temperature is lowered. The healing temperature is reported to be around 100°C with healing time more than 2 hours [36-38].

Ionomers are another class of thermally activated supramolecular self-healing polymers that possess the ability to heal ballistic impact damage. In ionomers, ionic metal salts are bonded to the polymer backbone creating electrostatic interactions. The local heat that is released upon impact enables these bonds to reform and thereby heal the material. Studies on ionomer healing focused on the autonomous healing after high speed ballistic impact [39, 40] and on the stimulated self-healing after quasi static damage production [41-44].

### **2.2.2 Photochemical triggered self-healing**

Besides thermal activation, self-healing behavior can be triggered by photochemical reactions. Based on photochemical [2+2] cycloaddition of cinnamoyl groups, Chung et al. developed a self-healing polymer from 1,1,1-tris-(cinnamoyloxymethyl)ethane,

which is a photo-cross-linkable cinnamate monomer[45]. In their study, healing was conducted by photoirradiation ( $\lambda > 280$  nm) for 10 minutes. More recently, Ling et al. and Oya et al. continued this line of research by synthesizing novel self-healing polymers based on [2+2] photocycloaddition [46, 47].

Another example of photochemically triggered healing was reported by Ghosh et al. who developed a self-healing oxetane-substituted chitosan polyurethane [48]. Upon fracture, four-membered oxetane rings open up thereby creating two reactive ends. When the crack plane is exposed to ultraviolet light ( $\lambda=302$  nm), chitosan chain scission occurs, which forms crosslinks between the reactive oxetane ends and repairs the network in less than 1 hour.

Amamoto et al. showed two novel studies on self-healing polymers by photoinduced reshuffling of disulphide bonds. First, they introduced self-healing in poly(*n*-butyl acrylate) by including repeatable trithiocarbonate units [49]. These polymers are capable of healing macroscopic cracks almost completely after UV irradiation ( $\lambda=330$  nm) for 48 hours. In a second study, they reported on macroscopic self-healing crosslinked polyurethanes based on radical reshuffling of thiuram disulfide units under the stimulation of visible light at room temperature [50].

Moreover, photochemical self-healing in metallosupramolecular polymers were reported by Burnworth et al.. Their low-molecular-mass polymers possess ligand end groups that are non-covalently linked through metal-ion binding [51]. Samples were healed by exposure to UV light leading to a temporary disengagement of the metal-ligand bonds.

### 2.2.3 Electrically triggered self-healing

Matrix healing upon electrical stimulus was proposed by Chuo et al. who prepared an electrically triggered self-healing polymeric material based on the complexation reaction between ferrocene modified poly(glycidylmethacrylate) and  $\beta$ -cyclodextrin groups [52]. A knife-cut crack on the surface of this sample mends almost completely after an electrical treatment of 9V for 24 hours followed by a resting period at room temperature for another 24 hours. The healing efficiency can be improved by an additional thermal treatment (85°C, 24 h) after the electrically induced repairing process.

#### **2.2.4 Moisture triggered self-healing**

Zhang et al. synthesized an isocyanate containing methacrylate monomer copolymer system that repairs macroscopic cracks after a relative humidity treatment (95% at 30°) of 12 hours and serves as a protecting fluorine-containing monomer component [53]. Healing is based on a zipper-like healing mechanism in which the isocyanate groups on both sides of the crack within the effective contact areas are coupled by reacting with environmental water. This process can be gradually extended to the ineffectively contacted areas which ultimately results in full closure and healing of the crack.

### **2.3 Structural composites containing an intrinsically self-healing polymer matrix**

Structural composites are optimized to give desirable mechanical properties, in particular (specific) stiffness and mechanical strength. The strength and stiffness of such composites depends on the properties of the constituent phases (polymer matrix and inorganic filler), their volume fraction and their configuration. To realize their full potential a perfect bonding between the matrix and the filler particles is required. As the inorganic fillers are based on strong irreversible (non-self-healing) covalent bonds, any self-healing has to come from the polymer matrix which (in principle) can restore the integrity of the matrix as well that of the interfacial bond. Below we demonstrate how the principal mechanical properties are to be affected by a self-healing polymer matrix.

#### **2.3.1 Stiffness recovery**

The stiffness of a material is defined by the ratio between stress and strain (Young's modulus or modulus of elasticity) at the elastic regime of tensile experiment and describes the resistance to elastic deformation of a material. To improve the typical low stiffness of polymers either particles or fibers of a high modulus material are integrated into the polymer matrix [2, 54, 55].

In particulate reinforced composites, the first factor that affects the stiffness is the weight percentage of the added particles. An increasing concentration of hard



particles in a polymer matrix improves the stiffness since the rigidity of fillers is much higher than that of matrix. This effect was described in many studies such as the work of Zhu et al. on polyimide/silica particle composites [56-60]. The polymer composite stiffness is less clearly affected by a change in particle size. For particles with sizes in the micrometer scale, the Young's modulus does not change with increasing diameter [58], but for nanometer-sized particles an increase in stiffness is observed when the average particle size is decreased [57]. Besides the particle size, the interfacial adhesion between the particles and the matrix has little effect on the stiffness as well. Since values for the stiffness are determined at relatively low deformation, there is insufficient dilation for interfacial adhesion parameters to have an effect on the Young's modulus [56, 59].

Besides adding particles, long continuous or short discontinuous fibers can also be used to increase the stiffness of a polymer matrix. The elastic modulus of common reinforcement fibers (glass, aramid, carbon) is typically a hundred times higher than that of conventionally used polymer matrices [55]. Based on the volume fraction of the fibers in the matrix, the overall stiffness of fiber reinforced polymer composite can be estimated by the 'rule of mixture':

$$E_c = \eta_L \eta_o V_f E_f + (1 - V_f) E_m \quad (2.1)$$

where  $E_c$ ,  $E_f$  and  $E_m$  are the stiffness of the composite, fiber and matrix respectively,  $V_f$  is the volume fraction of the fiber and  $\eta_L$  and  $\eta_o$  are the length efficiency and orientation factor respectively [61]. The fiber orientation factor has a value ranging from 0.2 (for randomly distributed fibers) till 1 (for unidirectional fibers). The length efficiency factor  $\eta_L$  depends on the critical fiber length ( $L_c$ ) of the filler material which is described by:

$$L_c = \frac{\sigma_f d_f}{2\tau} \quad (2.2)$$

where  $\sigma_f$  is the maximum fiber stress (or ultimate fiber strength),  $d_f$  is the fiber diameter and  $\tau$  is the interfacial shear stress which can be regarded as a measure for the interfacial adhesion between filler and matrix. When the fiber length is below  $L_c$ ,  $\eta_L$  has a value near zero and the filler material does not contribute to the composite stiffness. The value for  $\eta_L$  increases with increasing fiber length up till the point where the fiber length is ten times  $L_c$  and  $\eta_L$  has a value of 1. At this level, an increase

in interfacial adhesion does no longer add to the composite stiffness. For this reason the interfacial adhesion has only a small effect on the stiffness of a continuous fiber reinforced polymers. However, the effect of interfacial adhesion on short fiber reinforced composite stiffness is significant. A graphical description of the effect of interfacial adhesion on the composite stiffness is presented in Figure 2.4. In the case of complete debonding the fillers do not carry any load and the stiffness of the composite decreases with increasing filler content. In the case of perfect bonding the stiffness of the composite increases with filler content according to the physical limit given by equation 2.1. In the case of partial debonding intermediate stiffness values are obtained. Several studies described interfaces that are modified to improve the adhesion between fiber and matrix which show higher elastic moduli than their unmodified counterparts [55, 62, 63]. A study by Thomason et al. on continuous glass fiber reinforced polyimides shows that the composite stiffness is unaffected by changes in the fiber diameter because the fiber length greatly exceeds the  $L_c$  [64].

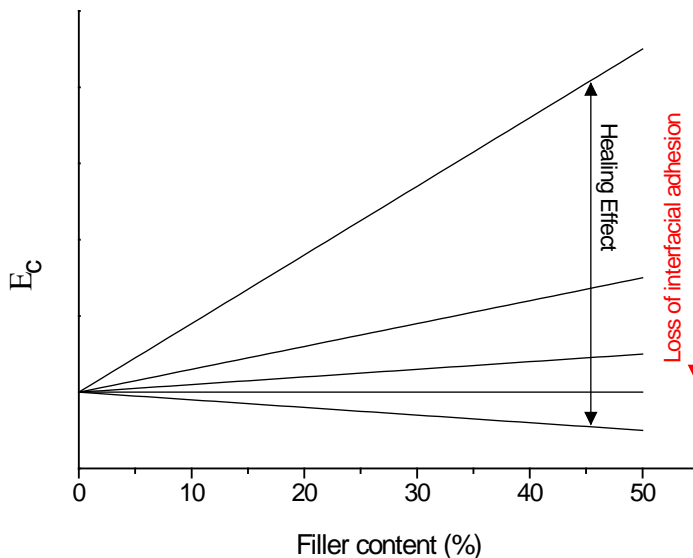


**Figure 2.4** Graphical representation of the relation between filler content, interfacial adhesion and the elastic modulus in a short discontinuous fiber reinforced polymer composite material. The relation is plotted for various values of  $\tau$  resulting in values for  $\eta_L$  ranging from 0 to 1 which directly shows the range of stiffness that can be healed by restoring the fiber–matrix interface. A similar model could be composed for the strength of a polymer composite.

Fatigue and impact damage are the most occurring types of damage in real-life applications of polymer composites. Fatigue damage results in cracks splitting either part of the polymer matrix or the matrix–filler interface and damage upon impact ranges from barely visible impact damage (micro–cracks or delamination) to large scale breakage like target penetration [6, 65]. In short fiber reinforced polymer composites the damage will initiate at the interface resulting in a reduction of  $\tau$  and  $\eta_L$  leading to a drop in composite stiffness. Figure 2.4 shows the stiffness range that can potentially be recovered by healing of the interfacial adhesion between filler and matrix. To repair the composite's damage and regain its structural properties, the focus should therefore be on healing the matrix and the composite interface which results in restoring the initial values of  $\tau$  and  $\eta_L$ . Studies that report on stiffness regeneration include the work of Yoshie et al. who reported on the recovery of tensile moduli of a self–mending polymer based on the Diels–Alder chemistry between anthracene and maleimide at both room temperature (17%) and 100°C (46%) [66]. Secondly, recovery rates of Young's moduli of almost 100% were reported by Amamoto et al. who designed a polyurethane that heals using radical reshuffling of thiuram disulphide bonds under ambient conditions (Figure 2.5) [50]. A third example of stiffness regeneration was shown in the study of Zako and Takano. They developed a composite blend material that consists of a rigid polymer matrix in which melt processable thermosetting epoxy particles are introduced. Specimens were damaged and healed at 120°C. After healing the stiffness of the composite material was fully recovered [67].

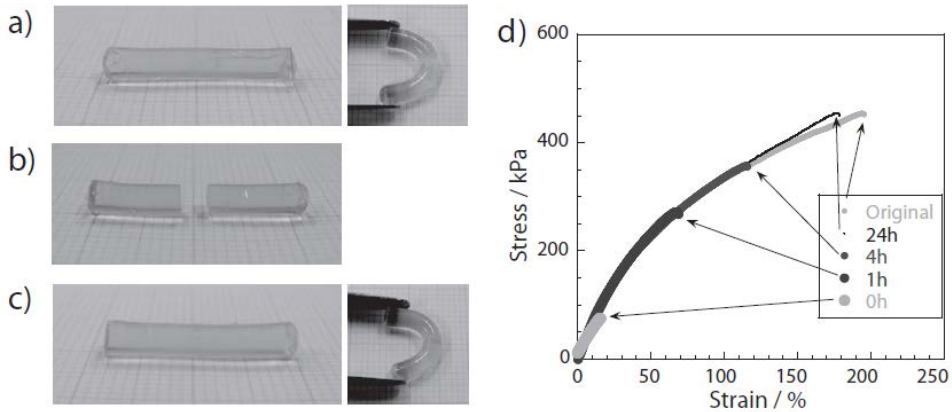


**Figure 2.5** Recovery of structural properties in a self-healing polymer matrix using photochemical reversible thiuam disulfide bonds. The polymer matrix is displayed prior cutting and self-healing (a), after cutting (b) and after 24h of self-healing (c). (d) shows a stress, strain curve in which the regeneration of mechanical properties is plotted at different stages of the self-healing process [50].

### 2.3.2 Strength recovery

The strength of a material can be described by several parameters. The tensile strength is defined as the maximum stress that a material can sustain under tensile loading and is also called the ultimate strength. The stress at fracture and the stress above which plastic deformation occurs are called the breaking strength and yield strength respectively [2]. In line with polymer stiffness improvement, the polymer composite stiffness can be increased by introducing particles or fibers that have much higher strength values than the matrix.

The strength of micro and nano-particulate composites is mainly determined by the effectiveness of the stress transfer between the matrix and the particles [54]. As for composite stiffness, the strength depends on the weight percentage of filler that is present in the matrix. However, no clear trend can be derived from literature as studies show that an increase in filler concentration can initially improve the composite strength while it is reduced upon further increase of particle concentration [54]. This is exemplified by the work of Zhu et al. who reported on polyimide films with silica fillers that show an increase in tensile strength up to a

silica weight fraction of 10% [60]. However, a decline of tensile strength is observed upon further increase of the silica concentration. This can be explained by the fact that the particle cluster size increases together with the weight fraction which suppresses the strength of the composite, since, in contrast to stiffness, there is a clear relation between the size of added micro- and nanoparticles and the strength of a polymer composite. Generally, a decrease in particle size will lead to an increase in tensile strength as is shown for epoxy/silica composites by Nakamura et al. [68]. A final crucial parameter is the strength of the interfacial particle/matrix adhesion which determines the stress transfer between the components. For polymer composites containing very well-bonded particles, the addition of particles will result into a higher material strength. Poorly adhered particles, however, have an ineffective stress transfer and therefore do not contribute to the reinforcement of the matrix which leads to a decrease in strength. This phenomenon was quantified by Zhang et al. who showed the effect of interfacial adhesion in polypropylene/silica nano-composites on the material's strength by treating the particles with various monomers [69, 70].

Short and continuous reinforcing fibers with high elastic moduli (carbon, aramid, glass) are used to enhance the strength of a polymer composite in a similar fashion as is described for stiffness modification. Therefore, the 'rule of mixture' can also be used to approach the strength of a composite based on the volume fraction of the fibers:

$$\sigma_c = \eta_L \eta_0 V_f \sigma_f + (1 - V_f) \sigma_m \quad (2.3)$$

where  $\sigma_c$ ,  $\sigma_f$  and  $\sigma_m$  are the strength of the composite, fibers and matrix respectively. For strength, the length efficiency factor,  $\eta_L$ , is again related to the critical thickness  $L_c$ , as is described by equation 2.2. Therefore a similar graphical relation between the strength, volume fraction and interfacial adhesion, similar to that depicted in Figure 2.4 could be composed. Such a graph would indicate that the interfacial adhesion between fiber and polymer also has a large effect on the composite strength [62, 71]. This is exemplified by a recent study that showed the coating of carbon fibers with carbon nanotubes in order to improve the interfacial stress transfer of polymer to fibers resulting in an increase of tensile strength of 64% [63].

As is described for stiffness, the strength of a composite will drop upon interfacial failure due to a reduction of effective stress transfer resulting from cracks and delamination in the matrix or at the interface. Therefore, studies on strength healing

should also focus on the recovery of  $\eta_L$  and  $\tau$  by intrinsic restoration of the polymer matrix or the matrix–filler interface. For this purpose mainly intrinsic covalent healing strategies, containing either thermo reversible or photo reversible chemistries, are used [22]. Healing of the strength of epoxy–amine thermoset composites by the addition of thermally reversible cross–linking gel based on Diels–Alder chemistry was reported by Peterson et al. [20]. Recovery of strength can be achieved by direct application of the gel (37%) and by incorporation as a secondary particulate phase (21%) [72]. A more recent study described strength recovery (41% healing efficiency) at the glass fiber–polymer interface by coating with DA functional groups (Figure 2.3) which results in restoration of stress transfer capacity between matrix and fiber [23]. A second thermo reversible route is the incorporation of disulphide bonds in epoxy thermosets which leads to the recovery of the material's tensile strength (>90%) [24] or adhesive strength (100%) [73].

Alternatively, self–healing of structural properties by photo reversible chemistry was introduced by Chung et al in 2004, however, the healing efficiency was rather low [45]. Later, Ling et al. managed to achieve tensile strength recoveries up to 100% by embedding coumarin groups in the main chains of a polyurethane network [47, 74].

Instead of using covalent healing chemistry Hayes et al. showed the recovery of strength by blending conventional thermosets with thermoplastic material. Their study showed that including 20 wt.% of thermoplastic material results in a regain of 70% of the virgin properties of the matrix [75]. More recent, Luo et al. showed a strength recovery of more than 100% in a polymerization–induced phase separated thermoset/thermoplastic blend that is capable of differential expansive bleeding [76].

## **2.4 Functional composites containing an intrinsically self–healing polymer matrix**

Polymer based composites are also widely used as functional materials such as electrically conductive materials, electromagnetic interference shielding materials, electromechanical materials, magnetic materials or thermally conductive materials. Like structural polymer composites their properties generally (but not always) rely on the absence of damage in the polymer matrix and the absence of interfacial delamination. The opportunities for restoration of functional properties due to a

self-healing polymer matrix are addressed below. The potential options are grouped according to the functional character of the composite.

### **2.4.1 Electrically conductive polymer composites**

2

Electrically conductive polymer composites consist of a non-conductive polymer matrix and electrically conductive fillers and are widely used in various commercial applications due to their light weight, high manufacturability, corrosion resistance and good electrical conductivity [77-84].

To analyze the electrical conductivity of filler-loaded polymer composites, the percolation theory is usually used. When the content of fillers is below the percolation threshold, a long-range connection of fillers does not exist, leading to a very low electrical conductivity. While above the percolation threshold, the electrical conductivity increases significantly due to the formation of a long-range filler connection. When the percolation threshold for a material with a fixed filler concentration is reduced an increase in electrical conductivity is observed. According to the statistic percolation theory [85], the percolation threshold is inversely proportional to the particle aspect ratio. Therefore carbon nanotubes are promising candidates as electrically conductive fillers. This is exemplified by the work of Sandler et al. who reported percolation thresholds below 0.01% in a carbon nanotube/epoxy system [77]. Additionally, the work of Bilotti et al. showed that a further reduction of percolation threshold can be achieved by the addition of secondary nano-fillers [86].

Other systems using graphite, carbon black and carbon fibers as fillers are also investigated and research focuses on improving the processability and reducing the costs. An effective strategy that can be applied to these systems is to form a double percolation phenomenon by localizing fillers at the interface or within one of the phases of an immiscible polymer blend [87, 88]. Furthermore, processing conditions will affect the particle alignment and the electrical conductivity of composites. For example, Kitajima et al. fabricated anisotropic electrically conductive polymer composites by applying a strong magnetic field to orient fillers [89]. The resulting composites showed much higher electrical conductivity along the direction of the magnetic field.

When micro- or macro-cracks are formed in the system, the connection of fillers may break down. Since the electrical conductivity of composites depends on the connection of fillers, this leads to a full or at least significant decrease of electrical conductivity and unexpected failure of electronic devices. These problems can be overcome by introducing an intrinsic self-healing polymer matrix that can heal the crack and restore the connection of fillers. Following this concept, Li et al. fabricated electrically conductive self-healing films by depositing Ag nanowires on top of healable polyelectrolyte multilayer films consisting of a layer-by-layer assembled branched poly(ethylenimine) and poly(acrylic acid)–hyaluronic acid blend [90]. Cuts can be autonomously repaired when water is sprayed on the films thereby recovering the electrical conductivity. A second example electrical conductivity healing was given by Tee et al.. They prepared an electrically and mechanically self-healing composite consisting of a supramolecular polymeric hydrogen-bonding network with self-healing ability filled with chemically compatible micro-nickel particles with nanoscale surface features [91]. The result showed a full recovery of electrical conductivity within 1 minute at room temperature upon complete fracture (as shown in Figure 2.6).

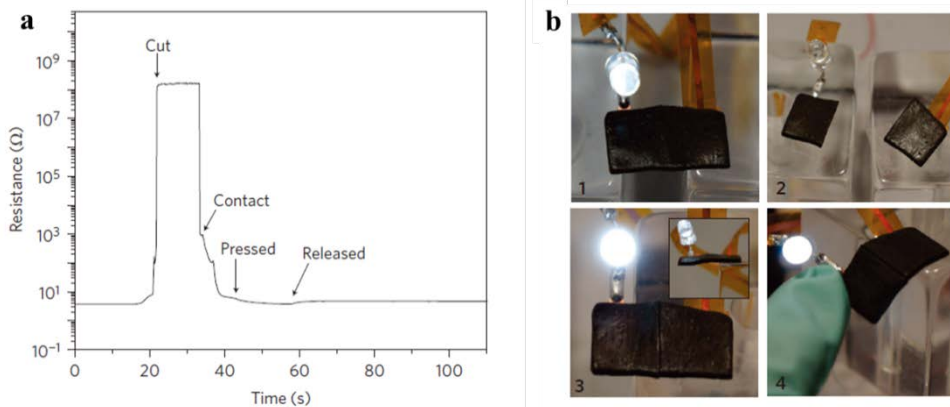


**Figure 2.6** Electrical conductivity healing characterization of self-healing composite. (a) Resistance measurement shows electrical conductivity healing at room temperature. (b) Demonstration of the healing process using an LED in series with a self-healing composite conductor. 1, undamaged; 2, completely severed (open circuit); 3, electrical healing (inset shows conductor being self-supporting); 4, healed film being flexed to show its mechanical healing after only 5 min at room temperature [91].



Self-healing of electrical properties in stretchable wires was reported by Palleau et al. who combined the self-healing Reverlink polymer produced by Arkema with liquid metal [92]. In their experiment, 2D or 3D structures were made after cutting a straight sample. The self-healing polymer provided the mechanical recovery and helped to re-align the liquid metal channel. Once re-aligned, the liquid metal components merged together and formed a conductive channel again. Self-healing wires are particularly important for the growing field of stretchable electronics in which electronic components may undergo significant deformation and lead to unexpected failure. In addition, these self-healing structures offer a simple method to rewire circuits.

Another example of self-healing electrically conductive polymer composite was reported by Wang et al.. They fabricated silicon micro-particle (SiMP) anodes for high-energy lithium-ion batteries, which are coated with a self-healing polymer composite consisting of a randomly branched hydrogen-bonding polymer matrix and carbon black nanoparticles [93]. The self-healing conductive composite coatings assist to heal the cracks, which are generated during the cycling process, and as such extend the cycle life ten times longer than state-of-the-art anodes made from SiMPs while still retaining a high capacity.

### 2.4.2 Electromagnetic polymer composites

All electrical and electronic devices emit electromagnetic signals, which can interfere with the operational properties of either the emitting equipment or any other equipment around it. To overcome this problem, the equipment can be shielded by electromagnetic interference (EMI) shielding materials. The first generation of EMI shielding materials were made of metals, but in recent years electrically conducting polymer composites have gained popularity for EMI shielding applications. EMI shielding polymer composites are lightweight, resistant to corrosion, flexible, and cost less than metals. The most important property of EMI shielding materials is the shielding effectiveness (SE). According to Simon's equation [94]:

$$SE(\text{dB}) = 50 + 10 \log_{10} \left( \frac{1}{\rho f} \right) + 1.7t \left( \frac{f}{\rho} \right)^{\frac{1}{2}} \quad (2.4)$$

where  $\rho$  is the volume resistivity in  $\Omega\cdot\text{cm}$ ,  $f$  is the frequency in MHz, and  $t$  is the thickness in cm, the EMI SE is higher when the electrical resistivity is lower. As discussed in section 2.4.1, the electrical conductivity can be restored after damage by introducing a self-healing polymer matrix to electrically conducting composites. Subsequently, the EMI shielding property can recover.

### 2.4.3 Electromechanical polymer composites

Polymers that possess the ability to convert electrical into mechanical energy or vice versa are used in composite materials for numerous applications, such as sensors, actuators and energy harvesting. The functionality of these so called electromechanical composites can be found either in the polymer matrix or in the added filler material. The driving force behind electromechanical polymer matrices can be electronic (driven by an electric field or Coulomb forces) or ionic (involving diffusion or mobility of ions). Electronically driven polymers operate at room temperature and show a rapid electroactive response (ms range), but the required voltages are high ( $\pm 200$  MV/m). Ionic electroactive polymers already operate at low voltage levels ( $< 5$  MV/m), but this is combined with a relatively slow response (in the order of seconds) [95, 96].

One of the most common electronically activated electromechanical functionalities is the piezoelectric effect. Piezoelectricity is found only in noncentrosymmetric materials and it is called ferroelectricity when such a material exhibits spontaneous polarization. Among the few polymers that show ferroelectric behavior, poly(vinylidene fluoride)(PVDF) and its copolymers have shown to have the best overall electroactive properties. Therefore PVDF is used in the majority of the research and industrial applications that involve piezoelectric polymers [97]. Another class of electronically driven polymers is that of the dielectric elastomers. This group of polymers includes silicones and acrylics with rubberlike properties such as low tensile strength and high deformability [98]. Studies of Pelrine et al. describe high strain rates ( $> 100\%$ ) for both silicone and acrylic polymers [99, 100].

Ionic electroactive polymers are used for the production of ionomeric polymer-metal composites (IPMC). IPMCs bend at low voltages due to an ionomer that provides mobility of positive ions between a fixed network of negative ions on metal clusters. Two types of ionomers are typically used for the production of IPMCs, being Nafion (DuPont) and Flemion (Asahi Glass). Both ionomers consist of a

tetrafluoroethylene backbone with a sidechain containing a negative sulfonate end group that is responsible for ion mobility. The majority of follow-up research in this field is based these two commercial ionomers [101, 102]. Recent studies describe the influence of the ionomer sidechains [103] and the effects of softening and heating processes [104]. A second class of ionic electroactive polymers is conducting polymers. Their electromechanical response is based on the reversible insertion and expulsion of ions that occurs during redox cycling which induces a considerable volume change of the polymer. Frequently used conducting polymers are polyaniline, polypyrrole and polythiophenes [105, 106].

Besides using an electroactive polymer as matrix material, composites with electrochemical properties can be developed by adding functional fillers to a conventional matrix. These fillers range from inorganic metallic fibers to organic polymer particles. A common strategy is to enhance a matrix with semi-crystalline ferroelectric ceramic particles (0-3 composites) or fibers (1-3 composites) of which lead zirconate titanate (PZT) is the most frequently used example. These composites typically have a high electromechanical sensitivity, high pressure tolerance and good acoustical impedance [107]. Another strategy that increases the electromechanical performance of non-electroactive polymers is the addition of highly conductive fillers such as metal powders (e.g. aluminum and nickel) and carbon based materials which changes the composite resistivity value with several orders of magnitude [98]. Many recent studies describe the high potential of carbon nanotubes (CNTs), however, many problems will have to be overcome before they will be used in industrial applications [108]. Another recent study describes the combination of PZT and aluminum particles in an electromechanical epoxy based material [109].

Since both electromechanical polymers and self-healing polymers are able to regain a previously adapted form it seems a logical step to combine these two material functionalities into one material. However, the amount of studies that report on the regeneration of electromechanical properties after fracture is rather limited. Still, Soroushian et al. report on the piezo-driven self-healing of fiber reinforced polymer composites. Here, the mechanical energy that is released upon fracture is converted into electrical energy by the PVDF based matrix. Healing of the composite is then achieved by an electrochemical reaction at the fiber-matrix interface [110]. A second study, that shows self-healing of electrical (as mentioned in section 2.4.1) and electromechanical properties was performed by Tee et al. Their piezo resistive polymer composite with tactile pressure- and flexion bending sensitive properties can be used in electronic skin applications (Figure 2.7). The healing is based on

supramolecular hydrogen bonding with high healing efficiencies, whereas the piezo resistive behavior is generated by adding  $\mu\text{Ni}$  particles to the polymer matrix. This resulted in an almost full recovery of the composite functionality, however, the mechanical properties were not fully restored [91]. A final option that can be employed to prepare self-healing electromechanical composites could be through the use of ionomers. Since ionomers possess both electromechanical and self-healing properties, they are ideal candidates to serve as matrix material for multifunctional materials. Recently, James et al were the first to report a self-healing piezoelectric PZT-ionomer based polymer. They showed that the loss of sensorial functionality after high cyclic tensile fatigue can be partially recovered by thermal healing at  $70^\circ\text{C}$  [111].

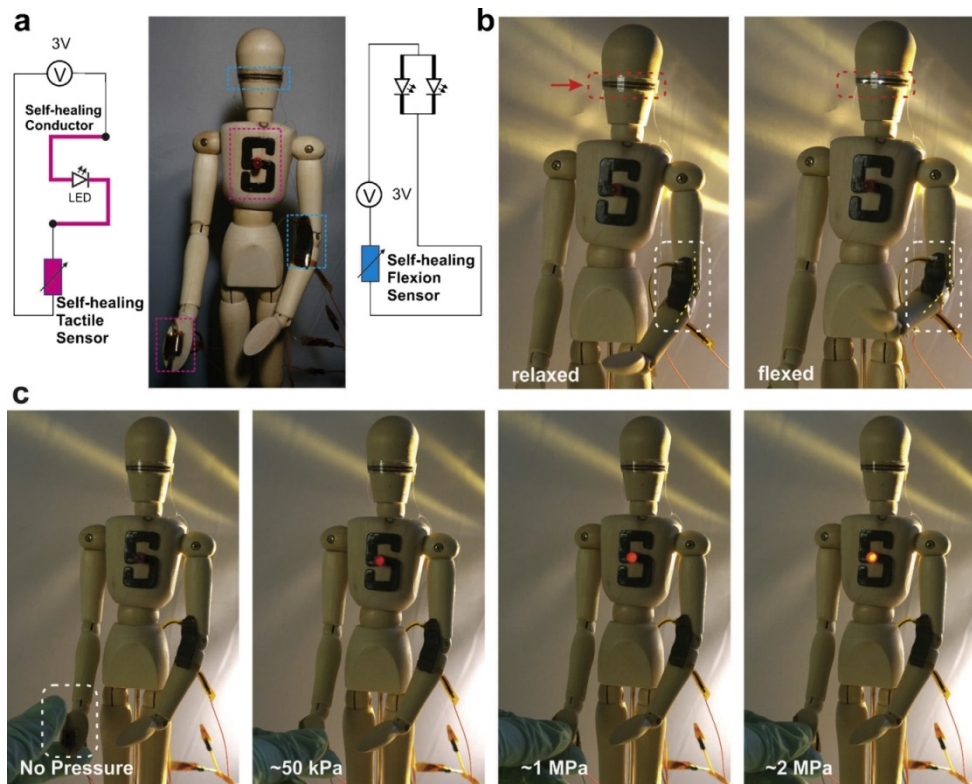


**Figure 2.7** Example of piezo resistive recovery in a fully articulated wooden mannequin. (a) A self-healing flexion and a self-healing tactile sensor were mounted on the elbow and palm of the mannequin respectively. LEDs in the eye and body region are used to transduce mechanical deformation into visible light. (b) shows the LED lights up with increasing elbow flexion. (c) shows LED lightening with increasing palm tactile pressure[91].

#### 2.4.4 Magnetic polymer composites

Magnetic polymer composites generally contain magnetic powders, such as  $\text{Fe}_3\text{O}_4$ ,  $\text{CoFe}_2\text{O}_4$ , strontium ferrite and nickel [112-115], whereas epoxies, polyurethanes and polyimides are often selected as matrix material [113, 116, 117]. Although they possess inferior magnetic properties compared to cast or sintered magnets, they have various advantages, such as a higher manufacturability and the possibility to produce complicated small and thin shapes with high precision. Therefore they are widely used for various applications, such as electronic and communications instruments, household tools and audio equipment [118]. Self-healing in magnetic polymer composites could be achieved by substituting conventional with intrinsically self-healing matrices, thereby creating more reliable and longer-lasting materials.

Magnetic gels are highly elastic hydrogels with magnetic fillers and they are an important group of magnetic polymer composites, which could greatly benefit from the self-healing effect. Controlled by the action of external magnetic fields, magnetic gels can perform elongation, contraction and coiling actions (as shown in Figure 2.8), which makes them suitable for actuator applications such as artificial muscles [119-121]. In these kinds of applications, the material will undergo significant deformation which may lead to unexpected failure. The mechanical damage can potentially be undone by introducing self-healing hydrogels, which are well developed [122-124], as polymer matrix in magnetic gels. This concept is exemplified by a study of Zhang et al.. They mixed  $\text{Fe}_3\text{O}_4$  nanoparticles into a chitosan solution and subsequently added synthetic telechelic difunctional polyethylene glycol into the ferrofluid. The result is that a magnetic self-healing hydrogel can be fabricated quickly and straightforward at room temperature within less than 2 minutes. The resulting composite is capable of regenerating itself after multiple complete fractures under the influence of an external magnetic field [125].

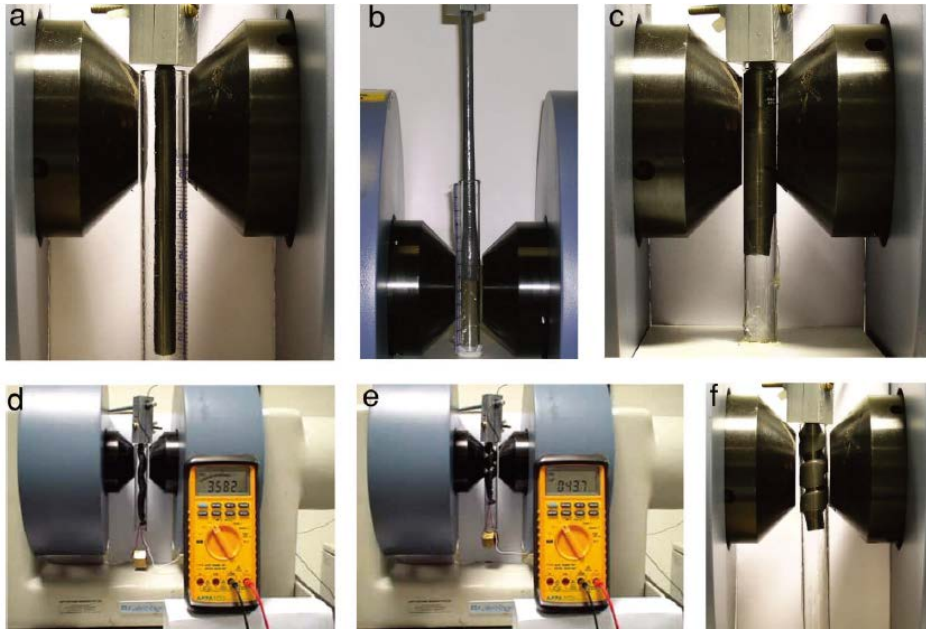


**Figure 2.8** Performance of magnetic gel (20 wt% Fe in silicone) controlled by external magnetic fields. (a) Relaxed mode without magnetic field; (b) elongation mode; (c) contraction mode; (d) and (e) coiling mode, the ohmmeter shows the resistance change of the sample during coiling process; (f) hybrid mode at  $B = 1T$ . [121]

### 2.4.5 Thermally conductive polymer composites

Thermally conductive polymer composites, consisting of a polymeric matrix and high thermally conductive fillers, such as carbon fibers, carbon nanotubes, aluminum oxide, zinc oxide, silicon carbide, boron nitride and metal powders, are widely used as thermal interface materials (TIMs), which play a key role in thermal management of the electronic industry [126-130].

Both modelling and experimental results indicate that the formation of thermally conductive chains leads to an increase in thermal conductivity of composites. For example, Devpura et al proposed a model on percolation phenomenon based thermal conductivity [131]. On the other hand, an experimental study by Hu et al. described the addition of carbon nanotubes into a silicone composite filled with spherical Nickel particles [132]. They found out that even small quantities of carbon nanotubes can effectively improve the heat conduction performance of the

composites by forming carbon nanotube–nickel sphere chains. Their work shows that a large increase in the thermal conductivity can be obtained by percolation phenomena, which is also justified in many recent studies [133-135]. Upon crack formation the thermally conductive chains can be cut off, which leads to a significant decrease in the thermal conductivity of the composite.

2

The adhesion at the interface between the polymer matrix and the fillers is essential to the thermal conductivity of composites. Many studies showed that the surface treatment with coupling agent can improve the matrix–filler interfacial adhesion, which increases the thermal conductivity of composites [136-138]. Thermal boundary resistance ( $R_b$ ) is a measure of an interface's resistance to thermal flow. Every et al. built a thermal conductivity model of spherical particle loaded composite material which took  $R_b$  into account, as shown in equation 2.5 [139],

$$(1 - V)^3 = \left(\frac{\lambda_m}{\lambda_c}\right)^{(1+2\alpha)/(1-\alpha)} \times \left[\frac{\lambda_c - \lambda_f(1 - \alpha)}{\lambda_m - \lambda_f(1 - \alpha)}\right]^{3/(1-\alpha)} \quad (2.5)$$

in which  $\lambda_c$ ,  $\lambda_m$  and  $\lambda_f$  are the thermal conductivity of composite material, matrix and filler, respectively,  $V$  is the volume fraction of filler,  $\alpha$  is a non-dimensional parameter with reference to the boundary resistance, which is defined by equation 2.6,

$$\alpha = \frac{2R_b\lambda_m}{d} \quad (2.6)$$

in which  $d$  is the diameter of filler. When  $\lambda_f \gg \lambda_m$ , equation 2.5 can be deduced to

$$\frac{\lambda_c}{\lambda_m} = \frac{1}{(1 - V)^{3(1-\alpha)/(1+2\alpha)}} \quad (2.7)$$

If crack formation occurs at the matrix–filler interface, the boundary resistance will increase significantly leading to a decrease of the composite's thermal conductivity, as shown schematically in Figure 2.9. As in its reference figure for mechanical stiffness (Figure 2.4), Figure 2.9 shows that upon full delamination the properties of the composite decrease with filler fraction and reach a value well below that of the matrix. Only for the case of perfect interface heat transfer, the properties of the

composite increase with the filler content to reach values that are substantially above that of the polymer matrix.

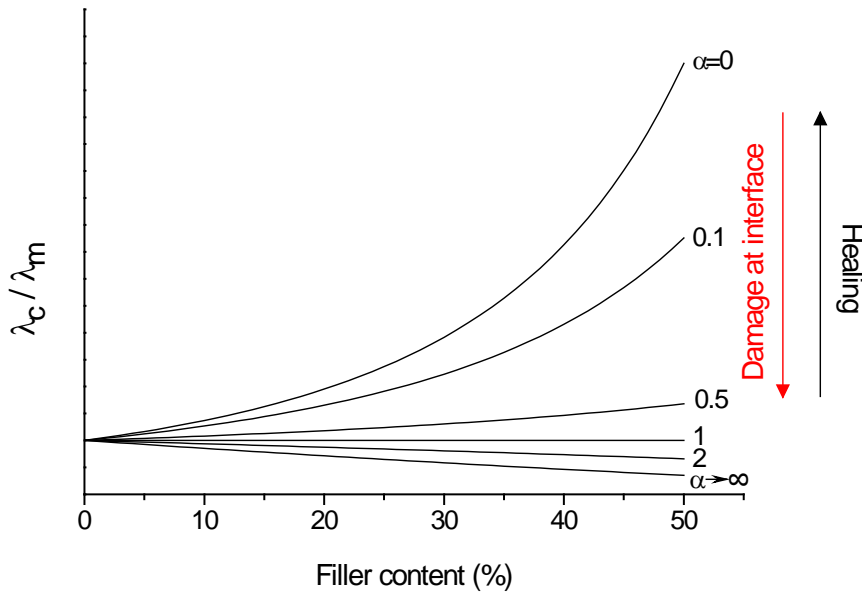


**Figure 2.9** Graphical representation of the relation between filler content, thermal boundary resistance and the thermal conductivity of spherical particle loaded composite material. The relation is plotted for various values of  $R_b$  resulting in values for  $\alpha$  ranging from 0 to  $\infty$  which directly shows the range of thermal conductivity that can be healed by restoring the filler-matrix interface.

Interfacial failure is a key failure mechanism in the use of Thermal Interface Materials (TIMs), which are composites designed to mechanically and thermally connect a heat source and component to minimize a potential temperature rise of the entire structure, hence TIMs and the components contacted to them usually have a mismatch in coefficient of thermal expansion (CTE) which leads to mechanical stress. After some thermal cycles, CTE mismatch may induce delamination between components and TIMs, which leads to an increase in thermal contact resistance and subsequent failure of the whole device [140-142].



In general, the functionality of TIMs will be damaged in three ways: cracks cutting off the thermally conductive chains, cracks separating matrix and fillers and delamination between components and TIMs. To introduce cohesive and adhesive self-healing ability to TIMs could be an effective way to solve this problem. Although much work has been done on both self-healing polymers and TIMs, only a few attempts have been made to fabricate self-healing TIMs. Lafont et al. prepared TIMs consisting of boron nitride or graphite particles and two types of self-healing polysulphide-based thermoset matrices [143]. The composites exhibit recovery of both cohesion and adhesion properties under a mild healing temperature (65°C). After multiple healing cycles, most of the samples show full recovery of initial adhesive strength. On the other hand, the samples behave differently on cohesion recovery: 20-100% recovery can be achieved depending on filler concentration, filler type and matrix type.

## 2.5 Conclusion

This review gives the first overview on the emerging field of self-healing behavior of composite materials. In polymer based composite materials, the damages in the matrix or at the matrix-filler interface lead to the loss of both structural and functional properties. By applying intrinsic self-healing polymer as matrix, those damages can be healed upon the stimulation of an external stimulus and subsequently both structural and functional properties can be partially or even fully restored.

As described, the majority of recent studies regarding self-healing composite materials focus on the restoration of structural properties, such as stiffness and strength. Research into the self-healing of functional properties (electrical, electromagnetic, electromechanical, magnetic and thermal conductive) is still in its early stage development. However, as the demand for functional polymer composites is increasing, it is expected that the focus of researchers will broaden to the development of materials that are capable of healing both structural and functional properties in the upcoming years.

## References

1. Gibson RF. A review of recent research on mechanics of multifunctional composite materials and structures. *Composite Structures*. 2010;92(12):2793-2810.
2. Chung DDL. *Composite Materials*. 2nd ed: Springer London; 2010.
3. Eadie L, Ghosh TK. Biomimicry in textiles: Past, present and potential. An overview. *Journal of the Royal Society Interface*. 2011;8(59):761-775.
4. Olszta MJ, Cheng X, Jee SS, Kumar R, Kim YY, Kaufman MJ, et al. Bone structure and formation: A new perspective. *Materials Science and Engineering R: Reports*. 2007;58(3-5):77-116.
5. Van Der Zwaag S. An Introduction to Material Design Principles: Damage Prevention versus Damage Management. In: Van Der Zwaag S, editor. *Self-Healing Materials an Alternative Approach to 20 Centuries of Materials Science* 2007.
6. Van Der Zwaag S, Grande AM, Post W, Garcia SJ, Bor TC. A review of current strategies to induce self-healing behaviour in fibre reinforced polymer based composites. *Materials Science and Technology*. 2014.
7. Dry C. Procedures developed for self-repair of polymer matrix composite materials. *Composite Structures*. 1996;35(3):263-269.
8. Dry CM, Sottos NR, editors. *Passive smart self-repair in polymer matrix composite materials* 1993.
9. White SR, Sottos NR, Geubelle PH, Moore JS, Kessler MR, Sriram SR, et al. Autonomic healing of polymer composites. *Nature*. 2001;409(6822):794-797.
10. Pang JWC, Bond IP. A hollow fibre reinforced polymer composite encompassing self-healing and enhanced damage visibility. *Composites Science and Technology*. 2005;65(11-12):1791-1799.
11. Billiet S, Hillewaere XKD, Teixeira RFA, Du Prez FE. Chemistry of crosslinking processes for self-healing polymers. *Macromolecular Rapid Communications*. 2013;34(4):290-309.
12. Garcia SJ. Effect of polymer architecture on the intrinsic self-healing character of polymers. *European Polymer Journal*. 2014;53(0):118-125.
13. Zhang Y, Broekhuis AA, Picchioni F. Thermally Self-Healing Polymeric Materials: The Next Step to Recycling Thermoset Polymers? *Macromolecules*. 2009;42(6):1906-1912.
14. Kavitha AA, Singha NK. "Click Chemistry" in Tailor-Made Polymethacrylates Bearing Reactive Furfuryl Functionality: A New Class of Self-Healing Polymeric Material. *ACS Applied Materials & Interfaces*. 2009;1(7):1427-1436.
15. Canary SA, Stevens MP. Thermally reversible crosslinking of polystyrene via the furan-maleimide Diels-Alder reaction. *Journal of Polymer Science Part A: Polymer Chemistry*. 1992;30(8):1755-1760.
16. Liu Y-L, Hsieh C-Y, Chen Y-W. Thermally reversible cross-linked polyamides and thermo-responsive gels by means of Diels-Alder reaction. *Polymer*. 2006;47(8):2581-2586.
17. Magana S, Zerroukhi A, Jegat C, Mignard N. Thermally reversible crosslinked polyethylene using Diels-Alder reaction in molten state. *Reactive and Functional Polymers*. 2010;70(7):442-448.

18. Tian Q, Rong MZ, Zhang MQ, Yuan YC. Synthesis and characterization of epoxy with improved thermal remendability based on Diels-Alder reaction. *Polymer International*. 2010;59(10):1339-1345.
19. Bai N, Saito K, Simon GP. Synthesis of a diamine cross-linker containing Diels-Alder adducts to produce self-healing thermosetting epoxy polymer from a widely used epoxy monomer. *Polymer Chemistry*. 2013;4(3):724-730.
20. Pratama PA, Peterson AM, Palmese GR. The role of maleimide structure in the healing of furan-functionalized epoxy-amine thermosets. *Polymer Chemistry*. 2013;4(18):5000-5006.
21. Du P, Liu X, Zheng Z, Wang X, Joncheray T, Zhang Y. Synthesis and characterization of linear self-healing polyurethane based on thermally reversible Diels-Alder reaction. *RSC Advances*. 2013;3(35):15475-15482.
22. Zhang MQ, Rong MZ. Intrinsic self-healing of covalent polymers through bond reconnection towards strength restoration. *Polymer Chemistry*. 2013;4(18):4878-4884.
23. Peterson AM, Jensen RE, Palmese GR. Thermoreversible and remendable glass-polymer interface for fiber-reinforced composites. *Composites Science and Technology*. 2011;71(5):586-592.
24. Canadell J, Goossens H, Klumperman B. Self-healing materials based on disulfide links. *Macromolecules*. 2011;44(8):2536-2541.
25. Pepels M, Filot I, Klumperman B, Goossens H. Self-healing systems based on disulfide-thiol exchange reactions. *Polymer Chemistry*. 2013;4(18):4955-4965.
26. Higaki Y, Otsuka H, Takahara A. A Thermodynamic Polymer Cross-Linking System Based on Radically Exchangeable Covalent Bonds. *Macromolecules*. 2006;39(6):2121-2125.
27. Otsuka H, Aotani K, Higaki Y, Amamoto Y, Takahara A. Thermal Reorganization and Molecular Weight Control of Dynamic Covalent Polymers Containing Alkoxyamines in Their Main Chains. *Macromolecules*. 2007;40(5):1429-1434.
28. Yuan Ce, Rong MZ, Zhang MQ, Zhang ZP, Yuan YC. Self-Healing of Polymers via Synchronous Covalent Bond Fission/Radical Recombination. *Chemistry of Materials*. 2011;23(22):5076-5081.
29. Sijbesma RP, Beijer FH, Brunsveld L, Folmer BJB, Hirschberg JHKK, Lange RFM, et al. Reversible Polymers Formed from Self-Complementary Monomers Using Quadruple Hydrogen Bonding. *Science*. 1997;278(5343):1601-1604.
30. Park T, Zimmerman SC, Nakashima S. A Highly Stable Quadruply Hydrogen-Bonded Heterocomplex Useful for Supramolecular Polymer Blends. *Journal of the American Chemical Society*. 2005;127(18):6520-6521.
31. Cordier P, Tournilhac F, Soulie-Ziakovic C, Leibler L. Self-healing and thermoreversible rubber from supramolecular assembly. *Nature*. 2008;451(7181):977-980.
32. Montarnal D, Tournilhac F, Hidalgo M, Leibler L. Epoxy-based networks combining chemical and supramolecular hydrogen-bonding crosslinks. *Journal of Polymer Science Part A: Polymer Chemistry*. 2010;48(5):1133-1141.
33. Colquhoun HM. Self-repairing polymers: Materials that heal themselves. *Nat Chem*. 2012;4(6):435-436.

34. Li G, Wie JJ, Nguyen NA, Chung WJ, Kim ET, Char K, et al. Synthesis, self-assembly and reversible healing of supramolecular perfluoropolyethers. *Journal of Polymer Science Part A: Polymer Chemistry*. 2013;51(17):3598-3606.
35. Zhang A, Yang L, Lin Y, Yan L, Lu H, Wang L. Self-healing supramolecular elastomers based on the multi-hydrogen bonding of low-molecular polydimethylsiloxanes: Synthesis and characterization. *Journal of Applied Polymer Science*. 2013;129(5):2435-2442.
36. Greenland BW, Burattini S, Hayes W, Colquhoun HM. Design, synthesis and computational modelling of aromatic tweezer-molecules as models for chain-folding polymer blends. *Tetrahedron*. 2008;64(36):8346-8354.
37. Burattini S, Colquhoun HM, Greenland BW, Hayes W. A novel self-healing supramolecular polymer system. *Faraday Discussions*. 2009;143:251-264.
38. Burattini S, Greenland BW, Merino DH, Weng W, Seppala J, Colquhoun HM, et al. A Healable Supramolecular Polymer Blend Based on Aromatic  $\pi$ - $\pi$  Stacking and Hydrogen-Bonding Interactions. *Journal of the American Chemical Society*. 2010;132(34):12051-12058.
39. Kalista Jr SJ, Ward TC. Thermal characteristics of the self-healing response in poly(ethylene-co-methacrylic acid) copolymers. *Journal of the Royal Society Interface*. 2007;4(13):405-411.
40. Kalista Jr SJ, Ward TC, Oyetunji Z. Self-healing of poly(ethylene-co-methacrylic acid) copolymers following projectile puncture. *Mechanics of Advanced Materials and Structures*. 2007;14(5):391-397.
41. Varley RJ, Shen S, van der Zwaag S. The effect of cluster plasticisation on the self healing behaviour of ionomers. *Polymer*. 2010;51(3):679-686.
42. Varley RJ, van der Zwaag S. Autonomous damage initiated healing in a thermo-responsive ionomer. *Polymer International*. 2010;59(8):1031-1038.
43. Varley RJ, van der Zwaag S. Towards an understanding of thermally activated self-healing of an ionomer system during ballistic penetration. *Acta Materialia*. 2008;56(19):5737-5750.
44. Varley RJ, Van der Zwaag S. Development of a quasi-static test method to investigate the origin of self-healing in ionomers under ballistic conditions. *Polymer Testing*. 2008;27(1):11-19.
45. Chung C-M, Roh Y-S, Cho S-Y, Kim J-G. Crack Healing in Polymeric Materials via Photochemical [2+2] Cycloaddition. *Chemistry of Materials*. 2004;16(21):3982-3984.
46. Oya N, Sukarsaatmadja P, Ishida K, Yoshie N. Photoinduced mendable network polymer from poly(butylene adipate) end-functionalized with cinnamoyl groups. *Polym J*. 2012;44(7):724-729.
47. Ling J, Rong MZ, Zhang MQ. Coumarin imparts repeated photochemical remendability to polyurethane. *Journal of Materials Chemistry*. 2011;21(45):18373-18380.
48. Ghosh B, Urban MW. Self-Repairing Oxetane-Substituted Chitosan Polyurethane Networks. *Science*. 2009;323(5920):1458-1460.
49. Amamoto Y, Kamada J, Otsuka H, Takahara A, Matyjaszewski K. Repeatable Photoinduced Self-Healing of Covalently Cross-Linked Polymers through Reshuffling of Trithiocarbonate Units. *Angewandte Chemie*. 2011;123(7):1698-1701.

50. Amamoto Y, Otsuka H, Takahara A, Matyjaszewski K. Self-healing of covalently cross-linked polymers by reshuffling thiuram disulfide moieties in air under visible light. *Advanced Materials*. 2012;24(29):3975-3980.
51. Burnworth M, Tang L, Kumpfer JR, Duncan AJ, Beyer FL, Fiore GL, et al. Optically healable supramolecular polymers. *Nature*. 2011;472(7343):334-337.
52. Chuo T-W, Wei T-C, Liu Y-L. Electrically driven self-healing polymers based on reversible guest-host complexation of  $\beta$ -cyclodextrin and ferrocene. *Journal of Polymer Science Part A: Polymer Chemistry*. 2013;51(16):3395-3403.
53. Zhang Z, Hu Y, Liu Z, Guo T. Synthesis and evaluation of a moisture-promoted healing copolymer. *Polymer*. 2012;53(14):2979-2990.
54. Fu SY, Feng XQ, Lauke B, Mai YW. Effects of particle size, particle/matrix interface adhesion and particle loading on mechanical properties of particulate-polymer composites. *Composites Part B: Engineering*. 2008;39(6):933-961.
55. Ku H, Wang H, Pattarachaiyakop N, Trada M. A review on the tensile properties of natural fiber reinforced polymer composites. *Composites Part B: Engineering*. 2011;42(4):856-873.
56. Dekkers MEJ, Heikens D. The effect of interfacial adhesion on the tensile behavior of polystyrene-glass-bead composites. *Journal of Applied Polymer Science*. 1983;28(12):3809-3815.
57. Mishra S, Sonawane SH, Singh RP. Studies on characterization of nano CaCO<sub>3</sub> prepared by the in situ deposition technique and its application in PP-nano CaCO<sub>3</sub> composites. *Journal of Polymer Science, Part B: Polymer Physics*. 2005;43(1):107-113.
58. Spanoudakis J, Young RJ. Crack propagation in a glass particle-filled epoxy resin - Part 1 Effect of particle volume fraction and size. *Journal of Materials Science*. 1984;19(2):473-486.
59. Wang K, Wu J, Ye L, Zeng H. Mechanical properties and toughening mechanisms of polypropylene/barium sulfate composites. *Composites Part A: Applied Science and Manufacturing*. 2003;34(12):1199-1205.
60. Zhu ZK, Yang Y, Yin J, Qi ZN. Preparation and properties of organosoluble polyimide silica hybrid materials by sol-gel process. *Journal of Applied Polymer Science*. 1999;73(14):2977-2984.
61. Wang Z, Ciselli P, Peijs T. The extraordinary reinforcing efficiency of single-walled carbon nanotubes in oriented poly(vinyl alcohol) tapes. *Nanotechnology*. 2007;18(45).
62. Nogueira CL, De Paiva JMF, Rezende MC. Effect of the interfacial adhesion on the tensile and impact properties of carbon fiber reinforced polypropylene matrices. *Materials Research*. 2005;8(1):81-89.
63. Shazed MA, Suraya AR, Rahmanian S, Mohd Salleh MA. Effect of fibre coating and geometry on the tensile properties of hybrid carbon nanotube coated carbon fibre reinforced composite. *Materials & Design*. 2014;54(0):660-669.
64. Thomason JL. The influence of fibre length, diameter and concentration on the modulus of glass fibre reinforced polyamide 6,6. *Composites Part A: Applied Science and Manufacturing*. 2008;39(11):1732-1738.
65. Agarwal BD, Broutman LJ, Chandrashekhara K. *Analysis And Performance Of Fiber Composites*. Third Edition ed: John Wiley & Sons; 2006.

66. Yoshie N, Saito S, Oya N. A thermally-stable self-mending polymer networked by Diels-Alder cycloaddition. *Polymer*. 2011;52(26):6074-6079.
67. Zako M, Takano N. Intelligent material systems using epoxy particles to repair microcracks and delamination damage in GFRP. *Journal of Intelligent Material Systems and Structures*. 2000;10(10):836-841.
68. Nakamura Y, Yamaguchi M, Okubo M, Matsumoto T. Effects of particle size on mechanical and impact properties of epoxy resin filled with spherical silica. *Journal of Applied Polymer Science*. 1992;45(7):1281-1289.
69. Rong MZ, Zhang MQ, Pan SL, Lehmann B, Friedrich K. Analysis of the interfacial interactions in polypropylene/silica nanocomposites. *Polymer International*. 2004;53(2):176-183.
70. Wu CL, Zhang MQ, Rong MZ, Friedrich K. Silica nanoparticles filled polypropylene: Effects of particle surface treatment, matrix ductility and particle species on mechanical performance of the composites. *Composites Science and Technology*. 2005;65(3-4):635-645.
71. Soutis C. Fibre reinforced composites in aircraft construction. *Progress in Aerospace Sciences*. 2005;41(2):143-151.
72. Peterson AM, Jensen RE, Palmese GR. Reversibly cross-linked polymer gels as healing agents for epoxy-amine thermosets. *ACS Applied Materials and Interfaces*. 2009;1(5):992-995.
73. Lafont U, Van Zeijl H, Van Der Zwaag S. Influence of cross-linkers on the cohesive and adhesive self-healing ability of polysulfide-based thermosets. *ACS Applied Materials and Interfaces*. 2012;4(11):6280-6288.
74. Ling J, Rong MZ, Zhang MQ. Photo-stimulated self-healing polyurethane containing dihydroxyl coumarin derivatives. *Polymer (United Kingdom)*. 2012;53(13):2691-2698.
75. Hayes SA, Jones FR, Marshiya K, Zhang W. A self-healing thermosetting composite material. *Composites Part A: Applied Science and Manufacturing*. 2007;38(4):1116-1120.
76. Luo X, Ou R, Eberly DE, Singhal A, Viratyaporn W, Mather PT. A thermoplastic/thermoset blend exhibiting thermal mending and reversible adhesion. *ACS Applied Materials and Interfaces*. 2009;1(3):612-620.
77. Sandler JKW, Kirk JE, Kinloch IA, Shaffer MSP, Windle AH. Ultra-low electrical percolation threshold in carbon-nanotube-epoxy composites. *Polymer*. 2003;44(19):5893-5899.
78. Gojny FH, Wichmann MH, Fiedler B, Kinloch IA, Bauhofer W, Windle AH, et al. Evaluation and identification of electrical and thermal conduction mechanisms in carbon nanotube/epoxy composites. *Polymer*. 2006;47(6):2036-2045.
79. Gubbels F, Blacher S, Vanlathem E, Jérôme R, Deltour R, Brouers F, et al. Design of electrical composites: determining the role of the morphology on the electrical properties of carbon black filled polymer blends. *Macromolecules*. 1995;28(5):1559-1566.
80. Zheng W, Wong S-C. Electrical conductivity and dielectric properties of PMMA/expanded graphite composites. *Composites Science and Technology*. 2003;63(2):225-235.

81. Sengupta R, Bhattacharya M, Bandyopadhyay S, Bhowmick AK. A review on the mechanical and electrical properties of graphite and modified graphite reinforced polymer composites. *Progress in Polymer Science*. 2011;36(5):638-670.
82. Feller JF, Linossier I, Grohens Y. Conductive polymer composites: comparative study of poly(ester)-short carbon fibres and poly(epoxy)-short carbon fibres mechanical and electrical properties. *Materials Letters*. 2002;57(1):64-71.
83. Choi MH, Jeon BH, Chung IJ. The effect of coupling agent on electrical and mechanical properties of carbon fiber/phenolic resin composites. *Polymer*. 2000;41(9):3243-3252.
84. Kim WJ, Taya M, Nguyen MN. Electrical and thermal conductivities of a silver flake/thermosetting polymer matrix composite. *Mechanics of Materials*. 2009;41(10):1116-1124.
85. Stauffer D, Aharony A. *Introduction to percolation theory*: CRC press; 1994.
86. Bilotti E, Zhang H, Deng H, Zhang R, Fu Q, Peijs T. Controlling the dynamic percolation of carbon nanotube based conductive polymer composites by addition of secondary nanofillers: The effect on electrical conductivity and tuneable sensing behaviour. *Composites Science and Technology*. 2013;74(0):85-90.
87. Calberg C, Blacher S, Gubbels F, Brouers F, Deltour R, Jérôme R. Electrical and dielectric properties of carbon black filled co-continuous two-phase polymer blends. *Journal of Physics D: Applied Physics*. 1999;32(13):1517.
88. Thongruang W, Spontak RJ, Balik CM. Bridged double percolation in conductive polymer composites: an electrical conductivity, morphology and mechanical property study. *Polymer*. 2002;43(13):3717-3725.
89. Kitajima S, Matsuda M, Yamato M, Tominaga Y. Anisotropic ionic conduction in composite polymer electrolytes filled with clays oriented by a strong magnetic field. *Polym J*. 2013;45(7):738-743.
90. Li Y, Chen S, Wu M, Sun J. Polyelectrolyte Multilayers Impart Healability to Highly Electrically Conductive Films. *Advanced Materials*. 2012;24(33):4578-4582.
91. Tee BCK, Wang C, Allen R, Bao Z. An electrically and mechanically self-healing composite with pressure- and flexion-sensitive properties for electronic skin applications. *Nat Nano*. 2012;7(12):825-832.
92. Palleau E, Reece S, Desai SC, Smith ME, Dickey MD. Self-Healing Stretchable Wires for Reconfigurable Circuit Wiring and 3D Microfluidics. *Advanced Materials*. 2013;25(11):1589-1592.
93. Wang C, Wu H, Chen Z, McDowell MT, Cui Y, Bao Z. Self-healing chemistry enables the stable operation of silicon microparticle anodes for high-energy lithium-ion batteries. *Nat Chem*. 2013;5(12):1042-1048.
94. Simon RM. EMI shielding through conductive plastics. *Polymer-Plastics Technology and Engineering*. 1981;17(1):1-10.
95. Bar-Cohen Y. Electroactive polymers as artificial muscles: A review. *Journal of Spacecraft and Rockets*. 2002;39(6):822-827.
96. Bar-Cohen Y, Zhang Q. Electroactive Polymer Actuators and Sensors. *MRS Bulletin*. 2008;33(03):173-181.
97. Martins P, Lopes AC, Lanceros-Mendez S. Electroactive phases of poly(vinylidene fluoride): Determination, processing and applications. *Progress in Polymer Science*. 2013.

98. Vinogradov AM, editor Accomplishments and future trends in the field of electroactive polymers 2008.
99. Pelrine R, Kornbluh R, Kofod G. High-strain actuator materials based on dielectric elastomers. *Advanced Materials*. 2000;12(16):1223-1225.
100. Pelrine R, Kornbluh R, Pei Q, Joseph J. High-speed electrically actuated elastomers with strain greater than 100%. *Science*. 2000;287(5454):836-839.
101. Akle BJ, Leo DJ, Hickner MA, McGrath JE. Correlation of capacitance and actuation in ionomeric polymer transducers. *Journal of Materials Science*. 2005;40(14):3715-3724.
102. Tiwari R, Garcia E. The state of understanding of ionic polymer metal composite architecture: A review. *Smart Materials and Structures*. 2011;20(8).
103. Liu Y, Ghaffari M, Zhao R, Lin JH, Lin M, Zhang QM. Enhanced electromechanical response of ionic polymer actuators by improving mechanical coupling between ions and polymer matrix. *Macromolecules*. 2012;45(12):5128-5133.
104. Akle BJ, Leo DJ. Softening and heating effects in ionic polymer transducers: An experimental investigation. *Journal of Intelligent Material Systems and Structures*. 2013;24(10):1266-1277.
105. Bhadra S, Khastgir D, Singha NK, Lee JH. Progress in preparation, processing and applications of polyaniline. *Progress in Polymer Science (Oxford)*. 2009;34(8):783-810.
106. Barisci JN, Lewis TW, Spinks GM, Too CO, Wallace GG. Conducting polymers as a basis for responsive materials systems. *Journal of Intelligent Material Systems and Structures*. 1999;9(9):723-731.
107. Tressler JF, Alkoy S, Newnham RE. Piezoelectric sensors and sensor materials. *Journal of Electroceramics*. 1998;2(4):257-272.
108. McClory C, Chin SJ, McNally T. Polymer/carbon nanotube composites. *Australian Journal of Chemistry*. 2009;62(8):762-785.
109. Banerjee S, Cook-Chennault KA. An investigation into the influence of electrically conductive particle size on electromechanical coupling and effective dielectric strain coefficients in three phase composite piezoelectric polymers. *Composites Part A: Applied Science and Manufacturing*. 2012;43(9):1612-1619.
110. Soroushian P, Nassar RUD, Balachandra AM. Piezo-driven self-healing by electrochemical phenomena. *Journal of Intelligent Material Systems and Structures*. 2013;24(4):441-453.
111. James NK, Lafont U, Van Der Zwaag S, Groen WA. Piezoelectric and mechanical properties of fatigue resistant, self healing PZT-ionomer composites. *Smart Materials and Structures*. 2014.
112. Ahmad H, Kumar K, Rahman MA, Rahman MM, Miah MAJ, Minami H, et al. Preparation and characterization of conducting polyaniline layered magnetic nano composite polymer particles. *Polymers for Advanced Technologies*. 2013;24(8):740-746.
113. Lagorce LK, Allen MG. Magnetic and mechanical properties of micromachined strontium ferrite/polyimide composites. *Microelectromechanical Systems, Journal of*. 1997;6(4):307-312.
114. Munoz Resta I, Horwitz G, Mendez Elizalde ML, Jorge GA, Molina FV, Soledad Antonel P. Magnetic and Conducting Properties of Composites of Conducting



Polymers and Ferrite Nanoparticles. *Magnetics*, IEEE Transactions on. 2013;49(8):4598-4601.

115. Song P, Peng Z, Yue Y, Zhang H, Zhang Z, Fan Y. Mechanical properties of silicone composites reinforced with micron-and nano-sized magnetic particles. *EXPRESS POLYMER LETTERS*. 2013;7(6):546-553.

116. Ramajo LA, Cristóbal AA, Botta PM, Porto López JM, Reboredo MM, Castro MS. Dielectric and magnetic response of Fe<sub>3</sub>O<sub>4</sub>/epoxy composites. *Composites Part A: Applied Science and Manufacturing*. 2009;40(4):388-393.

117. Senthur Pandi R, Chokkalingam R, Mahendran M. Thermal and Magnetic studies of Ni-Mn-Ga/PU Polymer Composites. *Indian J Phys*. 2012;86(9):787-790.

118. Gokturk HS, Fiske TJ, Kalyon DM. Electric and magnetic properties of a thermoplastic elastomer incorporated with ferromagnetic powders. *Magnetics*, IEEE Transactions on. 1993;29(6):4170-4176.

119. Szabó D, Zrínyi M. MUSCULAR CONTRACTION MIMICED BY MAGNETIC GELS. *International Journal of Modern Physics B*. 2001;15(06n07):557-563.

120. Nguyen VQ, Ramanujan RV. Novel Coiling Behavior in Magnet-Polymer Composites. *Macromolecular Chemistry and Physics*. 2010;211(6):618-626.

121. Nguyen VQ, Ahmed AS, Ramanujan RV. Morphing Soft Magnetic Composites. *Advanced Materials*. 2012;24(30):4041-4054.

122. Xu K, An H, Lu C, Tan Y, Li P, Wang P. Facile fabrication method of hydrophobic-associating cross-linking hydrogel with outstanding mechanical performance and self-healing property in the absence of surfactants. *Polymer*. 2013;54(21):5665-5672.

123. Kakuta T, Takashima Y, Nakahata M, Otsubo M, Yamaguchi H, Harada A. Preorganized Hydrogel: Self-Healing Properties of Supramolecular Hydrogels Formed by Polymerization of Host-Guest-Monomers that Contain Cyclodextrins and Hydrophobic Guest Groups. *Advanced Materials*. 2013;25(20):2849-2853.

124. Hao X, Liu H, Xie Y, Fang C, Yang H. Thermal-responsive self-healing hydrogel based on hydrophobically modified chitosan and vesicle. *Colloid Polym Sci*. 2013;291(7):1749-1758.

125. Zhang Y, Yang B, Zhang X, Xu L, Tao L, Li S, et al. A magnetic self-healing hydrogel. *Chemical Communications*. 2012;48(74):9305-9307.

126. Sim LC, Ramanan SR, Ismail H, Seetharamu KN, Goh TJ. Thermal characterization of Al<sub>2</sub>O<sub>3</sub> and ZnO reinforced silicone rubber as thermal pads for heat dissipation purposes. *Thermochimica Acta*. 2005;430(1-2):155-165.

127. Nakamura A, Iji M. Factors affecting the magnitudes and anisotropies of the thermal and electrical conductivities of poly(l-lactic) acid composites with carbon fibers of various sizes. *Journal of Materials Science*. 2011;46(3):747-751.

128. Fu S, Song P, Yang H, Jin Y, Lu F, Ye J, et al. Effects of carbon nanotubes and its functionalization on the thermal and flammability properties of polypropylene/wood flour composites. *Journal of Materials Science*. 2010;45(13):3520-3528.

129. Wattanakul K, Manuspiya H, Yanumet N. Thermal conductivity and mechanical properties of BN-filled epoxy composite: effects of filler content, mixing conditions, and BN agglomerate size. *Journal of Composite Materials*. 2011;45(19):1967-1980.

130. Ren F, Ren P-g, Di Y-y, Chen D-m, Liu G-g. Thermal, Mechanical and Electrical Properties of Linear Low-Density Polyethylene Composites Filled with Different Dimensional SiC Particles. *Polymer-Plastics Technology and Engineering*. 2011;50(8):791-796.
131. Devpura A, Phelan PE, Prasher RS, editors. Percolation theory applied to the analysis of thermal interface materials in flip-chip technology. *Thermal and Thermomechanical Phenomena in Electronic Systems, 2000 ITherm 2000 The Seventh Intersociety Conference on*; 2000 2000.
132. Xuejiao H, Linan J, Goodson KE, editors. Thermal conductance enhancement of particle-filled thermal interface materials using carbon nanotube inclusions. *Thermal and Thermomechanical Phenomena in Electronic Systems, 2004 ITherm '04 The Ninth Intersociety Conference on*; 2004 1-4 June 2004.
133. Kim B-W, Park S-H, Kapadia RS, Bandaru PR. Evidence of percolation related power law behavior in the thermal conductivity of nanotube/polymer composites. *Applied Physics Letters*. 2013;102(24):243105.
134. Kwon SY, Kwon IM, Kim Y-G, Lee S, Seo Y-S. A large increase in the thermal conductivity of carbon nanotube/polymer composites produced by percolation phenomena. *Carbon*. 2013;55(0):285-290.
135. Wang B, Hao J, Li H. Remarkable improvements in the stability and thermal conductivity of graphite/ethylene glycol nanofluids caused by a graphene oxide percolation structure. *Dalton Transactions*. 2013;42(16):5866-5873.
136. Zhou W. Effect of coupling agents on the thermal conductivity of aluminum particle/epoxy resin composites. *Journal of Materials Science*. 2011;46(11):3883-3889.
137. Zengbin W, Iizuka T, Kozako M, Ohki Y, Tanaka T. Development of epoxy/BN composites with high thermal conductivity and sufficient dielectric breakdown strength part I - sample preparations and thermal conductivity. *Dielectrics and Electrical Insulation, IEEE Transactions on*. 2011;18(6):1963-1972.
138. Zhang M, Gu A, Liang G, Yuan L. Preparation of high thermal conductive aluminum nitride/cyanate ester nanocomposite using a new macromolecular coupling agent. *Polymers for Advanced Technologies*. 2012;23(11):1503-1510.
139. Every AG, Tzou Y, Hasselman DPH, Raj R. The effect of particle size on the thermal conductivity of ZnS/diamond composites. *Acta Metallurgica et Materialia*. 1992;40(1):123-129.
140. Chou T-L, Huang C-F, Han C-N, Yang S-Y, Chiang K-N. Fabrication process simulation and reliability improvement of high-brightness LEDs. *Microelectronics Reliability*. 2009;49(9-11):1244-1249.
141. Longzao Z, Bing A, Yiping W, Shunhong L, editors. Analysis of delamination and darkening in high power LED packaging. *Physical and Failure Analysis of Integrated Circuits, 2009 IPFA 2009 16th IEEE International Symposium on the*; 2009 6-10 July 2009.
142. Lu G, Yang S, Huang Y, editors. Analysis on failure modes and mechanisms of LED. *Reliability, Maintainability and Safety, 2009 ICRMS 2009 8th International Conference on*; 2009: IEEE.
143. Lafont U, Moreno-Belle C, van Zeijl H, van der Zwaag S. Self-healing thermally conductive adhesives. *Journal of Intelligent Material Systems and Structures*. 2014;25(1):67-74.



# Chapter 3

---

**Numerical simulation of the thermal conductivity and mechanical properties of thermal interface materials with micro- or macro- damages**

---

### 3.1 Introduction

Thermal interface materials (TIMs) are widely used in all kinds of electronic devices to enable heat dissipation and mechanical anchoring of components thus increasing the reliability and service lifetime of electronic devices. Most TIMs are polymer based composites loaded with thermally conductive filler particles. Many experimental [1-4] and theoretical [5-9] investigations have been made to determine the effect of filler content, filler size, filler geometry and interfacial thermal resistance on the total thermal conductivity of the composites. Amongst all filler parameters influencing the thermal conductivity of composites, apart from the actual material properties of the constituent phases, the filler fraction is the most important one [10-12]. The filler orientation also plays an important role in the thermal conductivity of composites provided the fillers have a high aspect ratio. Feliciani et al. conducted a FEM simulation on thermal conductivity of fiber-reinforced thermoplastics injection molded parts. The simulation result shows good agreement with experimental data[13]. Moreover FEM has been successfully applied in predicting the thermal conductivity of porous materials [14-17] taking into account the actual internal geometry in the sample. Interfacial thermal resistance, which was first introduced by Kapitza[18], has a significant effect on the effective thermal conductivity of composites. Numerical studies taking interfacial thermal resistance into account predict that composites with a bigger particle size generally have a higher thermal conductivity than those with smaller particles, all other parameters being the same [19-21]. However Veyret et al. showed that in fibrous composites larger fiber diameters will slightly decrease the thermal conductivity of the material. This effect can be explained that at a constant volume concentration the increase in diameter implies fewer fibers, therefore less contact between them[22].

Most studies on TIMs performance reported in literature focus on the performance of perfect and freshly made samples. However, in reality the thermal properties of TIMs will decay with time during isothermal or cyclic thermal loading [23, 24]. Sun et al. [24] suggested that the debonding of filler-matrix interfaces due to the mismatch in coefficient of thermal expansion may be the reason of increase of thermal resistance. However, there are only a few computational studies on the effect of debonding on the thermal conductivity of composites. Tang et al. proposed a two-dimensional model and investigated the effect of mechanical loading on the thermal conductivity of concrete, which can be regarded as a composite of mortar and stones. The simulation showed that the decrease of the thermal conductivity of concrete specimen as a result of crack formation during uniaxial compression could

reach 24% [25]. Shen et al. improved Tang's model and showed that the thermal conductivity parallel to the crack decreased much less than that perpendicular to the crack[26]. However there are many damage parameters that will influence the decrease in thermal conductivity of particulate composites, due to internal and external micro- and macro-cracks, which have not been investigated in detail yet. In this study, we conducted many numerical simulations using COMSOL Multiphysics to investigate the effect of micro-damage at particle-matrix interfaces on the thermal conductivity of TIM. The effect of damage area ratio and thickness of gap at the particle-matrix interfaces and are taken into account for particulate composites with different combinations of particle fraction, particle size and thermal properties of the constituents.

Apart from thermal conductivity, mechanical properties are also essential for TIMs as the TIM is also responsible for keeping the heat producing component in place. This study will focus on the stiffness (Young's modulus) of TIMs as a function of its structure and the characteristics of the damage at the particle-matrix interface. The effects of filler content, filler size, filler geometry on the effective stiffness of the composite have been studied extensively [27-30]. Particle-matrix interface adhesion is another important parameter that influences the mechanical properties of composite. Wang et al. [31] and Wong et al. [32] argued that a better particle-matrix interface adhesion leads to a higher Young's modulus. However Dekkers et al. [33] and Dibenedetto [34] et al. showed that interfacial adhesion has little effect on the Young's modulus of particulate-filled composites because Young's modulus is measured at relatively low deformations at which there is insufficient dilation to cause interface separation. Nevertheless the debonding of particle-matrix interfaces will lead to decrease in mechanical properties. Ghosh et al. applied an analytical model to study the effect of debonding on various moduli of short fiber composites[35]. They showed that only a few percent debonding along the fiber length substantially reduces the elastic modulus. FEM is also widely used in mechanical damage analysis of composites considering the influence of debonding [36-39]. In the present study, we applied numerical simulation to investigate the effect of micro damage at particle-matrix interfaces on Young's modulus of TIMs in more detail for conditions relevant for thermal interface materials in microelectronics.

Macro damage at TIM-heat source interface will also lead to a decrease in the effective thermal conductivity of TIM and a reduction in the reliability of the system as a whole. Eleffndi et al. [40] showed that the change in the junction-to-case

thermal resistance can be estimated according to the residual attached area. Not only does macro-delamination lead to a reduced heat flux, it will also generate a thermal profile and hence thermal stresses [41-45] at the edges of the remaining bonded interface. In conventional TIMs the development of such a thermal profile will accelerate the breakdown of the interface. However, in polymer-based self-healing TIMs [46-48], the local temperature rise will stimulate the self-healing process and restore the functionality. Hence, both for current conventional and future self-healing TIMs, the analysis of the temperature rise at the edges of delaminated zones is important.

3

The present work aims to present a comprehensive overview of the effects of micro- and macro-cracks on the thermal and mechanical performance of thermal interface materials.

### 3.2 Numerical method

All calculations were performed using the 'Heat Transfer in Solids' interface and 'Solid Mechanics' interface of COMSOL Multiphysics software V5.2. Various filler materials such as glass (low thermal conductivity), alumina (medium thermal conductivity) and aluminum (high thermal conductivity) were selected while the thermal conductivity of the polymer matrix was fixed to a value characteristic for the polymer matrices currently in use. To study the effect of macro damage, the thermal interface composite material was homogenized (HOMO TIM). The thermal conductivities and mechanical properties of different materials used in this study are listed in Table 3.1. All materials are considered being homogeneous and isotropic themselves. Furthermore, all material properties are taken to be independent of temperature and all materials are to remain in their elastic regime during the simulations. The air in the delaminated zones is taken to be stagnant

**Table 3.1** The thermal conductivities and mechanical properties of different materials used in this study

Material	Thermal conductivity (W/(m·K))	Density (kg/m <sup>3</sup> )	C <sub>p</sub> (J/(kg·K))	Poisson's ratio	Young's modulus (MPa)	CTE (10 <sup>-6</sup> /K)
Polymer matrix	0.45	1180	1820	0.49	2	--
glass	1.13	2500	840	--	--	--
alumina	27	3900	880	0.222	300000	--
Aluminum	237	2700	897	0.33	70000	23
HOMO TIM	2	2550	1350	0.4	7	60
Air	0.026	1	1006	--	--	--

### 3.2.1 The effect of micro damage at particle–matrix interfaces on thermal conductivity

A cuboid matrix was created and spherical particles of the same size were embedded, as shown in Figure 3.1a. A boundary heat source  $Q_b$  of 40000 W/m<sup>2</sup> was applied at the bottom surface. A constant temperature of 300K was defined at the top surface. The four remaining walls of the cuboid matrix were set to be thermally insulated. The temperature distribution of the whole body can be simulated by applying stationary conditions. Then the thermal conductivity  $\lambda$  of the TIM can be calculated by equation 3.1:

$$\lambda = \frac{Q_b}{L\Delta T} \quad (3.1)$$

in which  $L$  is the height of the cuboid matrix and  $\Delta T$  is the temperature difference of top and bottom surface.

There are two methods to introduce the debonding of particle–matrix interface. Method 1: directly creating an air gap at the particle–matrix interface and then solving the thermal response over the system. Method 2: first calculating the thermal conductance  $h_g$  of an air gap with the desired thickness using equation 3.2 and then defining the heat transfer coefficient  $h_g$  at the particle–matrix interface.

$$h_g = \frac{\lambda_{air}}{l} \quad (3.2)$$

in which  $\lambda_{air}$  is the thermal conductivity of air and  $l$  is the matrix–particle separation distance. The difference in results according to methods 1 and 2 is less than 0.5%,



which is negligible. However calculations according to method 1 take much more time because of the required small mesh size to capture the air gap between the matrix and the particles. So in this study, method 2 was applied.

In order to investigate the effect of particle–matrix interface damage area on thermal conductivity of TIM, 0%, 25%, 50%, 75% and 100% of the particles were selected to be thermally detached, as shown in Figure 3.1. The additional contributions of particle volume concentration, particle size and thermal conductivity of particles are determined.

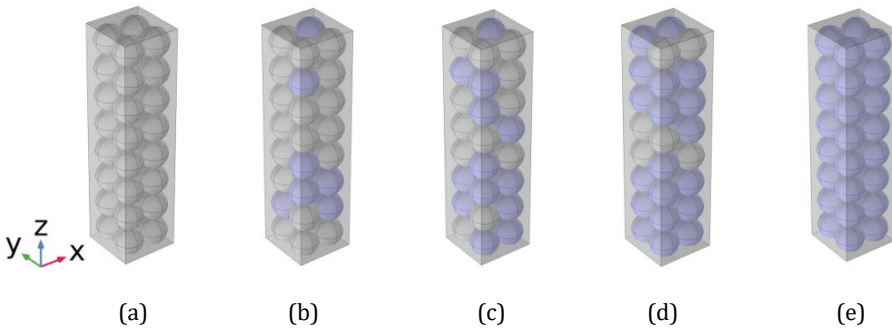


**Figure 3.1** The geometry of micro damage at particle–matrix interfaces. (a): 0% interface area debonding; (b): 25% interface area debonding; (c): 50% interface area debonding; (d): 75% interface area debonding; (e): 100% interface area debonding. The blue areas represent the debonding.

### 3.2.2 The effect of micro damage at particle–matrix interfaces on stiffness

The geometry is the same as shown in Figure 3.1. In the quasi–static mechanical analysis, the bottom surface is spatially fixed. A prescribed displacement in the Z direction, leading to 5% strain, is applied on the top surface. The other four external surfaces are set to be free boundaries. The apparent Young's modulus of the undamaged and damaged composites can be obtained by equation 3.3:

$$E = \frac{\bar{\sigma}_z}{\varepsilon} \quad (3.3)$$

in which  $\overline{\sigma_z}$  is the average stress tensor Z component on the top surface and  $\varepsilon$  is the imposed strain in the z-direction.

The de-bonded particles are randomly chosen as shown in Figure 3.1. Debonding is already in effect at the start of the simulation. The remaining particles do not show delamination even when the axial strain is applied during simulation. The effect of particle volume concentration, damage area ratio and particle size are discussed.

### 3.2.3 The effect of macro-damage at the TIM-heat source interface on the thermal conductivity and interfacial thermal stresses

The geometry used in the simulation of the effect of a macro delamination is shown in Figure 3.2. The TIM is considered to be square and to consist of a homogeneous and isotropic material with a thermal conductivity of 2 W/m·K. The thickness of the TIM is 1mm while the contact zone is 5 x 5 mm<sup>2</sup>. Two aluminum layers with the thickness of 0.05 mm are applied as heat source (at the bottom of TIM) and heat sink (at the top of TIM) respectively. The delamination is either located at the center, the corner or the edge of the TIM-heat source interface, as shown in Figure 3.2. A boundary heat source  $Q_b$  of 40000 W/m<sup>2</sup> is applied at the bottom surface. A constant temperature of 300K is defined at the top surface. The effective thermal conductivity of TIM was calculated using the same method as described in 2.1. By coupling the 'Solid Mechanics' interface to the 'Heat Transfer in Solids' interface, the thermal stress at TIM-heat source interface can be obtained. The zero-strain reference temperature was set to be 300K.

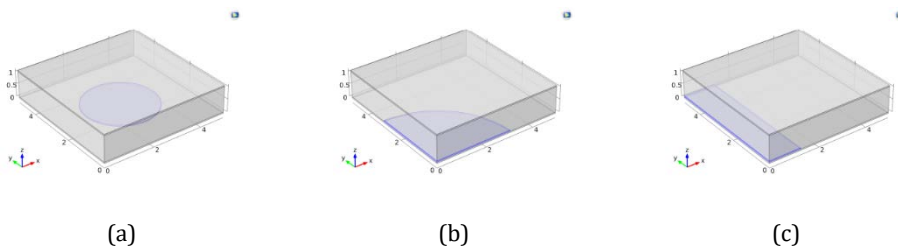


**Figure 3.2** The geometry of macro damage of TIM. The delamination is located at (a): center, (b): corner or (c): edge of the TIM-heat source interface. The blue areas represent the delamination. For clarity, the top heat sink is not shown in the figures.

### 3.3 Results and discussion

#### 3.3.1 The effect of micro damage at particle–matrix interfaces on thermal conductivity and Young’s modulus

Figure 3.3 shows that when the particle volume concentration is below 25%, the thermal conductivity of alumina (particle size 20  $\mu\text{m}$ ) loaded TIMs is not very sensitive to the degree of debonding at particle–matrix interfaces. With increasing particle volume fraction, the same degree of particle–matrix interface debonding leads to a greater decrease in thermal conductivity. In contrast, the Young’s modulus of TIM is rather sensitive to the degree of debonding at particle–matrix interfaces even when the particle volume concentration is low. Unless specified otherwise, in the remainder of this study the particle volume concentration is fixed at 50% and the particle material is fixed at alumina.

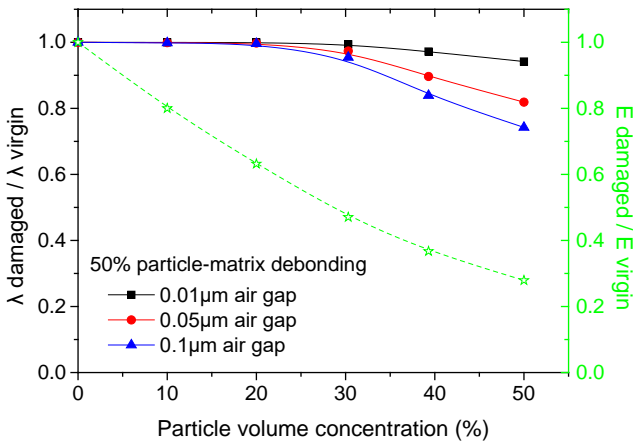


**Figure 3.3** The effect of particle volume concentration on the thermal conductivity and Young’s modulus of alumina (particle size 20  $\mu\text{m}$ ) loaded TIM

The thermal conductivity of 50 vol.% alumina (particle size 20  $\mu\text{m}$ ) loaded TIM nearly linearly decreases with debonded particle–matrix interface area, as shown in Figure 3.4. However the reduction is not dramatic. If the delamination distance at the interface is 0.01  $\mu\text{m}$ , the resulting thermal conductivity decrease is only 14% assuming all particles to be detached. If the separation distance is taken to be 0.1  $\mu\text{m}$ ,

the thermal conductivity will go down to 48 % when all interfaces are debonded. This result agrees with Sun's work [24] which shows that small crack openings only lead to a slight increase in thermal resistance. On the other hand, the Young's modulus of a TIM rapidly drops to 53% when only 25% particle-matrix interfaces are broken. When the percentage of debonding is over 60%, the modulus seems to become fairly constant and independent of further debonding. This trend is the same as in Ghosh's work[35]. It should be stated explicitly that, unlike the thermal conductivity, the reduction in sample stiffness is independent of the particle-matrix delamination distance.

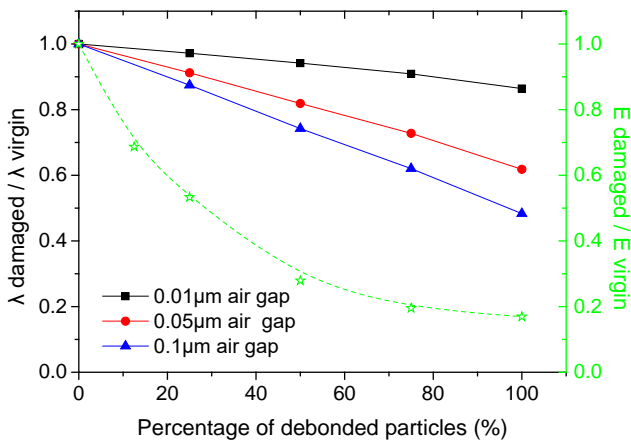
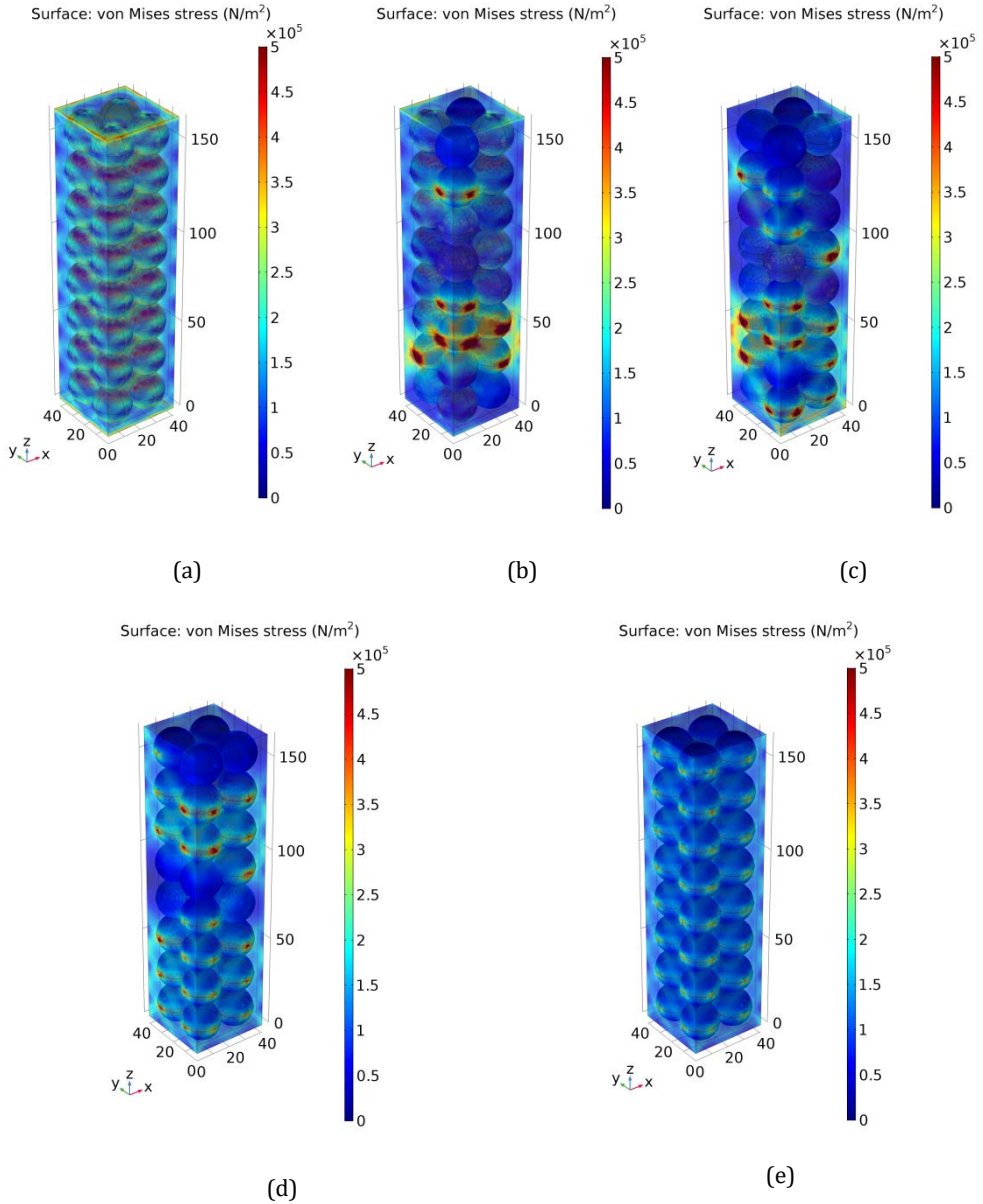


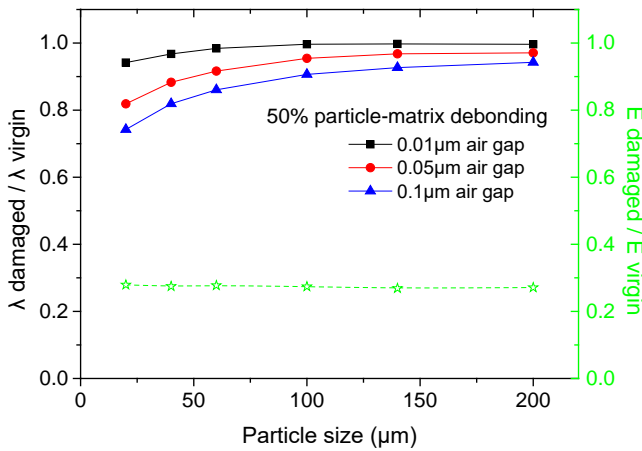
Figure 3.4 The effect of debonded particle percentage on the thermal conductivity and Young's modulus of 50 vol.% alumina (particle size 20 μm) loaded TIM.

Figure 3.5 shows the local (von Mises) stress distribution in 50 vol.% alumina (particle size 20 μm) loaded TIM for different degrees of particle-matrix interfaces debonding and a common 5% strain along Z direction. The regions of stress concentration clearly coincide with the regions containing the debonded samples (see Figure 3.1). It seems that for a fixed imposed strain conditions used in the present simulations, the amplitude of the absolute maximum stress in the debonded (red area) decreases with the area fraction of debonded interfaces. This is due to the fact that the total induced stress decreases dramatically with the debonded area fraction.



**Figure 3.5** The stress distribution in 50 vol.% alumina (particle size 20  $\mu\text{m}$ ) loaded TIM with (a): 0%, (b): 25%, (c): 50%, (d): 75%, (e): 100% alumina particle-polymer matrix interfaces debonding under 5% strain along Z direction. (Same delamination locations as in corresponding cases in Figure 3.1)

The decrease of the thermal conductivity due to particle–matrix interface debonding also depends on the particle size. Figure 3.6 clearly shows that the thermal conductivities of composites with smaller particles are more sensitive to the particle–matrix debonding. Under the same damage degree (50% of particle–matrix interfaces debonding and air gap 0.1  $\mu\text{m}$ ), the drop in thermal conductivity for a 20  $\mu\text{m}$  particle loaded TIM is 26% while for a 200  $\mu\text{m}$  particle loaded TIM the decrease is only 6%. However the decrease of Young’s modulus due to particle–matrix interface debonding is independent of particle size. This can be explained by the fact that in the micrometer range the particle size has no effect on the Young’s modulus of particulate filled composites [4].

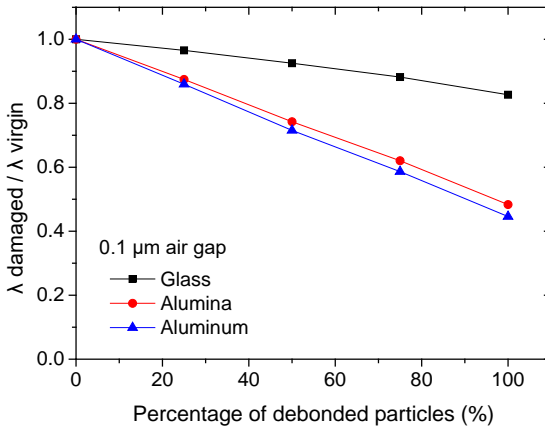


**Figure 3.6** The effect of particle size on the damage of TIM’s thermal conductivity and Young’s modulus due to particle–matrix interface debonding.

More importantly, it can be concluded from Figures 3.3, 3.4 and 3.6 that particle–matrix interface debonding always leads to greater relative decrease Young’s modulus than that in thermal conductivity regardless of particle volume concentration, particle size and damage area. This trend can also be found in Tang and Shen’s work [25, 26].

Finally, The thermal conductivity of loaded particles will also affect the decrease in thermal conductivity due to particle–matrix interface debonding. As shown in Figure

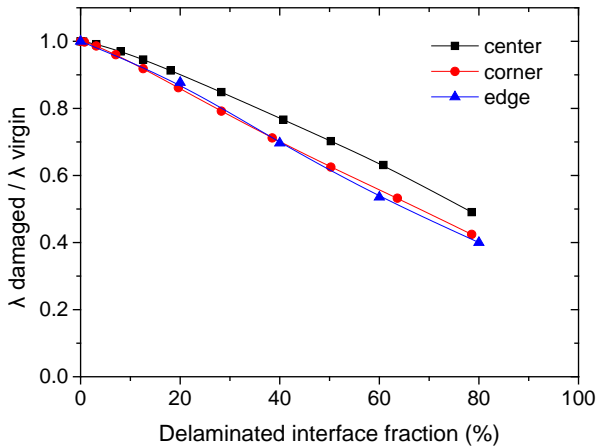
3.7, TIMs loaded with medium or high thermal conductive particles, for instance alumina (27 W/m·K) or Aluminum (237 W/m·K), are more sensitive to the particle–matrix interface damage than the one loaded with low thermal conductive glass beads (1.13 W/m·K).



**Figure 3.7** The effect of particle thermal conductivity on the decrease of the overall thermal conductivity due to particle–matrix interface debonding.

### 3.3.2 The effect of macro damage at TIM–heat source interface on thermal conductivity and interfacial thermal stress

Figure 3.8 shows the effect of delamination size on the effective thermal conductivity of TIM. When the delamination separation distance is fixed to 5% of the thickness of the TIM, the effective thermal conductivity of TIMs decreases nearly linearly with the delaminated areal fraction. When the delamination is located at the center of TIM–heat source interface, the effective thermal conductivity decreases a bit less than when the delamination is located at the corner or the edge. When the delamination size is bigger than 80%, which has been reported to occur in real applications, the effective thermal conductivity will be less than 50% of the virgin value irrespective of the damage location.



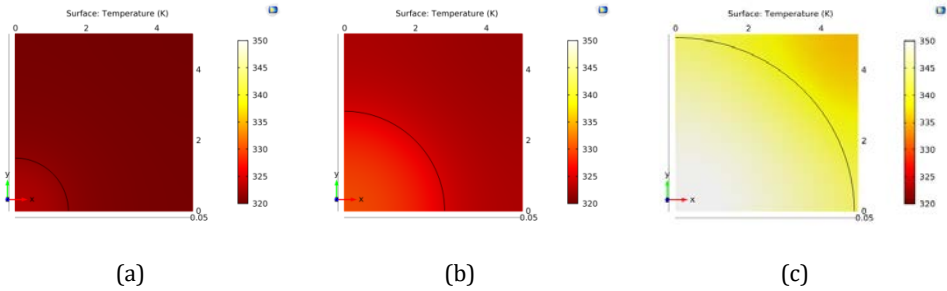
**Figure 3.8** The effect of the delaminated interface fraction on the effective thermal conductivity when the delamination distance is fixed to 5% of the thickness of the TIM.

Figure 3.9 shows the temperature distribution at the TIM–heat source interface for different delamination dimensions. With the delamination size increases, the average temperature at the TIM–heat source interface increases significantly due to the loss of effective thermal conductivity. As expected the temperature at the edge of the delamination is always higher than further into the well-adhered part. For conventional thermal interface materials the increase in local temperature at the “hot rim” will only lead to an increase in a stress concentration and a weakening of the polymer matrix. In the case of self-healing polymer matrices, the increase in temperature will lead to a temporary opening of the weaker secondary bonds, a flow of polymer into the crack gap and a restoration of the adhesion, ultimately resulting in a lowering of the interfacial temperature and restoration of performance. Hence for self-healing polymer matrices the occurrence of local healing around the damage site is the key to induce autonomous healing.

We will now look into the interfacial stresses in TIMs based on non-self-healing polymer matrices. The results are shown in Figure 3.10 for the three cases considered in Figure 3.9 and reveal significant stress concentrations at the rim. Figure 3.11a shows that the average thermal stress at TIM–heat source interface increases rapidly with the delamination size increasing. When the delamination size



is less than 40%, the location of delamination does not show a noticeable effect on the average interfacial thermal stress. When the delamination size is larger than 40%, delamination at the edge of TIM–heat source interface leads to the highest (von Mises) stresses. In Figure 3.11b the maximum thermal stress at the rim of the delamination is plotted as a function of the delaminated area for the three damage locations considered. If the delamination is at center, the maximum thermal stress at “hot rim” does not show a noticeable increase when delaminated interface is less than 15%. While for the other two locations the maximum thermal stresses increase more or less linearly and are larger than the former situation (delamination at center) over the whole studied range. It indicates that the damage evolution at the corner or edge is faster than the one at center.



**Figure 3.9** Temperature distribution at TIM–heat source interface with (a): 7%, (b): 25%, (c): 75% delamination size when the delamination thickness is fixed to 5% of the thickness of the TIM.

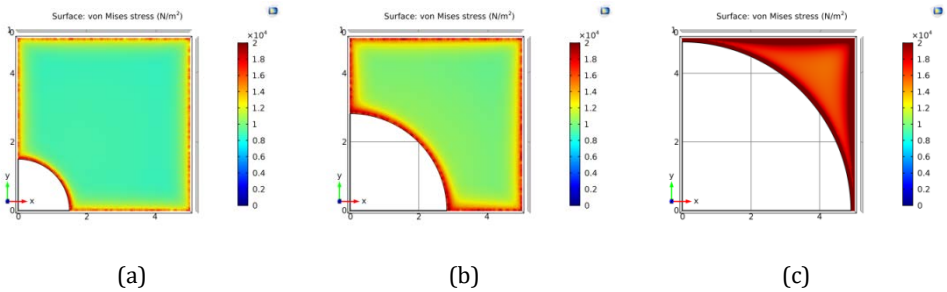


**Figure 3.10** Thermal stress distribution at TIM–heat source interface with (a): 7%, (b): 25%, (c): 75% delamination size when the delamination thickness is fixed to 5% of the thickness of the TIM.

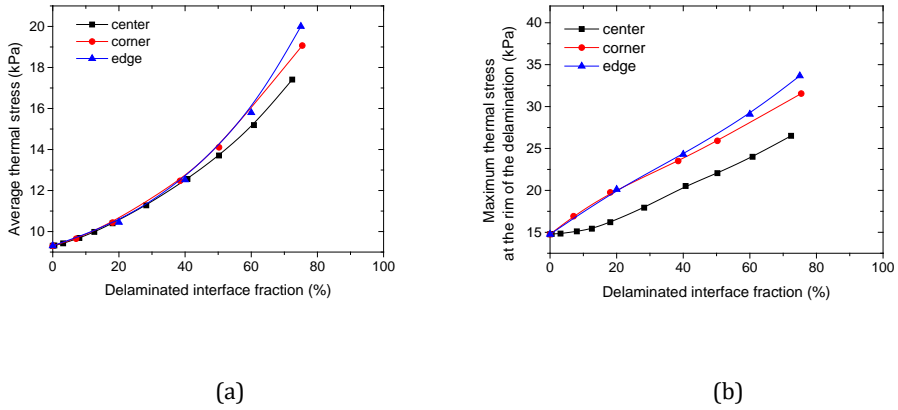


**Figure 3.11** The effect of delamination size on (a) the average thermal stress at TIM–heat source interface and (b) the maximum thermal stress at the “hot rim” when the delamination thickness is fixed to 5% of the thickness of the TIM.

For a fixed delaminated area fraction of 25%, the effect of the height of the delamination on the effective thermal conductivity is shown in Figure 3.12. The effective thermal conductivity of TIM first decreases rapidly to around 80% of its initial value when the up to a delamination height of 20% of thickness of the TIM. For even larger delamination heights the effective thermal conductivity barely changes. When the height of the delamination reaches 100%, the effective thermal conductivity of TIMs still remains around 72%. Figure 3.12 also shows that the effective thermal conductivity of TIM is more sensitive to delaminations at corners or edges than those in the center.

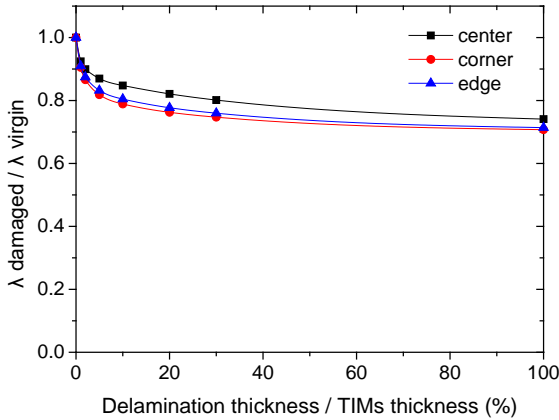


**Figure 3.12** The effect of delamination thickness on the effective thermal conductivity of TIM when the delamination size is fixed to 25% of the original TIM contact area.

### 3.4 Conclusion

In this study, we applied numerical simulations using COMSOL Multiphysics to investigate the effect of local delaminations on the thermal and mechanical properties of thermal interface materials (TIM) consisting of a polymer matrix filled with particles of a high thermal conduction material. We considered both micro delaminations at particle–matrix interfaces and macro delamination at the interface between the TIM and a substrate acting as the heat source. Local interfacial debonding between matrix and filler particle was found to have modest effect on overall thermal conductivity unless at higher filler volume fractions and for very conductive filler materials. In contrast, the elastic modulus was found to drop already sharply at low area debonding fractions. The height of the debonded region between filler particle was found to have a modest effect on thermal conductivity but to have no noticeable effect on overall material stiffness.

Loss of thermal conduction as a result of macroscopic delamination at the interface between the thermal interface material and the substrate (the heat source) was found to scale more or less linearly with the delaminated area fraction. Such macroscopic debonding leads to a rim of material near the edge of the delamination having a higher temperature and induced stresses. Both temperature levels and

stresses increase with increasing delaminated area. The degree of temperature rise at the edge is important to guide the development of next generation thermal interface materials based on (intrinsically) self-healing polymer matrices.

## References

1. Hasselman DPH, Donaldson KY, Geiger AL. Effect of Reinforcement Particle Size on the Thermal Conductivity of a Particulate-Silicon Carbide-Reinforced Aluminum Matrix Composite. *Journal of the American Ceramic Society*. 1992;75(11):3137-3140.
2. Lee G-W, Park M, Kim J, Lee JI, Yoon HG. Enhanced thermal conductivity of polymer composites filled with hybrid filler. *Composites Part A: Applied Science and Manufacturing*. 2006;37(5):727-734.
3. Mamunya YP, Davydenko VV, Pissis P, Lebedev EV. Electrical and thermal conductivity of polymers filled with metal powders. *European Polymer Journal*. 2002;38(9):1887-1897.
4. Fu S-Y, Feng X-Q, Lauke B, Mai Y-W. Effects of particle size, particle/matrix interface adhesion and particle loading on mechanical properties of particulate-polymer composites. *Composites Part B: Engineering*. 2008;39(6):933-961.
5. Tsao GT-N. Thermal Conductivity of Two-Phase Materials. *Industrial & Engineering Chemistry*. 1961;53(5):395-397.
6. Cheng SC, Vachon RI. The prediction of the thermal conductivity of two and three phase solid heterogeneous mixtures. *International Journal of Heat and Mass Transfer*. 1969;12(3):249-264.
7. Lewis TB, Nielsen LE. Dynamic mechanical properties of particulate-filled composites. *Journal of Applied Polymer Science*. 1970;14(6):1449-1471.
8. Hasselman DPH, Johnson LF. Effective Thermal Conductivity of Composites with Interfacial Thermal Barrier Resistance. *Journal of Composite Materials*. 1987;21(6):508-515.
9. Agari Y, Ueda A, Nagai S. Thermal conductivity of a polyethylene filled with disoriented short-cut carbon fibers. *Journal of Applied Polymer Science*. 1991;43(6):1117-1124.
10. Li Z, Sun WG, Wang G, Wu ZG. Experimental and numerical study on the effective thermal conductivity of paraffin/expanded graphite composite. *Solar Energy Materials and Solar Cells*. 2014;128:447-455.
11. Kumlutas D, Tavman IH. A Numerical and Experimental Study on Thermal Conductivity of Particle Filled Polymer Composites. *Journal of Thermoplastic Composite Materials*. 2006;19(4):441-455.
12. Zeng J, Fu R, Agathopoulos S, Zhang S, Song X, He H. Numerical Simulation of Thermal Conductivity of Particle Filled Epoxy Composites. *Journal of Electronic Packaging*. 2009;131(4):041006-041006.
13. Feliciani C, Takai Y. Measurement and numerical prediction of fiber-reinforced thermoplastics' thermal conductivity in injection molded parts. *Journal of Applied Polymer Science*. 2014;131(2):n/a-n/a.
14. Grandjean S, Absi J, Smith DS. Numerical calculations of the thermal conductivity of porous ceramics based on micrographs. *Journal of the European Ceramic Society*. 2006;26(13):2669-2676.
15. Chu K, Jia C, Tian W, Liang X, Chen H, Guo H. Thermal conductivity of spark plasma sintering consolidated SiCp/Al composites containing pores: Numerical study and experimental validation. *Composites Part A: Applied Science and Manufacturing*. 2010;41(1):161-167.

16. El Moumen A, Kanit T, Imad A, El Minor H. Computational thermal conductivity in porous materials using homogenization techniques: Numerical and statistical approaches. *Computational Materials Science*. 2015;97:148-158.
17. Akué Asséko AC, Cosson B, Duborper C, Lacrampe M-F, Krawczak P. Numerical analysis of effective thermal conductivity of plastic foams. *Journal of Materials Science*. 2016;51(20):9217-9228.
18. Kapitza P. The study of heat transfer in helium II. *J Phys(USSR)*. 1941;4(1-6):181-210.
19. Nan C-W, Birringer R, Clarke DR, Gleiter H. Effective thermal conductivity of particulate composites with interfacial thermal resistance. *Journal of Applied Physics*. 1997;81(10):6692-6699.
20. Kothari R, Sun CT, Dinwiddie R, Wang H. Experimental and numerical study of the effective thermal conductivity of nano composites with thermal boundary resistance. *International Journal of Heat and Mass Transfer*. 2013;66:823-829.
21. Haddadi M, Agoudjil B, Boudenne A, Garnier B. Analytical and Numerical Investigation on Effective Thermal Conductivity of Polymer Composites Filled with Conductive Hollow Particles. *International Journal of Thermophysics*. 2013;34(1):101-112.
22. Veyret D, Tsoiridis G. Numerical determination of the effective thermal conductivity of fibrous materials. Application to proton exchange membrane fuel cell gas diffusion layers. *Journal of Power Sources*. 2010;195(5):1302-1307.
23. Skuriat R, Li JF, Agyakwa PA, Matthey N, Evans P, Johnson CM. Degradation of thermal interface materials for high-temperature power electronics applications. *Microelectronics Reliability*. 2013;53(12):1933-1942.
24. Sun S, Chen S, Luo X, Fu Y, Ye L, Liu J. Mechanical and thermal characterization of a novel nanocomposite thermal interface material for electronic packaging. *Microelectronics Reliability*. 2016;56:129-135.
25. Tang S, Tang Ca, Liang Z, Zhang Y, Li L. Numerical Study of the Influence of Material Structure on Effective Thermal Conductivity of Concrete. *Heat Transfer Engineering*. 2012;33(8):732-747.
26. Shen L, Ren Q, Xia N, Sun L, Xia X. Mesoscopic numerical simulation of effective thermal conductivity of tensile cracked concrete. *Construction and Building Materials*. 2015;95:467-475.
27. Odegard GM, Clancy TC, Gates TS. Modeling of the mechanical properties of nanoparticle/polymer composites. *Polymer*. 2005;46(2):553-562.
28. Tan P, Tong L, Steven GP. Modelling for predicting the mechanical properties of textile composites—A review. *Composites Part A: Applied Science and Manufacturing*. 1997;28(11):903-922.
29. Huang Z-M. Simulation of the mechanical properties of fibrous composites by the bridging micromechanics model. *Composites Part A: Applied Science and Manufacturing*. 2001;32(2):143-172.
30. Alberola ND, Mele P. Interface and mechanical coupling effects in model particulate composites. *Polymer Engineering & Science*. 1997;37(10):1712-1721.
31. Wang K, Wu J, Ye L, Zeng H. Mechanical properties and toughening mechanisms of polypropylene/barium sulfate composites. *Composites Part A: Applied Science and Manufacturing*. 2003;34(12):1199-1205.

32. Wong CP, Bollampally RS. Thermal conductivity, elastic modulus, and coefficient of thermal expansion of polymer composites filled with ceramic particles for electronic packaging. *Journal of Applied Polymer Science*. 1999;74(14):3396-3403.
33. Dekkers MEJ, Heikens D. The effect of interfacial adhesion on the tensile behavior of polystyrene-glass-bead composites. *Journal of Applied Polymer Science*. 1983;28(12):3809-3815.
34. Dibenedetto AT, Wambach AD. The Fracture Toughness of Epoxy-glass Bead Composites. *International Journal of Polymeric Materials and Polymeric Biomaterials*. 1972;1(2):159-173.
35. Ghosh K, Carroll DR, Dharani LR. Effect of interface debonding on various moduli of short fiber composites. *Advanced Composite Materials*. 1994;4(1):17-32.
36. Alfano G, Crisfield MA. Finite element interface models for the delamination analysis of laminated composites: mechanical and computational issues. *International Journal for Numerical Methods in Engineering*. 2001;50(7):1701-1736.
37. Parmigiani JP, Thouless MD. The roles of toughness and cohesive strength on crack deflection at interfaces. *Journal of the Mechanics and Physics of Solids*. 2006;54(2):266-287.
38. Wang W, Sadeghipour K, Baran G. Finite element analysis of the effect of an interphase on toughening of a particle-reinforced polymer composite. *Composites Part A: Applied Science and Manufacturing*. 2008;39(6):956-964.
39. Cid Alfaro MV, Suiker ASJ, Verhoosel CV, de Borst R. Numerical homogenization of cracking processes in thin fibre-epoxy layers. *European Journal of Mechanics - A/Solids*. 2010;29(2):119-131.
40. Eleffendi MA, Yang L, Agyakwa P, Mark Johnson C. Quantification of cracked area in thermal path of high-power multi-chip modules using transient thermal impedance measurement. *Microelectronics Reliability*. 2016;59:73-83.
41. Suhir E. Analysis of interfacial thermal stresses in a trimaterial assembly. *Journal of Applied Physics*. 2001;89(7):3685-3694.
42. Kang Yong L, Chang Won S. Determination of thermal stress intensity factors for an interface crack under vertical uniform heat flow. *Engineering Fracture Mechanics*. 1991;40(6):1067-1074.
43. Carreño-Morelli E, Urreta SE, Schaller R. Mechanical spectroscopy of thermal stress relaxation at metal-ceramic interfaces in Aluminium-based composites. *Acta Materialia*. 2000;48(18-19):4725-4733.
44. Post D, Wood JD, Han B, Parks VJ, Gerstle JFP. Thermal Stresses in a Bimaterial Joint: An Experimental Analysis. *Journal of Applied Mechanics*. 1994;61(1):192-198.
45. Yeh M-K, Lu C-L. Reliability analysis of 3D heterogeneous microsystem module by simplified finite element model. *Microelectronics Reliability*. 2016;63:111-119.
46. Lafont U, Zeijl Hv, Zwaag Svd. Increasing the reliability of solid state lighting systems via self-healing approaches: A review. *Microelectronics Reliability*. 2012;52(1):71-89.
47. Lafont U, Moreno-Belle C, Zeijl Hv, Zwaag Svd. Self-healing thermally conductive adhesives. *Journal of Intelligent Material Systems and Structures*. 2014;25(1):67-74.
48. Nan Z, Santiago JG, Sybrand van der Z. The effect of filler parameters on the healing of thermal conductivity and mechanical properties of a thermal interface material based on a self-healable organic-inorganic polymer matrix. *Smart Materials and Structures*. 2016;25(8):084016.

# Chapter 4

---

**On the role of disulfide bond concentration and irreversible crosslink density on mechanical properties and crack healing efficiencies of organic–inorganic dual network polymers**

---



## 4.1 Introduction

Over the past few decades, self-healing polymeric materials have attracted the attention of many researchers because of their fascinating ability to restore their original properties after local mechanical damage (such as scratches or cracks) and their potential in applications such as coating, adhesives or as the matrix material for fibre reinforced composites[1-4]. While the field of self-healing polymers started with a landmark publication[5] on an extrinsic self-healing polymer (i.e. the polymer itself has no healing ability, but contains discrete entities containing the healing agent such as a liquid adhesive or solvent[6]), intrinsic self-healing polymers (i.e. the polymer itself can reform bonds over the former damage site) are now seen as more promising because of its ability of multiple healing and easier processing. In intrinsic self-healing polymer the re-establishment of bonds is due to the incorporation of reversible bonds/reactions (e.g. disulfide bonds, Diels-Alder reaction, hydrogen bonding or metal-ligand coordination) in the polymer networks [7-10]. A healing event can be triggered by applying appropriate stimulus (e.g. heat, moisture or UV light) to break the reversible bonds leading to temporary local network mobility which is necessary for local flow to fill the crack to and to cause damage repair[11-13].

As the presence of weaker and reversible bonds in the polymer must have a negative impact on mechanical properties, such as yield and tensile strength, a big challenge in the design of intrinsic self-healing polymer is a combination of good mechanical properties and a high healing efficiency. AbdolahZadeh et al. [14] used sol-gel chemistry to introduce tetra-sulfide groups into an epoxy resin to form a healable organic-inorganic dual network polymer which shows both excellent mechanical properties as coating and good healing performance. However a drawback of this polymer is a noticeable H<sub>2</sub>S gas release during curing process which limits its application as matrix material for fiber reinforced composites as it causes porosity and is environmentally unacceptable. Hernández et al. [15] showed that a compromise between mechanical performance and healing capability can be reached by tailoring the amount of sulfur, the cross-linking density, and the disulfide/polysulfide ratio in a self-healing sulfur vulcanized natural rubber. In this work, the organic-inorganic dual network polymer is modified and the effect of tetra-sulfide/disulfide on curing process, mechanical properties and healing performance of polymers is investigated. Post et al.[16] applied one of the modified disulfide-containing polymer system in this work as matrix material to develop an intrinsic healing glass fiber reinforced polymer (GFRP) composite, which shows a

combination of high mechanical properties, the ability to multiple thermally induced healing and process ability by conventional vacuum infusion process.

In principle, the disulfide exchange based self-healing can be achieved without the need for a catalyst [17]. However the application of disulfide cleavage catalyst is able to improve disulfide exchange based self-healing by enhancing the disulfide exchange reaction [18]. Tertiary amines[19], phosphines[20, 21], Rhodium[22] and  $\text{CuCl}_2$ [23] have been reported as efficient disulfide exchange catalysts. In this work, triethylamine (TEA) is chosen and the effect of this catalyst on the mechanical properties and healing performance of the bulk polymer is studied.

The polymer architecture plays an important role on the mechanical properties, and this dependence has been studied extensively since the beginning of the field of polymer science [24-28]. However only a few attempts have been made to systematically understand the influence of polymer architecture on healing behavior [29-31]. The work most relevant to the current work is done by Grande et al. [30] who controlled the crosslink density of self-healing poly(urea-urethane) networks by altering the ratio of bi-functional and tri-functional pre-polymers. They demonstrated that polymers with low crosslink density possess high crack healing efficiencies but low tensile strength values. Some other studies also showed that good healing ability can be achieved by sacrificing the mechanical properties [15, 32, 33]. In the present work, both reversible bond (disulfide bond) concentration and crosslink density of polymer are tuned to investigate the role of disulfide bond concentration versus crosslink density on mechanical and healing properties.

## 4.2 Experimental

### 4.2.1 Materials

Epoxy resin Epikote™ 828 (184-190 g/eq) and curing agent Ancamine® 2500 (105-110 g/eq) were provided by Akzo Noble. A fatty dimer diamine (from hereon called DD1), provided by Croda Nederland B.V., was also used as a substitute of curing agent Ancamine® 2500. (3-Aminopropyl)trimethoxysilane (purity 97%), Pentaerythritol tetrakis (3-mercaptopropionate) (purity>95%) and Triethylamine, from hereon called APS, tetrathiol and TEA respectively, were purchased from Sigma-Aldrich. Bis[3-(triethoxysilyl)propyl]tetrasulfide and Bis[3-(triethoxysilyl)propyl]disulfide, from hereon called BTS and BDS respectively, were

purchased from SiSiB Silanes. All chemicals were used as in their as-received well-packaged condition. The chemical structures of monomers used in this study are shown in Figure 4.1.

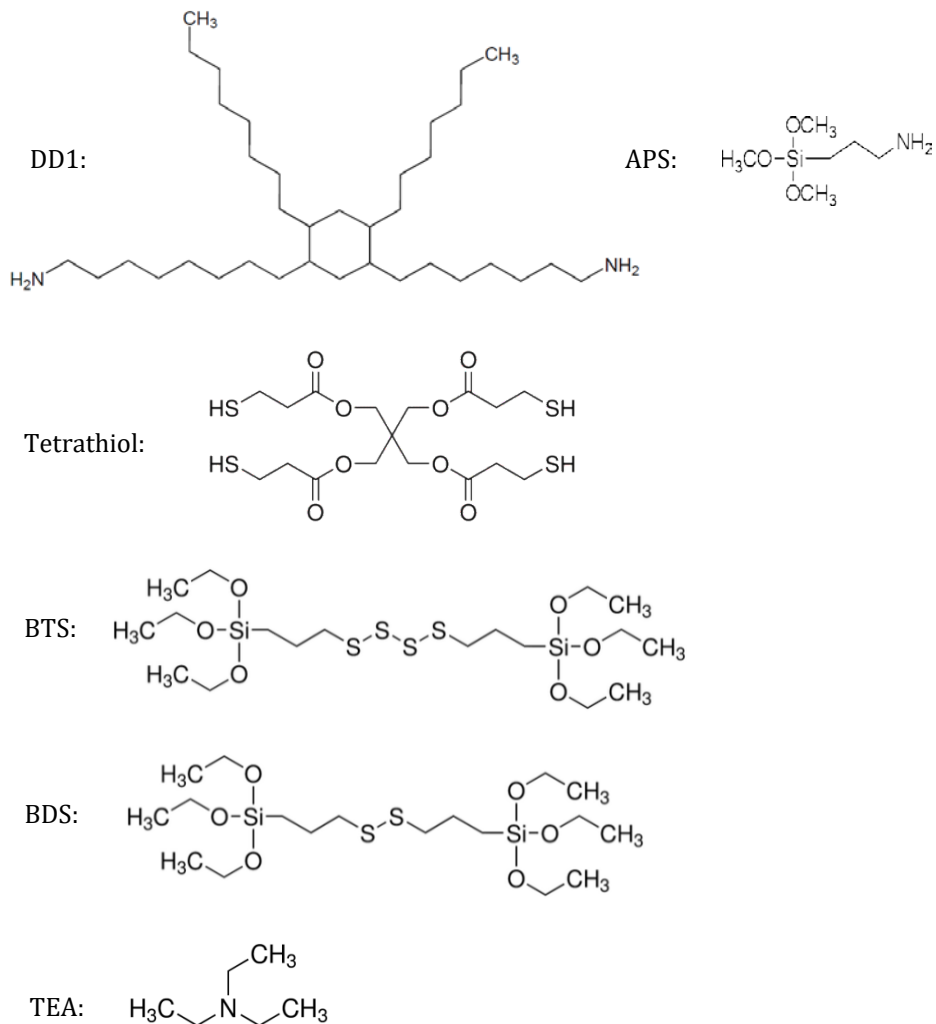


**Figure 4.1** Chemical structures of monomers used in this study.

### **4.2.2 Polymer preparation**

In the present study, organic–inorganic dual network polymers were prepared in a multi–step process. At first, Epoxy resin and APS were mixed using a magnetic stirrer at 100 rpm for 5 min at room temperature. Then BTS or BDS were added while continuously stirring at 300 rpm for 3 h at room temperature. Then, the curing agent Ancamine® 2500 or DD1 was mixed with the mixture in a high speed mixer operating at 2500 rpm for 5 min. Then tetrathiol and the catalyst TEA were added and mixed at 2500 rpm for 0.5 min. After casting the mixed product in a Teflon mold to yield a plaque of about 2 mm thickness, the polymer was cured at 70 °C for 2 h, 48 h, 120 h and 336 h respectively. The weight ratio of all components is shown in Table 4.1.

### **4.2.3 Characterization methods**

#### *4.2.3.1 Raman spectroscopy*

Raman spectroscopy tests were performed using a Renishaw InVia Raman microscope with a 785 nm laser source at a power of approximately 30 mW. The measured area was about 1 mm × 1 mm. The spectral response over the range 170 to 1360 cm<sup>-1</sup> was collected at room temperature.

#### *4.2.3.2 FTIR spectroscopy*

Fourier–transform infrared (FTIR) spectroscopy tests were performed using a Perkin Elmer spectrum 100 FTIR spectrometer. The spectral response over the region 600 to 4000 cm<sup>-1</sup> was collected at room temperature.

#### *4.2.3.3 SEM*

Scanning electron microscope (SEM) tests were performed using a JEOL JSM 7500F SEM. In order to avoid charging during SEM observation, the specimens were sputter coated with a 15 nm thick gold film using a Quorum Q300TD Sputtering System.

Table 4.1 Compositions of polymers studied in this work

Components	Polymers									
	BTS-An	BDS-An	BDS-An-TEA	BTS-DD1	BDS-DD1	BDS-DD1-TEA	0.2BTS0.8BDS-An	0.5BTS0.5BDS-An		
Epikote™ 828	1g	1g	1g	1g	1g	1g	1g	1g		
Ancamine® 2500	0.579g	0.579g	0.579g	0	0	0	0.579g	0.579g		
DD1	0	0	0	0.717g	0.717g	0.717g	0	0		
APS	0.076g	0.076g	0.076g	0.076g	0.076g	0.076g	0.076g	0.076g		
BTS	0.733g	0	0	0.733g	0	0	0.147g	0.367g		
BDS	0	0.646g	0.646g	0	0.646g	0.646g	0.517g	0.323g		
Tetrathiol	0.566g	0.566g	0.566g	0.566g	0.566g	0.566g	0.566g	0.566g		
TEA	0	0	0.014g	0	0	0.014g	0	0		

#### 4.2.3.4 Tensile test

Tensile tests using dog bone shaped samples (ASTM D1708, 2 mm thick) were performed at room temperature using an Instron 3365 tensile testing machine with a 1 kN load cell and a cross-head speed of 5 mm/min.

#### 4.2.3.5 DMTA test

Dynamic Mechanical Thermal Analysis (DMTA) was performed using a Perkin Elmer Pyris Diamond Dynamic Mechanical Analyzer. Rectangular samples (40×5×2 mm) were measured from -60 °C to 150 °C with a heating ramp of 2 °C/min.

#### 4.2.3.6 Fracture healing test

To evaluate the fracture healing efficiency (FHE), double edge notched tension (DENT) tests were performed. The size of the rectangular samples was 45×25×2 mm. Two 10 mm long notches were cut in the middle of the sample edges using a razor blade. The pristine samples were tested at room temperature using an Instron 3365 tensile testing machine with a 1 kN load cell and a cross-head speed of 10 mm/min. After complete failure, the fractured sample were repositioned carefully and put into a Teflon mold having a cavity with the same size as the pristine sample. After healing at 70 °C under 0.3 bar pressure for 4 h, the healed samples were then re-tested after thermal equilibration at room temperature (about 30 min) following the original DENT fracture protocol. A typical deformation sequence of a pristine DENT sample is shown in Figure 4.2.

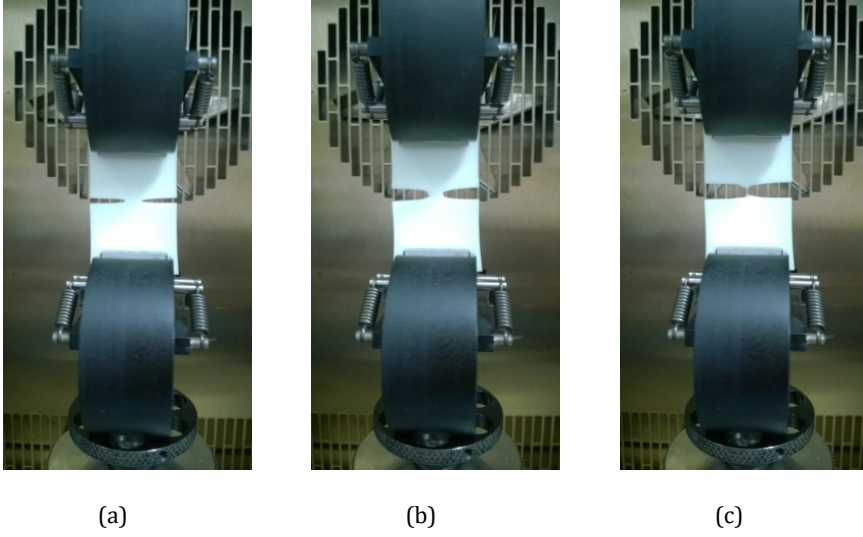


**Figure 4.2** Double edge notched tension (DENT) test sequence: (a) loading; (b) crack initiation and (c) complete failure.

From the Load–Displacement curves of DENT tests, critical fracture energy values ( $J_c$ ) can be calculated according to the following equation:

$$J_c \text{ [kJ/m}^2\text{]} = \frac{\eta U_c}{b(w-a)} \Big|_{u_c} \quad (4.1)$$

where  $U_c$  is the energy calculated as the area under the Load–Displacement curves up to the displacement  $u_c$  where crack initiation occurs,  $\eta$  is the proportionality factor (a value of 0.8 was selected according to literature [34]);  $b$ ,  $w$  and  $a$  are the sample thickness, sample width and pre-crack length, respectively. In order to quantify the recovery of fracture properties,  $J_c$  was selected as reference parameter [35, 36] and the fracture healing efficiency (FHE) can be calculated as the ratio between the measured  $J_c$  of healed ( $J_c^{Healed}$ ) and virgin samples ( $J_c^{Virgin}$ ):

$$FHE = \frac{J_c^{Healed}}{J_c^{Virgin}} \times 100\% \quad (4.2)$$

#### 4.2.3.7 Disulfide bond (S-S) concentration calculation and measurement.

For the polymers BDS-An and BDS-DD1, it is assumed that the S-S concentration is the same in the mixed base ingredients and the cured polymer, because neither the disulfide-thiol exchange reaction or the disulfide-disulfide exchange reaction will change the number of S-S bonds. Accordingly S-S concentration ( $v_{S-S}$ ) can be calculated by equation 4.3:

$$v_{S-S} [\text{mol}/\text{m}^3] = \frac{\rho w}{M_{BDS}} \quad (4.3)$$

where  $\rho$  is the density of polymer;  $w$  is the weight fraction of BDS in raw material and  $M_{BDS}$  is the molar mass of BDS, respectively.

For other polymers in this study,  $v_{S-S}$  was determined based on S-S bond peak area in the Raman spectrum. The  $v_{S-S}$  concentrations and the S-S bond peak area in the Raman spectrum of BDS-An and BDS-DD1 were used as the internal standards:

$$v_{S-S, \text{polymer X}} = \frac{\text{Area}_{S-S, \text{polymer X}}}{\text{Area}_{S-S, \text{reference}}} \times v_{S-S, \text{reference}} \quad (4.4)$$

#### 4.2.3.8 Irreversible crosslink density determination

According to the theory of rubber elasticity [37, 38], the crosslink density ( $v_e$ ) of highly crosslinked thermosets can be calculated by applying the simplified equation:

$$v_e = \frac{E'}{3RT} \quad (4.5)$$

where  $E'$  is the tensile storage modulus of rubbery plateau which as obtained by DMTA,  $T$  is pertinent temperature in Kelvin (in this study  $T = T_g + 60^\circ\text{C}$ ), and  $R$  is the gas constant.



## 4.3 Results

### 4.3.1 Without catalyst

#### 4.3.1.1 Ancamine system

The morphology of BTS-An polymer and BDS-An polymer are shown in Figure 4.3. A lot of 'cavities' can be observed in BTS-An polymer and BDS-An polymer cured for 2h. The 'cavity' size in BTS-An polymer is much smaller than that in BDS-An polymer. As the densities of BTS-An polymer and BDS-An polymers as a function of the curing time do not show significant changes, this indicates that the 'cavities' should be filled by a liquid phase which evaporated during gold sputtering in vacuum to prepare the samples for SEM analysis. To test the hypothesis new samples were cut in air and the liquid phase was carefully collected from fresh-cut cross sections of the BTS-An polymer and the BDS-An polymer after curing for 2h and the chemical composition of the liquid collected was measured by FTIR. The FTIR spectra clearly show that the liquid phase is mainly BTS or BDS monomer.

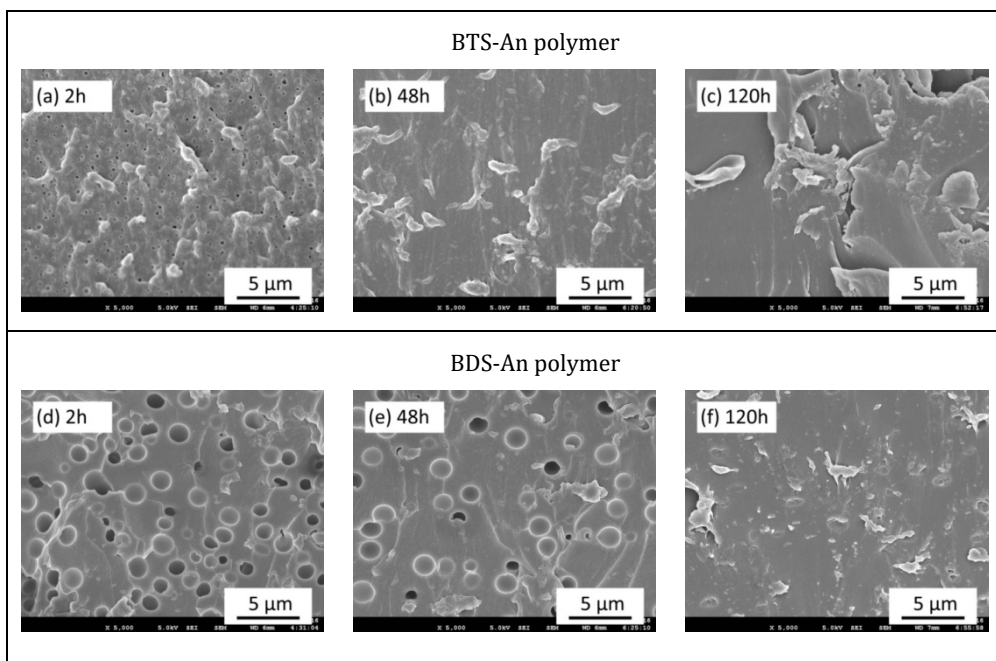
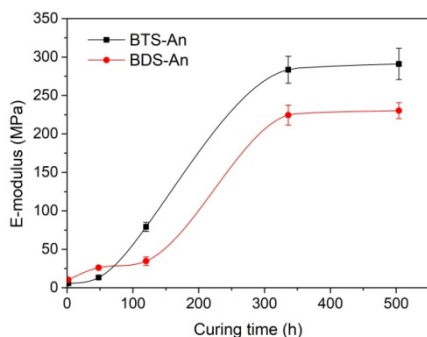
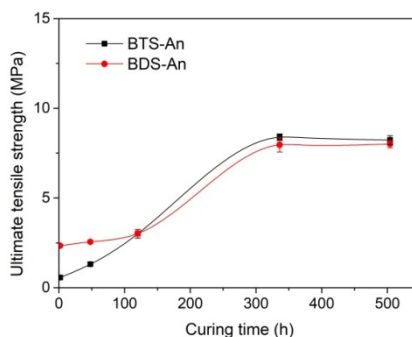


**Figure 4.3** SEM images of the fresh-cut cross section of BTS-An polymer curing for (a) 2h, (b) 48h, (c) 120h and BDS-An polymer curing for (d) 2h, (e) 48h, (f) 120h.

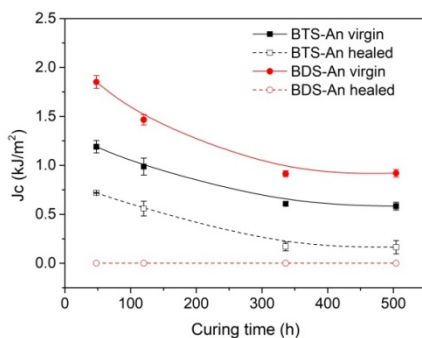
The mechanical properties of BTS-An polymer and BDS-An polymer are shown in Figure 4.4. The E-modulus and ultimate tensile strength of BTS-An polymer and BDS-An polymer both increase with curing time and reach maximum after 336h curing, which indicates that full curing has been achieved after 336h.  $J_c$  of virgin BTS-An polymer and virgin BDS-An polymer decreases with curing time. After healing at 70 °C under 0.3 bar pressure for 4 h,  $J_c$  of healed BTS-An polymer decreases with curing time leading to a decrease in FHE from 61% to 28% while BDS-An polymer does not show any effective healing no matter how long it cures.



(a)



(b)



(c)

**Figure 4.4** Mechanical properties of non-catalyst Ancamine system. (a) E-modulus; (b) ultimate tensile strength; (c)  $J_c$ , healing condition: 70 °C, 0.3 bar pressure, 4 h.

### 4.3.1.2 DD1 system

The morphology of BTS-DD1 polymer and BDS-DD1 polymer are shown in Figure 4.5. It is clear that after curing for only 2 h, both BTS-DD1 polymer and BDS-DD1 polymer are homogenous, no phase separation can be observed. Further curing does not change the polymer morphology.

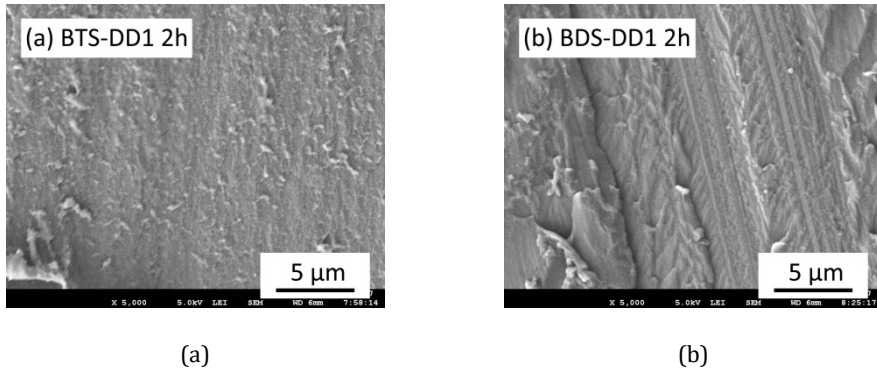


**Figure 4.5** SEM images of the fresh-cut cross section of (a) BTS-DD1 polymer curing for 2h, and (b) BDS-DD1 polymer curing for 2h.

The mechanical properties of BTS-DD1 polymer and BDS-DD1 polymer are shown in Figure 4.6. Data plotted the same range as Figure 4.4 for easy comparison. The evolution trend is very similar to Ancamine system. The E-modulus and ultimate tensile strength of BTS-DD1 polymer and BDS-DD1 polymer both increase with curing time.  $J_c$  of virgin BTS-DD1 polymer and virgin BDS-DD1 polymer decreases with curing time. After healing at 70 °C under 0.3 bar pressure for 4 h,  $J_c$  of healed BTS-DD1 polymer decreases with curing time leading to a decrease in FHE from 64% to 30% while BDS-DD1 polymer loses healing ability.

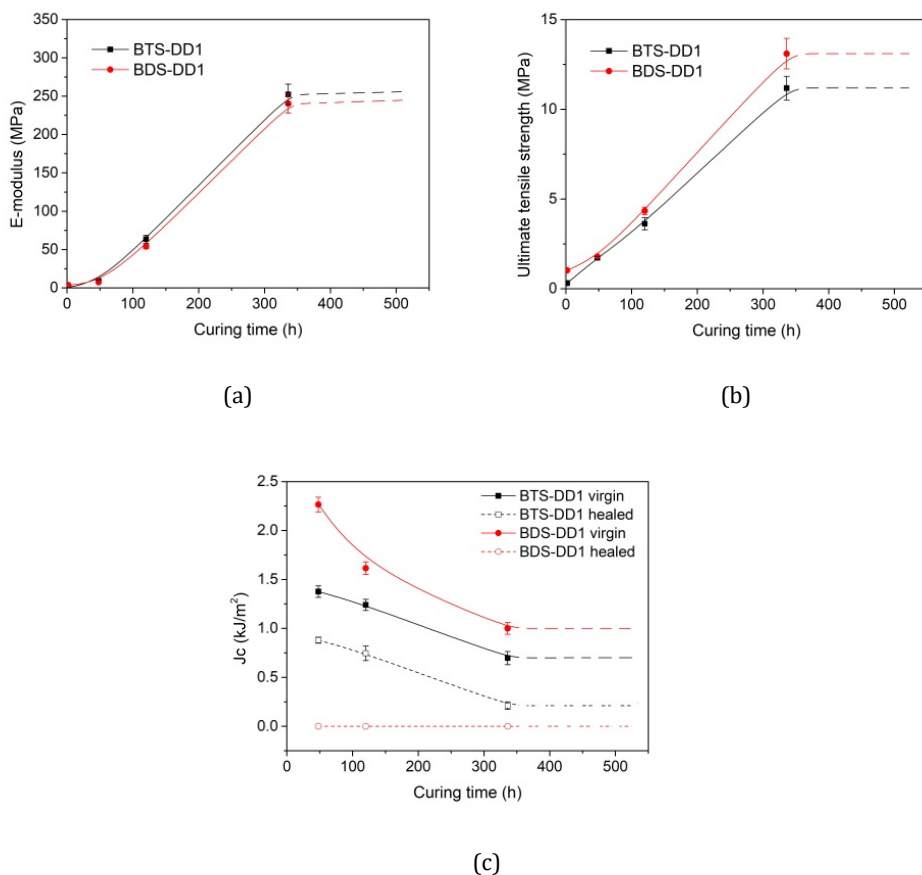


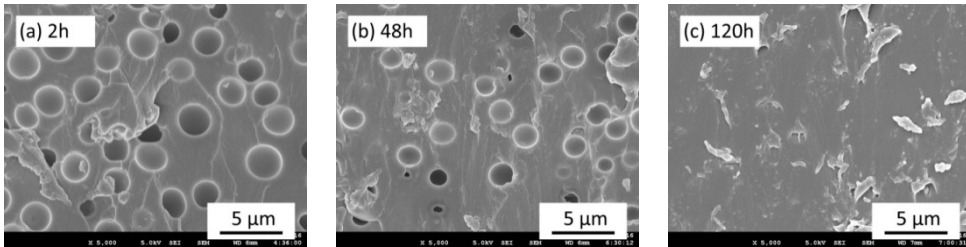
**Figure 4.6** Mechanical properties of non-catalyst DD1 system. (a) E-modulus; (b) ultimate tensile strength; (c)  $J_c$ , healing condition: 70 °C, 0.3 bar pressure, 4 h.

### 4.3.2 With catalyst

In order to improve healing in BDS based polymers, disulfide bond cleavage catalyst TEA was applied.

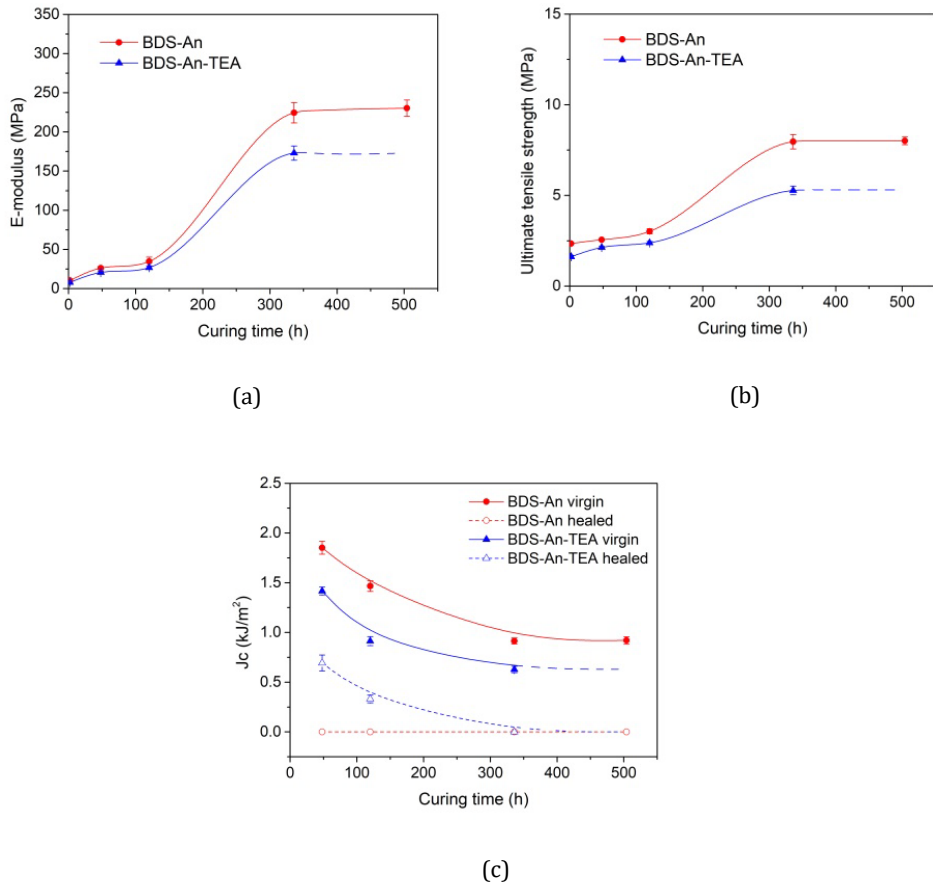
### 4.3.2.1 Ancamine system

Figure 4.7 shows the morphology of BDS-An-TEA polymer. Significant phase separation can be observed, which is similar to BDS-An polymer as shown in Figure 4.3.



**Figure 4.7** SEM images of the fresh-cut cross section of BDS-An-TEA polymer curing for (a) 2 h, (b) 48 h and (c) 120 h.

Figure 4.8 shows the effect of catalyst TEA on mechanical properties of BDS-Ancamine system. Comparing to BDS-An polymer, the addition of TEA makes the polymer softer and weaker. It is reasonable because TEA makes S-S bonds easier to break. After curing for 336 h, the E-modulus of BDS-An-TEA reaches 173 MPa (23% lower than that of BDS-An polymer) and ultimate tensile strength is 5.3 MPa (34% lower than that of BDS-An polymer). Although the application of TEA decreases the mechanical properties, it promotes self-healing in BDS based polymer, as shown in Figure 4.8(c).



**Figure 4.8** The effect of catalyst TEA on mechanical properties of BDS-Ancamine system. (a) E-modulus; (b) ultimate tensile strength; (c)  $J_c$ , healing condition: 70 °C, 0.3 bar pressure, 4 h.

#### 4.3.2.2 DD1 system

The effect of catalyst TEA on mechanical properties of BDS-DD1 system is shown in Figure 4.9. The evolution trend is also similar to BDS-Ancamine system.

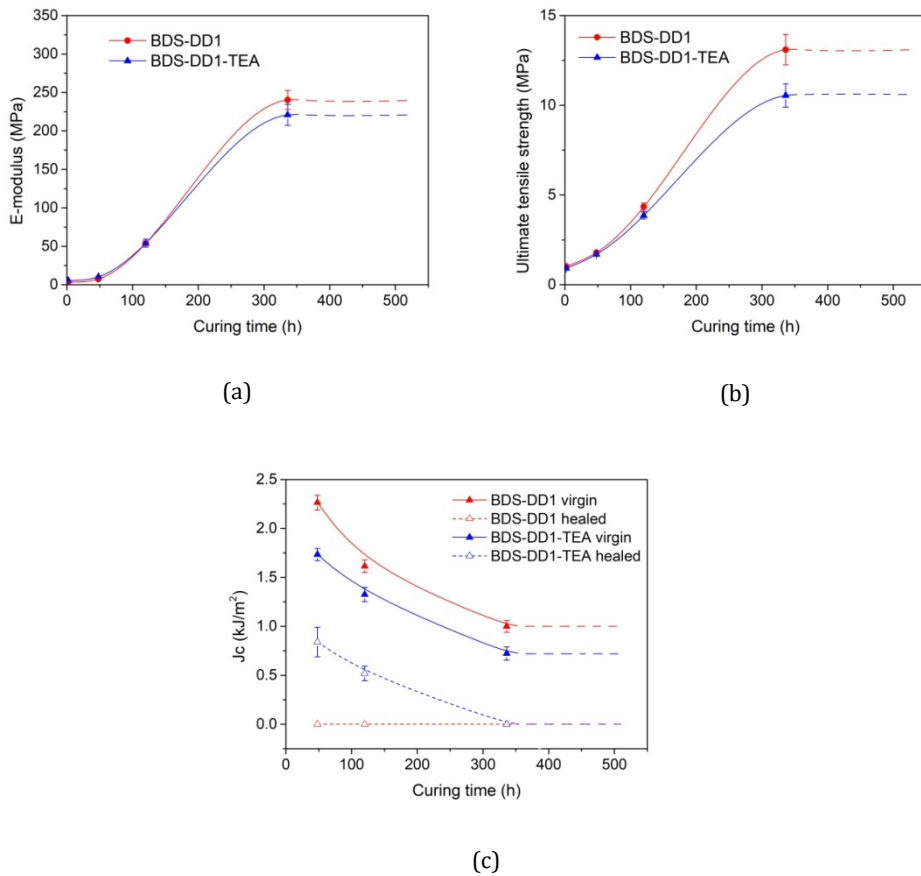


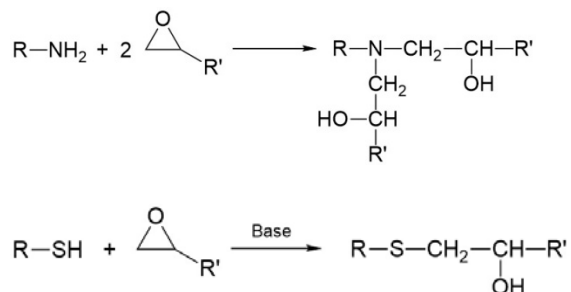
**Figure 4.9** The effect of catalyst TEA on mechanical properties of BDS-DD1 system. (a) E-modulus; (b) ultimate tensile strength; (c)  $J_c$ , healing condition: 70 °C, 0.3 bar pressure, 4 h.

## 4.4 Discussion

### 4.4.1 Curing mechanism

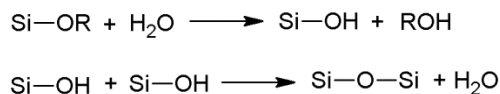
The curing of organic–inorganic dual network polymers in this work mainly consists of four kinds of reactions: (1) epoxy/amine reaction; (2) epoxy/thiol reaction; (3) alkoxy silane condensation reaction; (4) tetra–sulfide/thiol reaction.

Epoxy/amine reaction and epoxy/thiol reaction are shown in schematic 4.1. These two reactions complete in less than 2 h, which is confirmed by our previous work[14].



**Schematic 4.1** Epoxy/amine reaction and epoxy/thiol reaction.

The reason why E-modulus and ultimate tensile strength of samples in this work increase with curing time after 2h is alkoxy silane condensation reaction, as shown in schematic 4.2.



**Schematic 4.2** Alkoxy silane condensation reactions.

The alkoxy silane condensation reaction was monitored by FTIR, as shown in Figure 4.10. The absorption at 1100 cm<sup>-1</sup> corresponds to Si-OC<sub>2</sub>H<sub>5</sub> stretching, 1076 cm<sup>-1</sup> corresponds to Si-OCH<sub>3</sub> stretching, 1036 cm<sup>-1</sup> corresponds to Si-O-Si stretching and 957 cm<sup>-1</sup> corresponds to Si-OH stretching, respectively. It is very clear that the amount of Si-OC<sub>2</sub>H<sub>5</sub>, Si-OCH<sub>3</sub> and Si-OH decreases during curing resulting in formation of Si-O-Si bridges and increase of irreversible crosslink density. The effect of curing time on the irreversible crosslink density is shown in Figure 4.11.



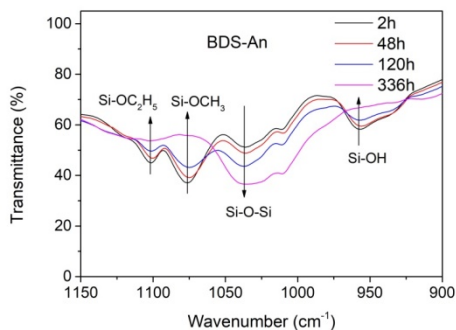
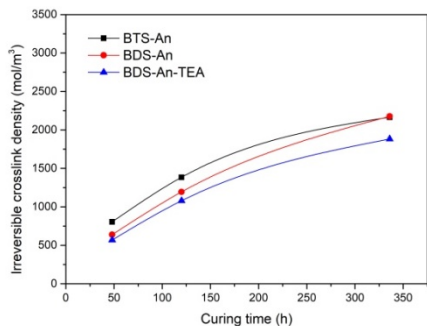
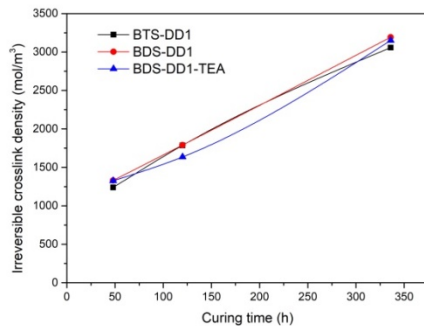


**Figure 4.10** FTIR spectra of BDS-An polymer curing for different time.



(a)



(b)

**Figure 4.11** The effect of curing time on the irreversible crosslink density, (a) Ancamine system; (b) DD1 system.

It needs to be addressed that at the beginning of the curing process (within the first few minutes) of BTS containing polymers (BTS-An and BTS-DD1), a noticeable and unpleasant  $\text{H}_2\text{S}$  gas release occurred, while this situation did not emerge during the curing process of the BDS containing polymers (BDS-An, BDS-An-TEA, BDS-DD1 and BDS-DD1-TEA). In order to understand what happens to tetra-sulfide unit in the polymers synthesized with BTS, the various S-based chemical bonds present were determined by Raman spectroscopy. In Figure 4.12, the peaks at  $458\text{ cm}^{-1}$  and  $489$

$\text{cm}^{-1}$  represent S–S bond in the middle of –S–S–S– in BTS while the peak at  $509 \text{ cm}^{-1}$  represents S–S bond in BDS. It can be noticed that the spectrum of BDS monomer also contains small peaks at  $458 \text{ cm}^{-1}$  and  $489 \text{ cm}^{-1}$ , which are due to impurity. Figure 4.12 clearly shows that the peaks at  $458 \text{ cm}^{-1}$  and  $489 \text{ cm}^{-1}$  disappear and the peak at  $509 \text{ cm}^{-1}$  appears in cured BTS-An polymer, which indicates that original tetra-sulfide bridges were mainly converted into disulfide bridges during curing, under the release of  $\text{H}_2\text{S}$ .

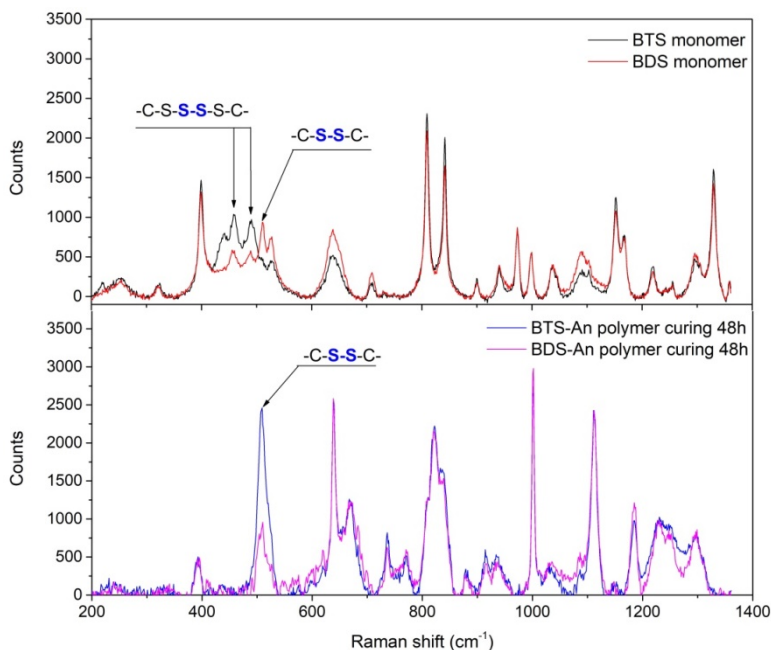


**Figure 4.12** Raman spectra of BTS monomer, BDS monomer, BTS-An polymer and BDS-An polymer.

It is interesting to see that the disulfide bond peak area of BTS-An polymer is 2.5 times as big as that of BDS-An polymer, although molar fraction of BTS and BDS are the same in raw materials (the spectra were normalized based on the peak at  $1112 \text{ cm}^{-1}$  which corresponds C–H stretching of aromatic ring in epoxy resin), which means that the disulfide bond concentration in BTS-An polymer is much higher than in the BDS-An polymer. We believe that the increasing of disulfide bond concentration in BTS-An polymer is due to the reaction of tetra-sulfide bond and thiol group, which also leads to the noticeable gas release (presumably  $\text{H}_2\text{S}$ ). The

disulfide bond concentrations of samples curing for different time are listed in Table 4.2.

**Table 4.2** Disulfide bond concentration of samples curing for different time.

Disulfide bond concentration $v_{S-S}$ (mol/m <sup>3</sup> )							
Sample	Curing time			Sample	Curing time		
	48h	120h	336h		48h	120h	336h
BTS-An	1407	1399	1397	BDS-DD1	508	508	513
BDS-An	556	570	570	BDS-DD1-TEA	508	510	513
BDS-An-TEA	558	570	570	0.2BTS0.8BDS-An	706	713	720
BTS-DD1	1140	1160	1147	0.5BTS0.5BDS-An	1006	1017	1024

#### 4.4.2 Healing mechanism

The healing mechanism of organic–inorganic dual network polymers in this work is dynamic disulfide exchange reaction which involves scission of the reversible sulfur–sulfur (S–S) bonds (generating thiyl radicals) to provide temporary local mobility of the polymer networks followed by their recombination to yield new polymer chains.

The scission of disulfide bond is promoted either by UV light or by elevated temperature[39, 40]. So the healing temperature in this work is set at 70°C. At the same healing temperature, higher disulfide bond concentration provides more bond cleavage hence leading to higher temporary local mobility that is essential for healing. This is the reason why BTS-An polymer shows good healing ability while BDS-An polymer does not. (The disulfide bond concentration in BTS-An polymer is about 2.5 times as high as that in the BDS-An polymer, as shown in Figure 4.12.)

Experiments show that nucleophiles such as TEA or tri-*n*-butyl phosphine can effectively promote the cleavage of disulfide bonds [19-21]. So when TEA is applied in BDS based systems (BDS-An-TEA polymer and BDS-DD1-TEA polymer), the

amount of debonded disulfide bonds is high enough to provide necessary local network mobility for healing.

Although alkoxy silane condensation reaction is still going on during healing process, it is not responsible for healing. Because in BDS-An and BDS-DD1 polymer alkoxy silane condensation reaction also exists however these two polymer do not show effective healing. TEA promotes healing in BDS-An-TEA and BDS-DD1-TEA polymer by catalyze the disulfide interchange reactions.

#### **4.4.3 The effect of disulfide bond concentration versus irreversible crosslink density on the healing of polymers**

Polymer architecture plays an important role in designing self-healing materials. The reversible bond (disulfide bond) concentration is one essential parameter. The work done by Canadell et al.[7] and AbdolahZadeh et al.[14] show that healing efficiency decreases with disulfide bond concentration decreasing. Another key parameter is irreversible crosslink density. A lot of studies show that higher irreversible crosslink density always provides better mechanical property but worse healing efficiency [30-33]. The dual network polymer provides an ideal system to study the effect of polymer architecture on healing behavior. By using BTS or BDS or mixture of BTS and BDS, the disulfide bond concentration can be tuned. By curing for different time, the irreversible crosslink density can be adjusted. Figure 4.13(a) shows that without the help of catalyst TEA, polymers in this work can only heal if the disulfide bond (reversible bond) concentration is higher than  $900 \text{ mol/m}^3$ . This is due to the break of reversible bonds leading to temporary local network mobility which is necessary for flow and damage repair. If the reversible bond concentration is not high enough the local network mobility cannot lead to effective flow and healing. Among all healable polymers, the fracture healing efficiency decreases with the irreversible crosslink density increasing (curing time increasing) because high irreversible crosslink density will restrict the local network mobility. In Figure 4.13(a) data by other researchers [7, 30] are also included for low crosslink density region.

The application of disulfide cleavage catalyst TEA significantly expands the L-shaped "healing zone", as shown in Figure 4.13(b). Polymers containing low reversible bond concentration (about  $500 \text{ mol/m}^3$ ) can heal with the help of TEA. Because TEA

makes disulfide bond easier to break thereby reduces the minimum reversible bond concentration to provide enough local network mobility for healing.

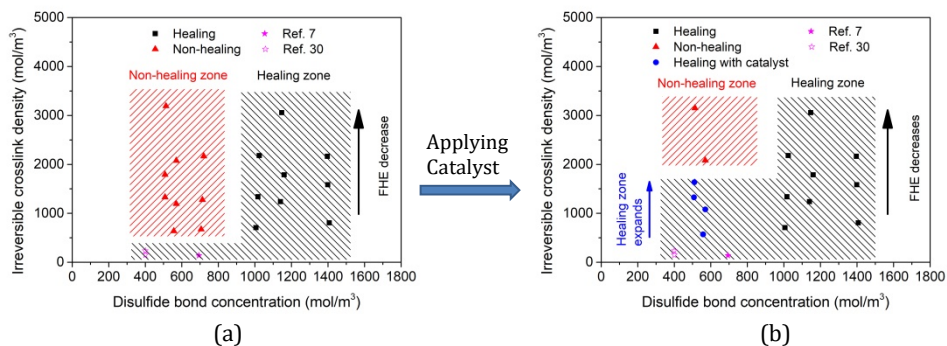


**Figure 4.13** The effect of disulfide bond concentration versus irreversible crosslink density on the healing of polymers: (a) without catalyst; (b) with catalyst TEA.

4

## 4.5 Conclusion

In this study, healable organic–inorganic dual network polymers, which have potential application as the matrix of TIMs and other composites, are developed. Using BDS monomer instead of BTS monomer significantly reduces gas production during curing while decreases disulfide bond concentration in polymer that leads to the loss of healing ability. The reversible bond (disulfide bond) concentration should be high enough to provide enough local network mobility for flow and damage repair. The irreversible crosslink density increases with curing time leading to decrease of fracture healing efficiency because high irreversible crosslink density will restrict the local network mobility. The application of disulfide cleavage catalyst TEA can promote self-healing in polymers with low reversible bond concentration due to its ability to make disulfide bond easier to break.

## References

1. Wu DY, Meure S, Solomon D. Self-healing polymeric materials: a review of recent developments. *Progress in Polymer Science*. 2008;33(5):479-522.
2. Yuan Y, Yin T, Rong M, Zhang M. Self healing in polymers and polymer composites. Concepts, realization and outlook: A review. *Express Polymer Letters*. 2008;2(4):238-250.
3. Cho SH, White SR, Braun PV. Self-healing polymer coatings. *Advanced Materials*. 2009;21(6):645-649.
4. Hager MD, Greil P, Leyens C, van der Zwaag S, Schubert US. Self-healing materials. *Advanced Materials*. 2010;22(47):5424-5430.
5. White SR, Sottos NR, Geubelle PH, Moore JS, Kessler MR, Sriram SR, et al. Autonomic healing of polymer composites. *Nature*. 2001;409:794.
6. Mookhoek SD. Novel routes to liquid-based self-healing polymer systems. 2010.
7. Canadell J, Goossens H, Klumperman B. Self-Healing Materials Based on Disulfide Links. *Macromolecules*. 2011;44(8):2536-2541.
8. Liu Y-L, Chuo T-W. Self-healing polymers based on thermally reversible Diels-Alder chemistry. *Polymer Chemistry*. 2013;4(7):2194-2205.
9. Cordier P, Tournilhac F, Soulié-Ziakovic C, Leibler L. Self-healing and thermoreversible rubber from supramolecular assembly. *Nature*. 2008;451(7181):977.
10. Bode S, Zedler L, Schacher FH, Dietzek B, Schmitt M, Popp J, et al. Self-Healing Polymer Coatings Based on Crosslinked Metallosupramolecular Copolymers. *Advanced Materials*. 2013;25(11):1634-1638.
11. van der Zwaag S, Grande AM, Post W, Garcia SJ, Bor TC. Review of current strategies to induce self-healing behaviour in fibre reinforced polymer based composites. *Materials Science and Technology*. 2014;30(13):1633-1641.
12. Zhong N, Post W. Self-repair of structural and functional composites with intrinsically self-healing polymer matrices: A review. *Composites Part A: Applied Science and Manufacturing*. 2015;69:226-239.
13. Zhang Z, Hu Y, Liu Z, Guo T. Synthesis and evaluation of a moisture-promoted healing copolymer. *Polymer*. 2012;53(14):2979-2990.
14. AbdolahZadeh M, Esteves C, Catarina A, Zwaag S, Garcia SJ. Healable dual organic-inorganic crosslinked sol-gel based polymers: crosslinking density and tetrasulfide content effect. *Journal of Polymer Science Part A: Polymer Chemistry*. 2014;52(14):1953-1961.
15. Hernández M, Grande AM, Dierkes W, Bijleveld J, van der Zwaag S, García SJ. Turning Vulcanized Natural Rubber into a Self-Healing Polymer: Effect of the Disulfide/Polysulfide Ratio. *ACS Sustainable Chemistry & Engineering*. 2016;4(10):5776-5784.
16. Post W, Cohades A, Michaud V, van der Zwaag S, Garcia SJ. Healing of a glass fibre reinforced composite with a disulphide containing organic-inorganic epoxy matrix. *Composites Science and Technology*. 2017;152:85-93.
17. Rekondo A, Martin R, Ruiz de Luzuriaga A, Cabanero G, Grande HJ, Odriozola I. Catalyst-free room-temperature self-healing elastomers based on aromatic disulfide metathesis. *Materials Horizons*. 2014;1(2):237-240.

18. Nevejans S, Ballard N, Miranda JJ, Reck B, Asua JM. The underlying mechanisms for self-healing of poly (disulfide) s. *Physical Chemistry Chemical Physics*. 2016;18(39):27577-27583.
19. Sarma RJ, Otto S, Nitschke JR. Disulfides, imines, and metal coordination within a single system: interplay between three dynamic equilibria. *Chemistry-A European Journal*. 2007;13(34):9542-9546.
20. Lei ZQ, Xiang HP, Yuan YJ, Rong MZ, Zhang MQ. Room-temperature self-healable and remoldable cross-linked polymer based on the dynamic exchange of disulfide bonds. *Chemistry of Materials*. 2014;26(6):2038-2046.
21. Caraballo R, Rahm M, Vongvilai P, Brinck T, Ramström O. Phosphine-catalyzed disulfide metathesis. *Chemical Communications*. 2008(48):6603-6605.
22. Arisawa M, Yamaguchi M. Rhodium-catalyzed disulfide exchange reaction. *Journal of the American Chemical Society*. 2003;125(22):6624-6625.
23. Xiang H, Qian H, Lu Z, Rong M, Zhang M. Crack healing and reclaiming of vulcanized rubber by triggering the rearrangement of inherent sulfur crosslinked networks. *Green Chemistry*. 2015;17(8):4315-4325.
24. Landel RF, Nielsen LE. *Mechanical properties of polymers and composites*: CRC press; 1993.
25. Lötters JC, Olthuis W, Veltink P, Bergveld P. The mechanical properties of the rubber elastic polymer polydimethylsiloxane for sensor applications. *Journal of micromechanics and microengineering*. 1997;7(3):145.
26. Van Krevelen DW, Te Nijenhuis K. *Properties of polymers: their correlation with chemical structure; their numerical estimation and prediction from additive group contributions*: Elsevier; 2009.
27. Kannurpatti AR, Anseth JW, Bowman CN. A study of the evolution of mechanical properties and structural heterogeneity of polymer networks formed by photopolymerizations of multifunctional (meth)acrylates. *Polymer*. 1998;39(12):2507-2513.
28. Clark AH, Ross-Murphy SB. *Structural and mechanical properties of biopolymer gels*. *Biopolymers*: Springer; 1987. p. 57-192.
29. Garcia SJ. Effect of polymer architecture on the intrinsic self-healing character of polymers. *European Polymer Journal*. 2014;53:118-125.
30. Grande AM, Martin R, Odriozola I, van der Zwaag S, Garcia SJ. Effect of the polymer structure on the viscoelastic and interfacial healing behaviour of poly(urea-urethane) networks containing aromatic disulphides. *European Polymer Journal*. 2017;97:120-128.
31. Lafont U, van Zeijl H, van der Zwaag S. Influence of Cross-linkers on the Cohesive and Adhesive Self-Healing Ability of Polysulfide-Based Thermosets. *ACS Applied Materials & Interfaces*. 2012;4(11):6280-6288.
32. Chen Q, Zhu L, Chen H, Yan H, Huang L, Yang J, et al. A Novel Design Strategy for Fully Physically Linked Double Network Hydrogels with Tough, Fatigue Resistant, and Self-Healing Properties. 2015;25(10):1598-1607.
33. Zechel S, Geitner R, Abend M, Siegmann M, Enke M, Kuhl N, et al. Intrinsic self-healing polymers with a high E-modulus based on dynamic reversible urea bonds. *Npg Asia Materials*. 2017;9:e420.

34. Ramorino G, Agnelli S, De Santis R, Riccò T. Investigation of fracture resistance of natural rubber/clay nanocomposites by J-testing. *Engineering Fracture Mechanics*. 2010;77(10):1527-1536.
35. Grande AM, Garcia SJ, van der Zwaag S. On the interfacial healing of a supramolecular elastomer. *Polymer*. 2015;56(0):435-442.
36. Grande AM, Bijleveld JC, Garcia SJ, van der Zwaag S. A combined fracture mechanical - rheological study to separate the contributions of hydrogen bonds and disulphide linkages to the healing of poly(urea-urethane) networks. *Polymer*. 2016;96:26-34.
37. Hill LW. Calculation of crosslink density in short chain networks. *Progress in Organic Coatings*. 1997;31(3):235-243.
38. Garcia SJ, Serra A, Suay J. Lanthanide triflates as curing initiators for solid DGEBA resin: Thermal and mechanical characterization. *Journal of applied polymer science*. 2007;105(5):3097-3107.
39. Koval' IVEJRCR. The chemistry of disulfides. 1994;63(9):735-750.
40. Nevejans S, Ballard N, Miranda JI, Reck B, Asua JM. The underlying mechanisms for self-healing of poly(disulfide)s. *Physical Chemistry Chemical Physics*. 2016;18(39):27577-27583.





# Chapter 5

---

**The effect of filler parameters on the healing of thermal conductivity and mechanical properties of a thermal interface material based on a self-healable organic-inorganic polymer matrix**

---

**This chapter has been published as:**

**Zhong N, Garcia SJ, van der Zwaag S**

*The effect of filler parameters on the healing of thermal conductivity and mechanical properties of a thermal interface material based on a self-healable organic-inorganic polymer matrix*

Smart Materials and Structures. 2016;25(8):084016.

## 5.1 Introduction

Nowadays with electronic devices becoming smaller and more powerful, the heat dissipation from the active component has become one of the most important issues in determining the product life times and a factor which restricts the development of the electronics and solid state lighting industry. Usually a relatively large metallic heat sink is used to dissipate the heat produced during operation. However direct bonding of the active die to the heat sink is generally not possible [1]. Thermal interface materials (TIMs), consisting of a flexible polymeric matrix filled with highly thermally conductive filler particles, are widely used as gap-filler materials between heat sink and electronic device to control the heat dissipation and to provide mechanical anchoring as shown in Figure 5.1. Aging of TIMs may lead to delamination and internal crack formation causing loss of heat transfer and mechanical integrity leading to premature device failure. In order to make electronic devices more reliable and longer lasting, in the present study the self-healing concept was introduced to TIMs using the guidelines presented in the recent literature[2].

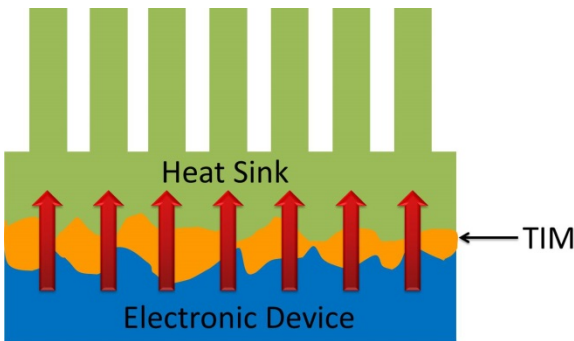


**Figure 5.1** Schematic of the location of Thermal Interface Materials (TIMs) in electronic devices between the heat source (electronic device) and the heat sink. Note that the drawing is not at scale to real systems.

Over the last decade, several concepts leading to materials which have the ability to autonomously repair damage and restore lost or degraded properties using resources inherently available to the system, the so-called intrinsic healing strategy, have been presented [3-6]. During the early stages of development of the field of self-healing materials, the extrinsic healing strategy, in which the healing was due to

the inclusion of discrete 'foreign' healing particles in an otherwise inert and conventional matrix material, was popular [7-10]. While the approach certainly has merit and was shown to work well, an intrinsic negative feature of the approach is that once activated the healing particles are not available for a second healing operation. More recently, intrinsic self-healing polymers based on reversible bond such as hydrogen bonding, Diels-Alder/retro-Diels-Alder reaction, and disulfide chemistry have been developed which have the potential to locally heal damage many times [11-14]. By applying an intrinsic self-healing polymer as the matrix in which functional particles are distributed, granulate composites can be created which can restore mechanical or functional properties (e.g. electrically conductivity, piezoelectric properties, etc.) after the occurrence of local damage [15-18]. Although it seems attractive to introduce self-healing concept to TIMs [19, 20], only a few attempts have been made in this field so far. Early work led to the development of thermally conductive adhesives consisting of self-healing polysulfide-based thermoset matrices containing boron nitride or graphite particles [2]. These composites exhibit recovery of both cohesion and adhesion properties at a mild healing temperature (65°C). However, a systematic study of the effect of particle parameters such as particle volume concentration (PVC) and particle size on the thermal and mechanical healing efficiency has not been presented yet. Aim of the present work is to present such a study using a novel organic-inorganic network polymer containing reversible tetra-sulfide units as the matrix. As model fillers, glass spheres were used.

## 5.2 Experimental

### 5.2.1 Material preparation

In the present study, a dual organic (epoxy-amine) –inorganic (siloxane) crosslinked polymer containing non-reversible crosslinks and reversible groups based on tetra-sulfides [14] was used as the matrix and glass beads with four different mean particle sizes (6µm, 63µm, 96µm, 185µm, respectively) were used as filler. It should be noted that low thermally conductive glass beads were used in this work because, opposite to highly thermally conductive particles typically used in industry such as alumina, aluminum nitride, graphite, and metal powders, they offer a wide range of sizes with the same geometry therefore allowing for systematic analysis of the effect of the particle parameters on the healing. At first, a pre-mixture of Bis[3-

(triethoxysilyl)propyl]tetrasulfide (purity 99%, total sulfur content > 20%, from SiSiB SILANES, China), (3-Aminopropyl)trimethoxysilane (purity 97%, from Sigma-Aldrich, the Netherlands) and an epoxy resin Epikote™ 828 (184-190 g/eq, from Akzo Nobel, the Netherlands) was stirred using a magnetic stirrer at 300 rpm for 3 h at room temperature. Then the required amount of organic crosslinker Ancamine® 2500 (105-110 g/eq, from Akzo Nobel, the Netherlands) and glass beads (from Sigmund Lindner GmbH, Germany) with a volume fraction between 30 vol.% and 50 vol.% were mixed with the pre-mixture in a high speed mixer at 2500 rpm for 5 min. The mixture was degassed in a vacuum chamber for 20 min. Pentaerythritol tetrakis (3-mercaptopropionate) (purity>95%, from Sigma-Aldrich, the Netherlands) was then mixed with the mixture in a high speed mixer at 2500 rpm for 0.5 min and the solution was cast in a rectangular Teflon mold to create a 2 mm thick film, relatively free of air bubbles. Finally, the resulting composite was cured at 70 °C for 48 h in the Teflon mold. The weight ratio of all components in the self-healing polymer matrix was stated in Table 5.1. A polymer epoxy Epikote™ 828 -amine Ancamine® 2500 with Pentaerythritol tetrakis (3-mercaptopropionate) in the same amounts as the self-healing systems was used as the reference non-self-healing polymer.

**Table 5.1** Weight ratio of all components in the self-healing polymer matrix

Chemicals	Weight ratio
Epikote™ 828	1 g
Bis[3-(triethoxysilyl)propyl]tetrasulfide	0.733 g
(3-Aminopropyl)trimethoxysilane	0.076 g
Ancamine® 2500	0.579 g
Pentaerythritol tetrakis(3-mercaptopropionate)	0.566 g

### 5.2.2 Mechanical healing test

To investigate the mechanical healing, tensile strength tests using dog bone shaped samples (ASTM D1708) were performed. A notch (approximately 0.5 mm in length and cut through the thickness of samples) was applied using a fresh scalpel on one side of the dog bone shaped sample and the ultimate tensile strength was evaluated at room temperature using an Instron 3365 tensile testing machine with a 1 kN load cell and a cross-head speed of 5 mm/min. After complete failure during tensile testing, the two parts of the sample were repositioned carefully and put into a Teflon

mold with the same size as the original sample. A contrast experiment was performed by rotating one of the broken parts 180° and reconnected. A healing step at 70°C for 2 h under 1 bar pressure followed based on our previous works [14, 21]. Then the same tensile testing procedure on the healed samples was carried out. The tensile strength healing efficiency (TSHE) was calculated using the following equation 5.1:

$$\text{TSHE} = \frac{\sigma_{\text{healed}}}{\sigma_{\text{virgin}}} \times 100\% \quad (5.1)$$

where  $\sigma_{\text{healed}}$  and  $\sigma_{\text{virgin}}$  are the ultimate tensile strength of healed sample and original sample, respectively.

### 5.2.3 Thermal conductivity restoration test

To monitor the recovery of the thermal conductivity, two kinds of samples were prepared. The first set of samples, which is called the “virgin system”, is made by curing a TIM cylinder ( $\Phi$  36 mm, height 5 mm) on a smooth aluminum foil (40×40×0.2 mm). The second system, which is called “crack system”, was prepared by increasing the surface roughness of the TIM by scratching it about 30 times with a fresh scalpel before bringing the damaged surface in contact with the aluminum foil. The contact area of the ‘crack system’ is the same as that of the ‘virgin system’. This approach ensures the formation of air gap between the TIM and the aluminum foil (leading to a decrease of the thermal conductivity of the system) to mimic delamination in actual de-bonded TIMs. After evaluation of the initial thermal conductivity of the ‘crack system’, a healing step at 70°C for 2h under 0.3 bar pressure was then performed leading to a so-called “healed system”. The thermal conductivity of both the pure TIMs and the whole systems was measured at room temperature using a modified transient source technique on a TCi C-Therm ® apparatus. Distilled water was used as the contact agent.

### 5.3 Results and discussion

In TIM composites, a high PVC is preferred because of the higher fraction of thermally conductive material. Therefore in the present work a minimum PVC of 30 vol.% is used and the effect of particle size on mechanical healing and thermal conductivity restoration was studied in more detail for TIMs with a 50 vol.% loading.

#### 5.3.1 The effect of PVC on mechanical properties and healing efficiency

Figure 5.2 shows that the ultimate tensile strength of self-healing TIMs loaded with glass beads (mean particle size of 6  $\mu\text{m}$ ) increases with increasing PVC. When the PVC is up to 50 vol%, the ultimate tensile strength of TIMs reaches a value of 3.26MPa, which is about 6 times that of the pure polymeric matrix (0.52MPa). For other particle sizes similar effects were obtained. The rise in tensile strength with PVC indicates that there is strong adhesion between the polymeric matrix and the glass beads, which is probably due to the silanes presenting in the self-healing polymeric matrix. Figure 5.2 also shows that after healing at 70°C for 2 h under 1 bar pressure, the tensile strength of self-healing TIMs reach almost the same value (about 0.6 MPa) independently of the glass beads loading (PVC). This suggests that the type of interface created is independent of the particle size and similar to that one created in the unloaded healed polymer (0.5 MPa). Accordingly, the tensile strength healing efficiency decreases significantly with increasing PVC as shown in Figure 5.3.

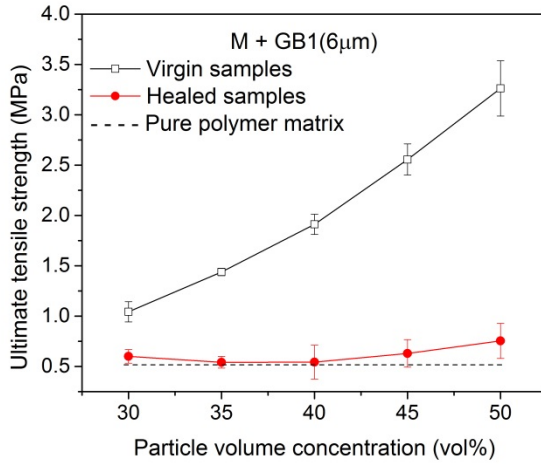


**Figure 5.2** The effect of particle volume concentration on ultimate tensile strength of glass beads loaded TIMs (black solid squares: virgin samples; red hollow circles: healed samples; dash line: indication of the interfacial healed strength level of the unloaded polymer matrix).

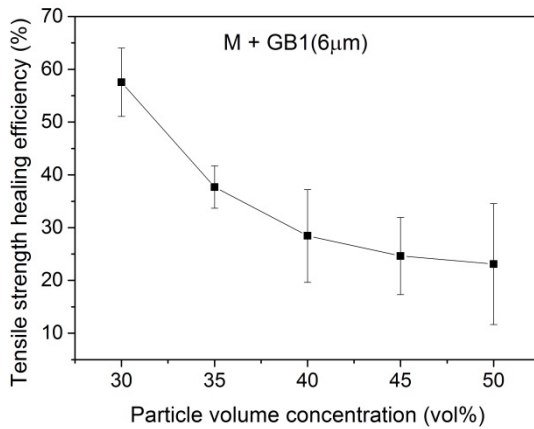


**Figure 5.3** The effect of particle volume concentration on tensile strength healing efficiency of glass beads loaded TIMs.



### 5.3.2 The effect of particle size on mechanical healing

The ultimate tensile strength of 50 vol% glass beads loaded TIMs was found to decrease when the particle size increases, as shown in Figure 5.4. The ultimate tensile strength of TIMs loaded with bigger particles (diameter 185  $\mu\text{m}$ ) was only half that of composites filled to the same PVC but containing smaller particles (diameter 6  $\mu\text{m}$ ). As it can be seen in Figure 5.4, after healing at 70°C for 2h under 1 bar pressure, the well repositioned TIMs recover to similar ultimate tensile strength values independently of the particle size (i.e. 0.7 MPa). Consequently the tensile strength healing efficiency increases with increasing particle size due to the general decreasing of ultimate tensile strength of virgin TIMs, as shown in Figure 5.5. A maximum healing efficiency of 50% can be achieved when bigger particles (185  $\mu\text{m}$ ) are applied. However when rotating one of the sample halves over 180° before reassembly only some restoration of mechanical properties occurs for the composites with the smallest particles (see Figure 5.5). In the case the registry is very poor and only in the samples loaded with smallest particles the fracture surface is relatively smooth and local polymer–polymer contact may exist across the interface explaining a healing efficiency similar, but still lower, than the well repositioned sample.

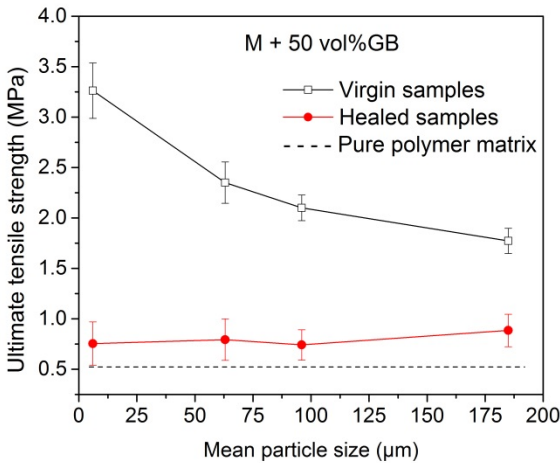


**Figure 5.4** The effect of particle size on ultimate tensile strength of glass beads loaded TIMs (black solid squares: virgin samples; red hollow circles: healed samples; dash line: indication of the interfacial healed strength level of the unloaded polymer matrix)

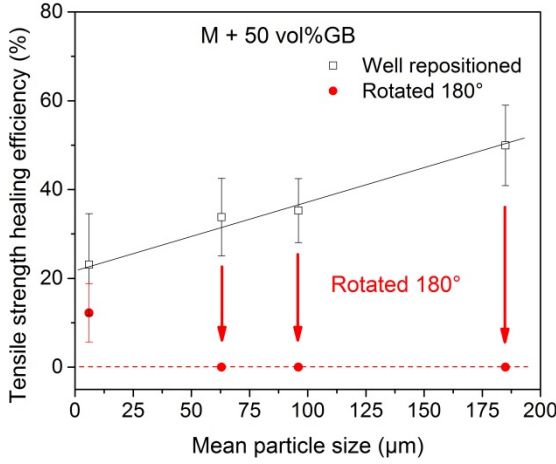


**Figure 5.5** The effect of particle size on tensile strength healing efficiency of glass beads loaded TIMs.

### 5.3.3 The effect of particle size on thermal conduction and healing efficiency

For a fixed PVC, the thermal conductivity of pure glass beads loaded TIM increases with increasing particle size, as shown in Figure 5.6 for a PVC of 50%. When bigger particles (185 μm) were used, the thermal conductivity is 0.77 W/m·K, which is less than twice that of the pristine polymer matrix (0.45 W/m·K) due to the fact that the thermal conductivity of glass beads is rather low for a filler material in a TIM. When using particles with higher thermal conductivity (e.g. Alumina, Aluminum Nitride, et al.) more thermally conductive TIMs can be obtained. Every et al. [22] built a thermal conductivity model of spherical particle loaded composite material which took thermal boundary resistance ( $R_b$ ) into account, as presented in equation 5.2,

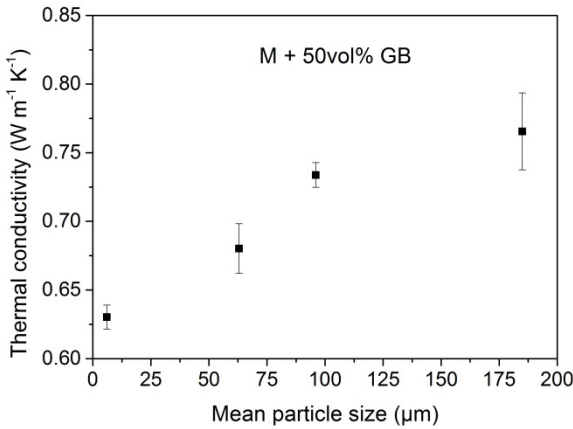
$$(1 - V)^3 = \left(\frac{\lambda_m}{\lambda_c}\right)^{(1+2\alpha)/(1-\alpha)} \times \left[\frac{\lambda_c - \lambda_f(1 - \alpha)}{\lambda_m - \lambda_f(1 - \alpha)}\right]^{3/(1-\alpha)} \quad (5.2)$$

where  $\lambda_c$ ,  $\lambda_m$  and  $\lambda_f$  are the thermal conductivity of composite material, matrix and filler, respectively,  $V$  is the volume fraction of filler,  $\alpha$  is a non-dimensional

parameter with reference to the boundary resistance, which is defined by equation 5.3,

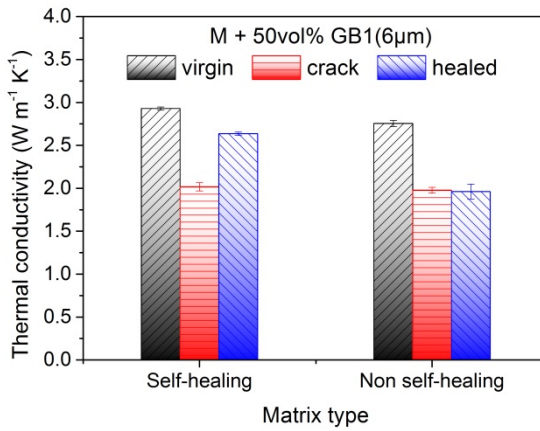
$$\alpha = \frac{2R_b\lambda_m}{d} \quad (5.3)$$

in which  $d$  is the diameter of the filler particle. From equation 5.2 and 5.3, it can be derived that the thermal conductivity of composite will increase when filler particle size increases. This trend also agrees with the modeling work on the effect of particle size on thermal conductivity of particle loaded polymer based composites done by Devpura et al. [23].



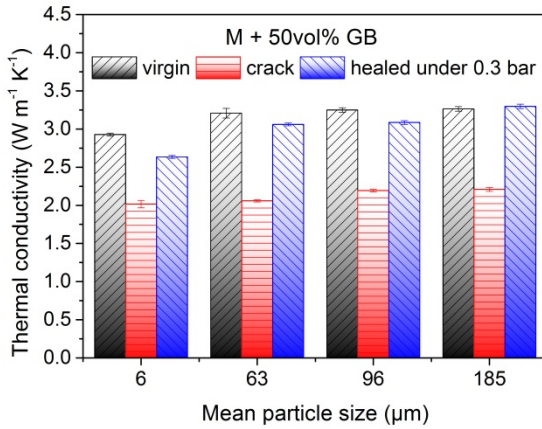
**Figure 5.6** The effect of particle size on thermal conductivity of glass beads loaded TIMs.

Figure 5.7 shows the effect of matrix type (self-healing vs. non-self-healing) on the thermal conductivity recovery of glass beads loaded TIMs. It is clear that the thermal conductivity of 'crack system' is lower than that of 'virgin system', which indicates that the intentionally produced air gap between the TIM and the aluminum foil can be detected by the evaluation method applied in present work. After healing at 70°C for 2h under 0.3 bar pressure, the thermal conductivity of the system with self-healing polymer based TIM restores significantly while the system with non-self-healing polymer does not show any thermal conductivity recovery.



**Figure 5.7** The effect of matrix type on the thermal conductivity recovery of glass beads loaded TIMs. (The thermal conductivity showed in this figure is the thermal conductivity of the system consisting of one layer of TIM and one layer of aluminum foil.)

Figure 5.8 shows how the thermal conductivity of the virgin system increases slightly with the particle size, which is due to the general increase of the thermal conductivity of TIMs made with bigger particles. Meanwhile the thermal conductivity recovery of TIMs shows the same trend as mechanical healing efficiency. It is interesting to note that a 100% thermal conductivity recovery of TIMs can be achieved when bigger particle (185μm) are used even though the tensile strength healing efficiency is low (50%).



**Figure 5.8** The effect of particle size on the thermal conductivity recovery of glass beads loaded TIMs. (The thermal conductivity showed in this figure is the thermal conductivity of the system consisting of one layer of TIM and one layer of aluminum foil.)

## 5

## 5.4 Conclusion

Thermal Interface Materials capable of restoring mechanical properties and thermal conduction can be obtained when a self-healing organic-inorganic network polymer containing reversible tetra-sulfide bonds is used as the matrix. For the same particle size, higher particle volume concentration (PVC) increases the mechanical strength. For a fixed PVC, larger particle sizes cause lower mechanical properties. Under the same healing conditions, the mechanical properties of the TIMs recover to similar values independently of the particle size or PVC. However, in terms of healing efficiency it was found that this property increases with the particle size and decreases with the PVC indicating that this factor is highly dependent on the mechanical properties of the virgin samples. Moreover, such healing efficiency is greatly reduced if the registry of the fracture surfaces brought in contact is destroyed. Thermal conductivity restoration of TIMs can reach 100% even though mechanical healing efficiency remains modest.

## References

1. Prasher R. Thermal Interface Materials: Historical Perspective, Status, and Future Directions. *Proceedings of the IEEE*. 2006;94(8):1571-1586.
2. Lafont U, Moreno-Belle C, van Zeijl H, van der Zwaag S. Self-healing thermally conductive adhesives. *Journal of Intelligent Material Systems and Structures*. 2014;25(1):67-74.
3. Blaiszik B, Kramer S, Olugebefola S, Moore JS, Sottos NR, White SR. Self-healing polymers and composites. *Annual Review of Materials Research*. 2010;40:179-211.
4. Hager MD, Greil P, Leyens C, van der Zwaag S, Schubert US. Self-healing materials. *Advanced Materials*. 2010;22(47):5424-5430.
5. van der Zwaag S. *Self healing materials: an alternative approach to 20 centuries of materials science*: Springer Science+ Business Media BV; 2008.
6. Wool RP. Self-healing materials: a review. *Soft Matter*. 2008;4(3):400-418.
7. Toohey KS, Sottos NR, Lewis JA, Moore JS, White SR. Self-healing materials with microvascular networks. *Nat Mater*. 2007;6(8):581-585.
8. White SR, Sottos NR, Geubelle PH, Moore JS, Kessler MR, Sriram SR, et al. Autonomic healing of polymer composites. *Nature*. 2001;409(6822):794-797.
9. Pang JWC, Bond IP. A hollow fibre reinforced polymer composite encompassing self-healing and enhanced damage visibility. *Composites Science and Technology*. 2005;65(11-12):1791-1799.
10. Kessler MR, Sottos NR, White SR. Self-healing structural composite materials. *Composites Part A: Applied Science and Manufacturing*. 2003;34(8):743-753.
11. Cordier P, Tournilhac F, Soulie-Ziakovic C, Leibler L. Self-healing and thermoreversible rubber from supramolecular assembly. *Nature*. 2008;451(7181):977-980.
12. Liu Y-L, Hsieh C-Y, Chen Y-W. Thermally reversible cross-linked polyamides and thermo-responsive gels by means of Diels-Alder reaction. *Polymer*. 2006;47(8):2581-2586.
13. Canadell J, Goossens H, Klumperman B. Self-Healing Materials Based on Disulfide Links. *Macromolecules*. 2011;44(8):2536-2541.
14. AbdolahZadeh M, C. Esteves AC, van der Zwaag S, Garcia SJ. Healable dual organic-inorganic crosslinked sol-gel based polymers: Crosslinking density and tetrasulfide content effect. *Journal of Polymer Science Part A: Polymer Chemistry*. 2014;52(14):1953-1961.
15. Palleau E, Reece S, Desai SC, Smith ME, Dickey MD. Self-Healing Stretchable Wires for Reconfigurable Circuit Wiring and 3D Microfluidics. *Advanced Materials*. 2013;25(11):1589-1592.
16. Wang C, Wu H, Chen Z, McDowell MT, Cui Y, Bao Z. Self-healing chemistry enables the stable operation of silicon microparticle anodes for high-energy lithium-ion batteries. *Nat Chem*. 2013;5(12):1042-1048.
17. Tee BCK, Wang C, Allen R, Bao Z. An electrically and mechanically self-healing composite with pressure- and flexion-sensitive properties for electronic skin applications. *Nat Nano*. 2012;7(12):825-832.
18. James NK, Lafont U, Zwaag Svd, Groen WA. Piezoelectric and mechanical properties of fatigue resistant, self-healing PZT?ionomer composites. *Smart Materials and Structures*. 2014;23(5):055001.

19. Lafont U, Zeijl Hv, Zwaag Svd. Increasing the reliability of solid state lighting systems via self-healing approaches: A review. *Microelectronics Reliability*. 2012;52(1):71-89.
20. Zhong N, Post W. Self-repair of structural and functional composites with intrinsically self-healing polymer matrices: A review. *Composites Part A: Applied Science and Manufacturing*. 2015;69:226-239.
21. Abdolah Zadeh M, van der Zwaag S, García SJ. Assessment of healed scratches in intrinsic healing coatings by AC/DC/AC accelerated electrochemical procedure. *Surface and Coatings Technology*.
22. Every AG, Tzou Y, Hasselman DPH, Raj R. The effect of particle size on the thermal conductivity of ZnS/diamond composites. *Acta Metallurgica et Materialia*. 1992;40(1):123-129.
23. Devpura PEP, Ravi S. Prasher, Amit. Size effects on the thermal conductivity of polymers laden with highly conductive filler particles. *Microscale Thermophysical Engineering*. 2001;5(3):177-189.

# Chapter 6

---

**Thermal cycling test of self-healing TIMs**

---



## 6.1 Introduction

Thermal interface materials (TIMs) are widely used as gap-filler materials between electronic devices and their heat sink and aim to control the heat dissipation and to provide mechanical anchoring. As the rated power densities of electronic devices are increasing rapidly nowadays, there is an increased demand for reliable and efficient TIMs [1-3]. Low quality or inappropriately chosen TIMs will degrade faster than expected causing the thermal resistance of heat transfer path and the junction temperature of the electronic device to increase substantially, leading to premature device failure. In order to know whether the TIMs can deliver the required functionality under the foreseen conditions for the desired time, reliability and life time tests are required.

However, from what appears in the literature, the TIM reliability test is not as mature as those of other components in electronic devices such as solder joints. Besides, the reliability of a TIM highly depends on the system to which it is installed, the environment to which it is exposed to and the cyclic nature of its operation. As a result a particular TIM used in two completely different devices may show a different reliability. So, there is not a universal reliability test protocol for TIMs. Specific reliability test protocols need to be designed according to the application conditions of a particular TIM [4-6].

### 6

Actual reliability and life time test can be done in several ways. For instance, the test can be done under the regular operating conditions and continued until the first failure occurs. However this method is generally too time consuming. In order to shorten the time to failure, accelerated life time testing (ALT) is usually performed [7-9]. In ALT components, devices or entire systems are exposed to stresses and other conditions that are more severe than those under normal or application conditions. There are three most common ALT categories for TIMs: temperature and humidity stress test (THT/HAST), high temperature storage test (HTS) and thermal/power cycling test (TC/PC). From a material selection and screening point of view all three stress tests are essential and informative and reveal different aspects of damage evolution. . In THT and HTS the failure mechanism is mainly (chemical) degradation (oxidation, phase separation, etc.) of the TIM itself [10-14] while in thermal cycling the periodic variation in test temperature will lead to delamination and cracks due to a mismatch in the coefficient of thermal expansion (CTE) between the TIM and the attached components (heat sink, die, etc.). Thermal cycling test may also cause warpage of components, leading to a 'pump-out' effect for

some low viscosity thermal grease [15, 16]. It has been proposed that self-healing TIMs can promote the reliability and service lifetime of electronic devices due to their ability to heal delamination and cracks in the system [17, 18]. So in this study the thermal cycling test, rather than THT and HTS is chosen to test the reliability of the TIM.

The two key parameters in a thermal cycling test are the temperature range and the number of cycles. In order to allow self-healing TIMs to heal autonomously, the maximum temperature in each cycle should be equal to or higher than the healing temperature of the material (70°C). Two temperature cycling ranges were chosen: a mild condition (cycling between 20°C to 70°C) and a harsh condition (cycling from -196°C to 70°C). For the mild condition thermal cycling was continued for as long as the testing time was available (more than 10,000 cycles). For the harsh condition cycling was continued till clear damage could be detected. In some tests lap shear testing after cycling was performed to quantify the damage and healing. A commercial TIM was used to set the reference levels. The purpose of this study is to get a general impression whether the self-healing concept works or not, rather than targeting at a specific application.

## 6.2 Experimental

### 6.2.1 Material preparation

In this chapter, two self-healing thermal interface materials (TIMs), each containing 50 vol.% alumina particles, are employed: (1) a dual-network self-healing polymer-based system (from hereon called 'DN') and (2) a polysulfide self-healing thermoset (from hereon called 'EPS25'). The healing temperature for both TIMs is 70°C. 3M™ Thermally Conductive Interface Tape 8926 was chosen as the reference material (from hereon called 'Refer').

#### 6.2.1.1 Dual-network self-healing polymer-based TIM

First, a pre-mixture of Bis[3-(triethoxysilyl)propyl]tetrasulfide (purity 99%, total sulfur content > 20%, from SiSiB SILANES, China), (3-Aminopropyl)trimethoxysilane (purity 97%, from Sigma-Aldrich, the Netherlands) and an epoxy resin Epikote™ 828 (184–190 g/eq, from Akzo Nobel, the Netherlands) was mixed together and stirred using a magnetic stirrer at 300 rpm for 3 h at room temperature. Then, an

organic crosslinker Ancamine® 2500 (105–110 g/eq, from Akzo Nobel, the Netherlands) and (spherical) alumina powder (mean particle size 20 µm, from Denka Company Limited, Japan) were mixed with the pre-mixture in a high speed mixer at 2500 rpm for 5 min. Then, the mixture was degassed in a vacuum chamber for 20 min. Subsequently, Pentaerythritol tetrakis (3–mercaptopropionate) (purity>95%, from Sigma–Aldrich, the Netherlands) was mixed with this degassed mixture in a high speed mixer at 2500 rpm for 0.5 min. Finally, the resulting composite was cast on a Teflon plate to form a film with a thickness of 0.5 mm which was cured in an oven at 70°C for 48 h. The weight ratios of all components in the dual network self-healing polymer based TIM are listed in Table 6.1.

**Table 6.1** Weight ratios of all components in the DN thermal interface material

Chemicals	Weight ratio
Epikote™ 828	1 g
Bis[3-(triethoxysilyl)propyl]tetrasulfide	0.733 g
(3–Aminopropyl)trimethoxysilane	0.076 g
Ancamine® 2500	0.579 g
Pentaerythritol tetrakis(3–mercaptopropionate)	0.566 g
Spherical alumina powder*	9.807 g

\* The volume fraction of the alumina powder in the composite is 50 vol.%.

### 6.2.1.2 Polysulfide self-healing thermoset-based TIM

The synthesis procedure is based on a basic catalyzed addition reaction of epoxy groups with thiols. At first, a stoichiometric amount of epoxidized polysulfide Thioplast™ EPS25 (640 g/eq, from Akzo Nobel, the Netherlands) was mixed with Pentaerythritol tetrakis(3–mercaptopropionate) (purity>95%, from Sigma–Aldrich, the Netherlands) in a high speed mixer at 2500 rpm for 3 min. Then, the catalyst 4–dimethylaminopyridine (purity>99%, from Sigma–Aldrich, the Netherlands) and the filler (spherical alumina powder (mean particle size 20 µm, from Denka Company Limited, Japan)) were added. After mixing at 2500 rpm for 5 min, the mixture was then degassed in a vacuum chamber for 20 min. Finally, the resulting composite was cast on a Teflon plate to form a film with a thickness of 0.5 mm which was then cured in an oven at 70°C for 48 h. The weight ratios of all components in the polysulfide self-healing thermoset-based TIM are shown in Table 6.2.

**Table 6.2** Weight ratios of all components in the polysulfide self-healing thermoset-based TIM

Chemicals	Weight ratio
Thioplast™ EPS25	1 g
Pentaerythritol tetrakis(3-mercaptopropionate)	0.185 g
4-dimethylaminopyridine	0.012 g
Spherical alumina powder*	3.628 g

\* The volume fraction of the alumina powder in the composite is 50 vol.%.

## 6.2.2 Thermal cycling test protocols

### 6.2.2.1 Drop-off test

In order to investigate whether the adhesion of thermal interface materials can withstand the shear stress generated by the weight of typical heat sinks (based on discussions with industrial partners set to 0.6 kPa in this study) during thermal cycling, a drop-off test was performed. Cured thermal interface material films were cut into 10mm × 10mm pieces and placed between a copper heat sink and a glass fiber/epoxy composite substrate, forming a sandwich structure, to mimic a TIM application in an electronic device. To ensure good initial adhesion, a normal pressure of 10 kPa was applied on the assembly and the whole sandwich structure was kept in an oven at 70°C for 24 h. Then, the sandwich structure was taped onto Peltier elements for thermal cycling. The Peltier elements acted both as heater and as cooler simply by altering the applied DC voltage. The whole thermal cycling system was placed vertically in a climate chamber which was kept at an ambient temperature of 20°C. The setup is shown in Figure 6.1.



**Figure 6.1** The setup of drop-off test thermal cycling system in the climate chamber.

The entire thermal cycling history in drop-off testing consisted of 4 periods. Period I: 8000 cycles at temperatures from 20°C to 70°C; In each thermal cycle of 55 seconds, it took 20 seconds for the temperature to rise from 20°C to 70°C, 10 seconds for isothermal annealing at 70°C and then another 25 seconds to lower the temperature to 20°C. Period II: ageing at room temperature for 5 months; Period III: another 10000 cycles at temperatures from 20°C to 70°C; Period IV: a final 8000 cycles at temperatures ranging from 20°C to 70°C with an additional block of steel hanging on the heat sink to apply 13 kPa shear stress on the TIM in order to simulate more severe testing and to create more damage. The temperature profile of the drop-off test is shown schematically in Figure 6.2.

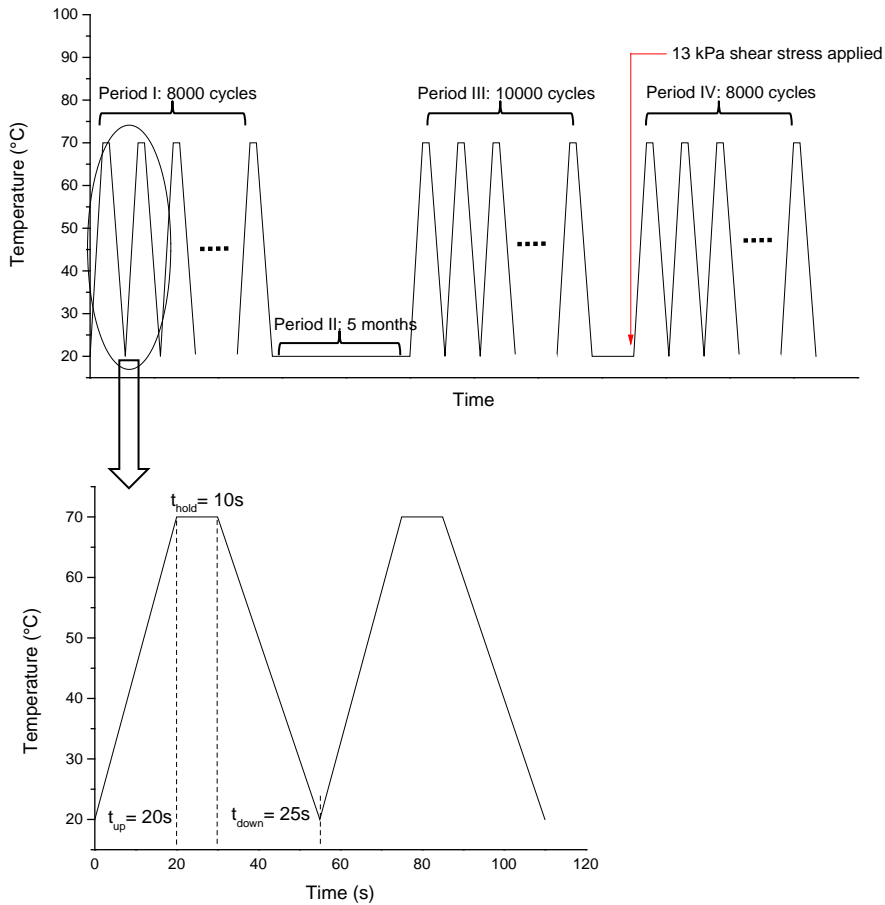


**Figure 6.2** The schematic temperature profile of the drop-off test.

### 6.2.2.2 Adhesion decay test

Single lap shear tests were performed to quantify the adhesive strength decay during thermal cycling. Specimens were prepared by bonding two (degreased) Aluminum plates (50mm × 20mm × 1mm) to each other using cured TIM films with a thickness of 0.5mm. The overlap length is 20mm and the test geometry is shown in Figure 6.3.

The adhesion was established in a 24 h thermal treatment at 70°C. During the thermal treatment the TIMs and the two Aluminum plates were kept in contact using a paper clip.

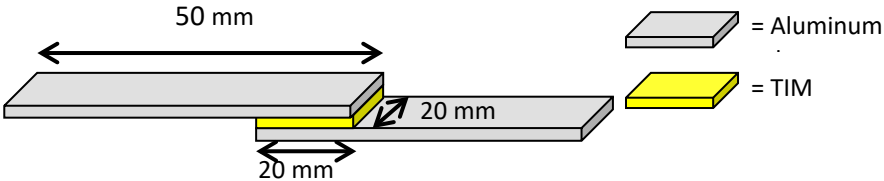


**Figure 6.3** Schematic lap shear test geometry.

Four different thermal cycling conditions were applied. Condition 1: samples were positioned on the Peltier elements and the whole thermal cycling system was placed horizontally in a climate chamber which kept the ambient temperature always at 20°C, as shown in Figure 6.4(a). The temperature of the samples was cycled between 20°C and 70°C. For each cycle, the temperature profile was the same as that in drop-off test (Figure 2). After every 1000 regular cycles, 10 temperature shocking events (temperature of the samples was cycled between 0°C and 90°C, with heating and cooling in 25 and 30 seconds respectively) were introduced. In this case, the larger thermal mismatch strain between the TIMs and the Al plate may lead to crack initiation and growing, which should result in a decrease of adhesion strength. On the other hand, the 90°C is above the healing temperature, so any damage formed could be healed and the adhesion strength should be maintained. Condition 2: samples were taped on the Peltier elements and the whole thermal cycling system was placed vertically. A block of copper was adhered to the lower end of the Al plate so that a constant shear stress of 0.8 kPa was applied on the TIMs/Al plate interface, as shown in Figure 4(b). The thermal history of condition 2 is the same as condition 1. Condition 3: the samples went through even more drastic temperature changes. At first, samples were manually kept in liquid nitrogen (-196°C) for 20s, then samples were placed on a table at room temperature to warm up by ambient temperature for 120s, and so on. No shear stress was applied during this cycling. Condition 4: samples were cycled between liquid nitrogen (-196°C, 20s) and a hot stage (70°C, 120s). The hot stage was kept in a hot oil bath to maintain the temperature of the upper surface, which contacted with samples, stable at 70°C, as shown in Figure 6.4(d). In this condition, samples suffered from greater temperature change than

condition 3 however a self-healing event could be triggered during heating period. All four conditions are summarized in Table 6.3. Three samples were tested per condition and per material.

After testing single lap shear tests were performed on an Instron 3365 tensile testing machine fitted with a 1 kN load cell. The cross-head speed was 1 mm/min. In order to determine the adhesion recovery of self-healing TIMs after complete failure in the lap shear tests, the sample ends were repositioned carefully, kept together using a paper clip and annealed at 70°C for 24h. After this healing treatment, the lap shear strength was measured again.

**Table 6.3** Details of the four conditions in the adhesion decay test.

	<b>Constant shear stress</b>	<b>Thermal history</b>
Condition 1	0	Every 1000 normal cycles (from 20°C to 70°C) introducing 10 shocking cycles (from 0°C to 90°C)
Condition 2	0.8 kPa	Every 1000 normal cycles (from 20°C to 70°C) introducing 10 shocking cycles (from 0°C to 90°C)
Condition 3	0	Temperature cycled from -196°C to room temperature
Condition 4	0	Temperature cycled from -196°C to 70°C



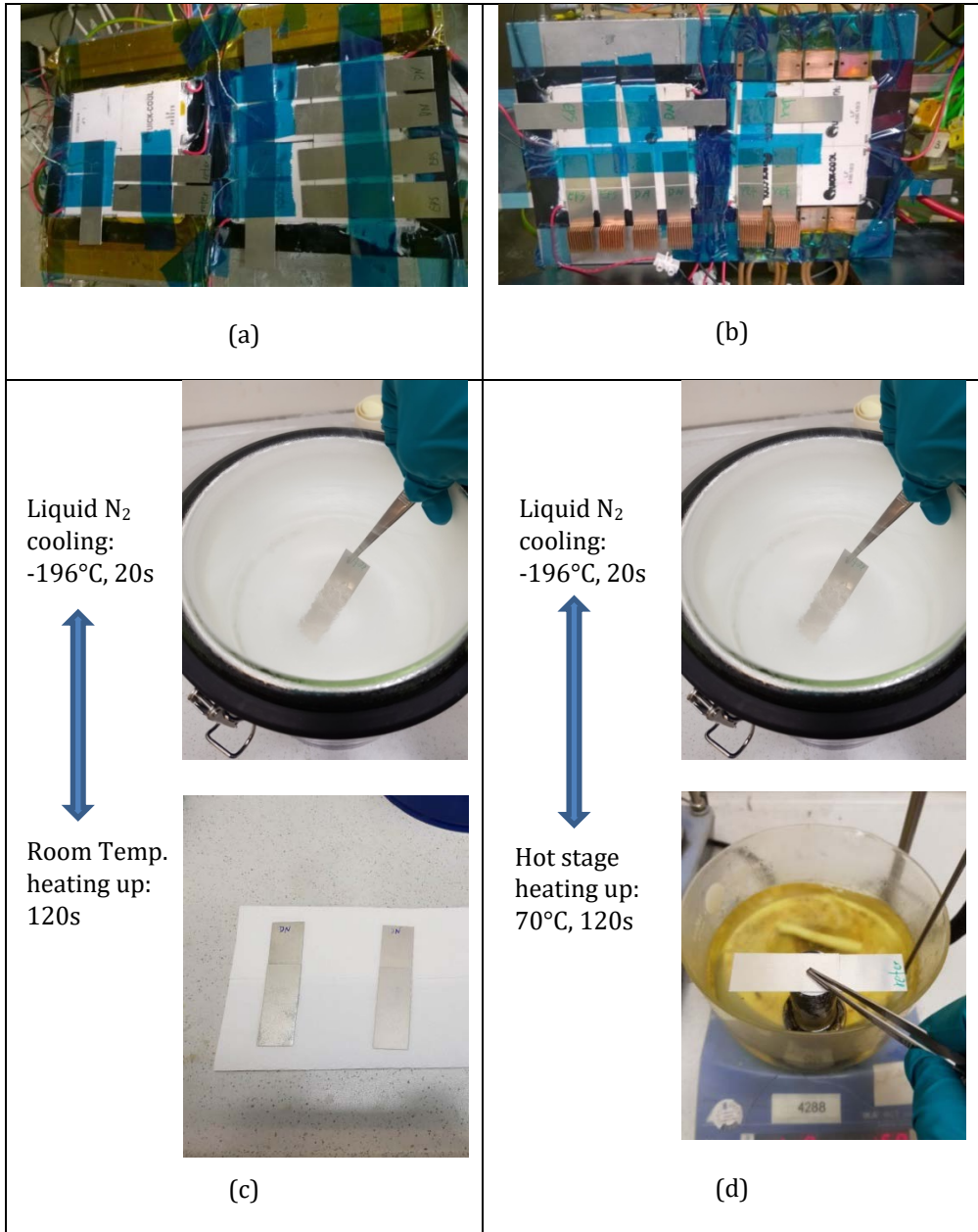


**Figure 6.4** Four conditions for the adhesion-decay test: (a) condition 1; (b) condition 2; (c) condition 3; (d) condition 4.

## 6.3 Results and discussion

### 6.3.1 Drop-off test

In the drop-off test, Refer samples, DN samples and EPS25 samples all stayed attached to the substrate after Period I (8000 cycles from 20°C to 70°C), Period II (aged at room temperature for 5 months) and Period III (10000 cycles from 20°C to 70°C). However, upon the application of 13 kPa shear stress, one Refer sample lost adhesion after only 50 cycles and the other Refer sample failed after 100 cycles, as shown in Figure 6.5. The DN samples and EPS25 samples survived the 8000 cycles till the end of the experiment.

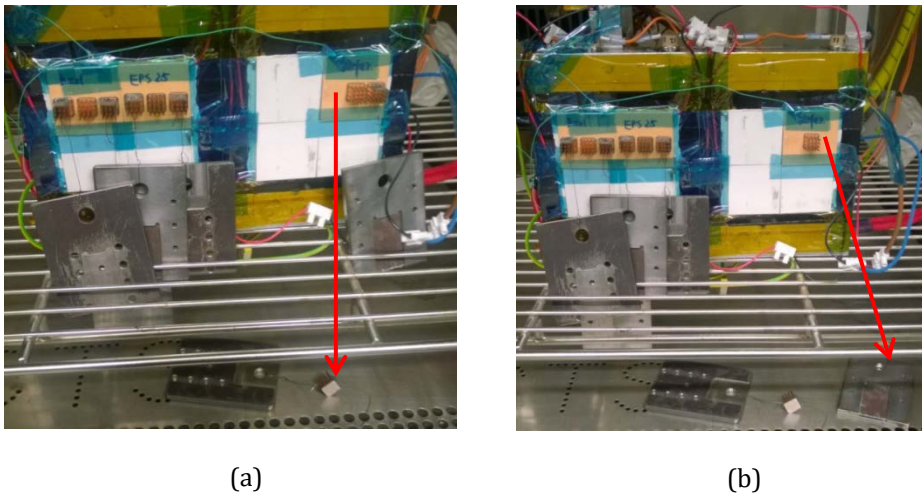


**Figure 6.5** Refer sample failed after (a) 50 cycles and (b) 100 cycles during Period IV in the drop-off test

In order to explain this result, the initial adhesive strengths of Refer, DN and EPS25 between a copper plate and a glass fiber/epoxy composite plate were measured both at room temperature and at 70°C, as shown in Figure 6.6. At room temperature, DN showed the highest adhesive strength (0.68 MPa), EPS25 showed a lower adhesive strength (0.43 MPa) and Refer showed the lowest strength (0.24 MPa). At 70°C, the adhesive strength of DN decreased by 24% to 0.52 MPa, EPS25 decreased by 28% to 0.31 MPa and Refer showed an 85% drop to 0.036 MPa. So, the early failure of Refer

samples is probably due to its low adhesive strength (in particular at the higher temperature) and the relatively high applied shear stress (the applied shear stress is about one third of its initial adhesive strength). For the record, all samples broke at the composite plate/TIM interface due to the stronger adhesion between TIM and copper. Nevertheless, the data show that DN and EPS25 have a better endurance during thermal cycling than the commercial thermal interface adhesive.

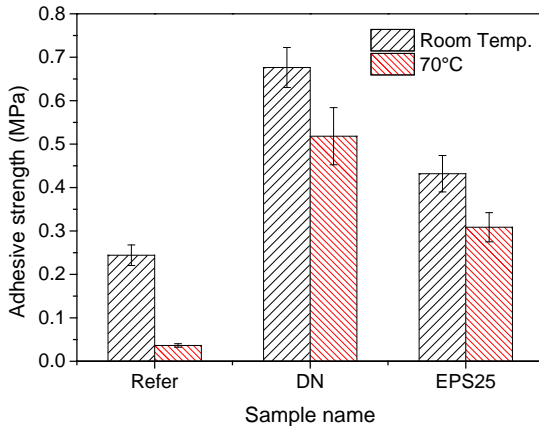


**Figure 6.6** Adhesive strength of Refer, DN and EPS25 between a copper plate and a glass fiber/epoxy composite plate.

### 6.3.2 Adhesion decay test

Figure 6.7 shows that the adhesive strength of Refer and EPS25 remained almost constant after 20000 temperature cycles from 20°C to 70°C including 10 shocking cycles (from 0°C to 90°C) per 1000 normal cycles (i.e. the adhesion decay test condition 1). The adhesive strength of DN even increased slightly. This is due to the aging of the DN TIMs, which has been discussed extensively in Chapter 4. The data show that the applied cycling condition were not harsh enough to result in a decrease of adhesion strength for any of the three systems tested.

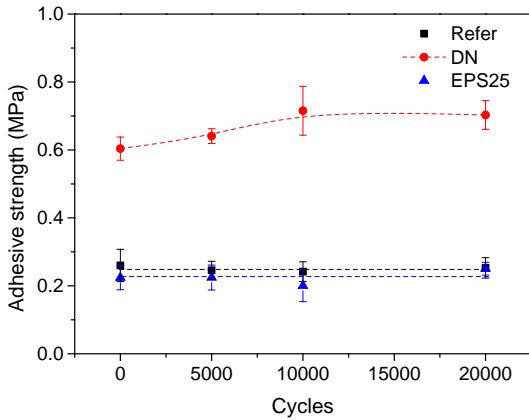


**Figure 6.7** Adhesive strength changes of Refer, DN and EPS25 samples between two Aluminum plates in adhesion decay test condition 1.

Even when 0.8 kPa shear stress was applied during thermal cycling, no significant reduction in the adhesive strength of Refer, DN and EPS25 samples was observed, as shown in Figure 6.8. The black bars represent the initial value while the red bars represent adhesive strength after 20000 temperature cycles from 20°C to 70°C including 10 shocking cycles (from 0°C to 90°C) per 1000 normal cycles at 0.8 kPa shear stress. However it is interesting to note that the self-healing samples (DN and EPS25) and the non-healing samples (Refer) broke differently in the final lap shear test. Figure 6.9 (a), (b) and (c) shows the morphologies of Refer, DN and EPS25 samples after completely failure in lap shear test. All Refer samples delaminated at the lower interface which is nearer to Peltier elements and the complete TIM film adhered to the upper aluminum plate. Meanwhile, all DN and EPS25 samples broke at both interfaces so that one part of the TIMs adhered to the upper aluminum plate and the other part adhered to the lower aluminum plate. The different failure locations of healing samples and non-healing samples are schematically shown in Figure 6.9(d). It seems that in the Refer samples the lower interface is weaker than the upper interface while in DN and EPS25 samples both interfaces are of the same strength. It is important to point out that the sample construction is symmetric so the upper interface and the lower interface strength of each sample should be all the same initially. In Refer samples, the lower interface suffers relatively harsher temperature variations than the upper interface so that more defects are introduced

and accumulated at the lower interface leading to delamination only to occur at the lower interface. In DN and EPS25 samples, although the lower interface suffered relatively harsher temperature variations, the same as in Refer sample, the defects seemed to have healed so that both lower interface and upper interface strength remained the same after thermal cycling. It should be pointed out that a larger number of samples need to be tested to validate the statements on preferred failure location made above.

After the complete failure of the thermally cycled samples in the lap shear test, DN and EPS25 samples were put back in the oven for healing at 70°C for 24h. After this healing treatment, the lap shear strength was measured again. As the blue bars in Figure 6.8 show, the adhesive strength of DN and EPS25 recovered for 95% and 98%, respectively. It indicates that the self-healing ability of DN and EPS25 TIMs still exists after 20000 temperature cycles from 20°C to 70°C.

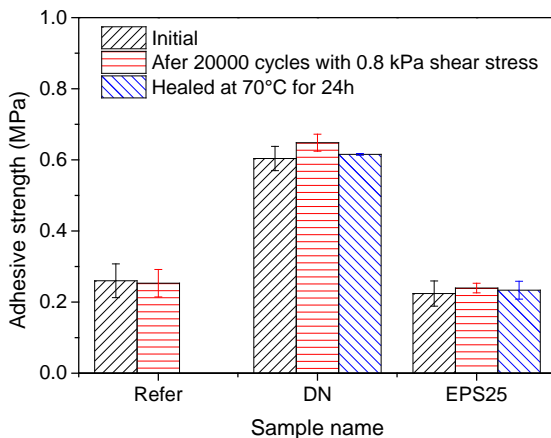


**Figure 6.8** Adhesive strength changes of Refer, DN and EPS25 samples in adhesion decay test condition 2 and healing results. Healing condition: 70°C for 24h.

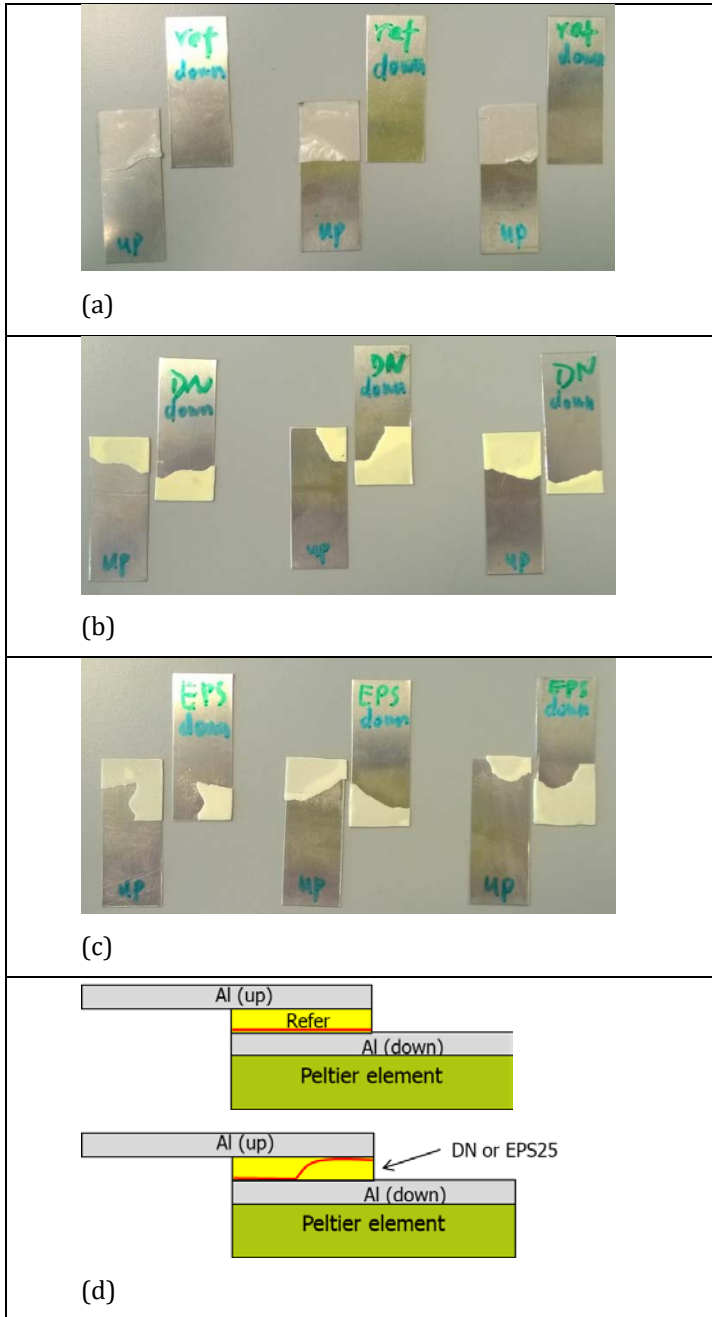


**Figure 6.9** Sample morphologies after lap shear test (a) Refer samples, (b) DN samples and (c) EPS25 samples, (d) different failure locations of healing samples (DN and EPS25) and non-healing samples, red lines indicate delamination.

In order to introduce more damage, harsher thermal cycling conditions (from  $-196^{\circ}\text{C}$  to room temperature and from  $-196^{\circ}\text{C}$  to  $70^{\circ}\text{C}$ ) were applied. After 100 cycles from  $-196^{\circ}\text{C}$  to room temperature, the adhesive strength of Refer, DN and EPS25 samples decreased to 77%, 86% and 78% of the initial adhesive strength values respectively, as the red bars in Figure 6.10 shows. The Figure shows that a certain amount of damage has been introduced successfully to all samples by fast thermal cycling from liquid nitrogen to room temperature. More interestingly, if the thermal cycling condition is from  $-196^{\circ}\text{C}$  to  $70^{\circ}\text{C}$ , the adhesive strength of Refer samples still decreased to 80% of the initial value while the adhesive strengths of DN and EPS25 samples remained almost the same as the initial value. Although the samples suffered greater temperature variations and more defects or micro cracks were formed, healing events were triggered in the DN and EPS25 samples leading to no loss in adhesive strength. This result clearly shows that self-healing TIMs can be more reliable than common TIMs by healing small damage (if there is) spontaneously if the healing condition is appropriate.

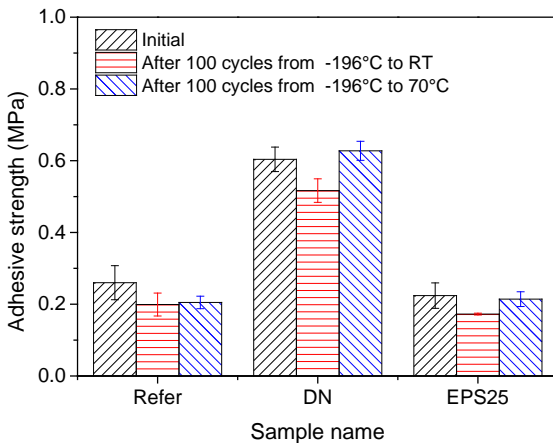


**Figure 6.10** Adhesive strength values for Refer, DN and EPS25 samples in adhesion decay test conditions 3 and 4.

## 6.4 Conclusion

In this study, several thermal cycling tests were performed to investigate the long-term reliabilities of two self-healing TIMs with a healing temperature of  $70^{\circ}\text{C}$  and

one commercial non-healing TIM. When large shear stresses are applied the chosen self-healing TIMs have a much better endurance during thermal cycling than the commercial non-healing TIMs due to their higher adhesive strength at the higher temperature (70°C). Under moderate thermal cycling condition (from 20°C to 70°C) both self-healing TIMs and the commercial non-healing TIM show good long-term reliability, as the testing conditions were too mild to induced damage. However under harsh thermal cycling condition (from -196°C to 70°C) self-healing TIMs were found to be more reliable than the reference commercial non-healing TIM because the damage due to thermal cycling was healed autonomously.



## References

1. Prasher R. Thermal interface materials: historical perspective, status, and future directions. *Proceedings of the IEEE*.94:p.1571-1586.
2. Rodgers P, Evelyn V, Rahim E, Morgan D, editors. *Thermal Performance and Reliability of Thermal Interface Materials: A Review*. 7th International Conference on Thermal, Mechanical and Multiphysics Simulation and Experiments in Micro-Electronics and Micro-Systems; 2006.
3. Le KC, Nguyen M. Thermal interface materials. *Journal of Materials Engineering Performance*. 2001;10(1):56-59.
4. Due J, Robinson AJ. Reliability of thermal interface materials: A review. *Applied Thermal Engineering*. 2013;50(1):455-463.
5. Gwinn JP, Webb RL. Performance and testing of thermal interface materials. *Microelectronics Journal*. 2003;34(3):p.215-222.
6. Jarrett RN, Merritt CK, Ross JP, Hisert J, editors. *Comparison of Test Methods for High Performance Thermal Interface Materials*. Twenty Third Annual IEEE Semiconductor Thermal Measurement and Management Symposium; 2007.
7. Escobar LA, Meeker WQ. A Review of Accelerated Test Models. *Statistical Science*. 2006;21(4):p.552-577.
8. Bharatham L, Fong WS, Chan JL, Chiu CP, editors. *A Study of Application Pressure on Thermal Interface Material Performance and Reliability on FCBGA Package*. International Conference on Electronic Materials and Packaging; 2006.
9. Fu HK, Ying SP, Chen TT, Hsieh HH, Yang YC. Accelerated Life Testing and Fault Analysis of High-Power LED. *IEEE Transactions on Electron Devices*. 2018;65(99):1-7.
10. Goel N, Anoop TK, Bhattacharya A, Cervantes JA, Pan JH, editors. *Technical Review of Characterization Methods for Thermal Interface Materials (TIM)*. 11th Intersociety Conference on Thermal and Thermomechanical Phenomena in Electronic Systems 2008.
11. Chen CI, Ni CY, Pan HY, Chang CM, Liu DS. Practical Evaluation for Long-term Stability of Thermal Interface Material. *Experimental Techniques*. 2008;33(1):28-32.
12. Bharatham, Fong WS, Torresola, Chen CK, editors. *Qualification of phase change thermal interface material for wave solder heat sink on FCBGA package*. Electronics Packaging Technology Conference, Shenzhen, China; 2005.
13. Ramaswamy C, Shinde S, Pompeo F, Sablinski W, Bradley S, editors. *Phase Change Materials as a Viable Thermal Interface Material for a High-Power Electronic Applications*. Conference on Thermal & Thermomechanical Phenomena in Electronic Systems; 2004.
14. Lira S, Dal B, editors. *Degradation mechanisms of siloxane-based thermal interface materials under reliability stress conditions*. 42nd Annual International Reliability Physics Symposium, Phoenix; 2004.
15. Khuu V, BarCohen A. Effects of Temperature Cycling and Elevated Temperature/Humidity on the Thermal Performance of Thermal Interface Materials. *IEEE Transactions on Device and Materials Reliability*. 2009;9(3):379-391.
16. Paisner SN, Touzelbaev M, Refai-Ahmed G, Yang Y, editors. *New developments for a no-pump-out high-performance thermal grease*. Thermal and Thermal-mechanical Phenomena in Electronic Systems, ITherm 10, Las Vegas 2010.

17. van der Zwaag S, Grande AM, Post W, Garcia SJ, Bor TC. Review of current strategies to induce self-healing behaviour in fibre reinforced polymer based composites. *Materials Science and Technology*. 2014;30(13a):1633-1641.

18. Lafont U, Moreno-Belle C, van Zeijl H, van der Zwaag S. Self-healing thermally conductive adhesives. *Journal of Intelligent Material Systems and Structures*. 2014;25(1):67-74.



# Chapter 7

---

**Laser Speckle Imaging observation of collective molecular motion during curing and adhesive bond formation of a sol-gel hybrid polymer**

---

## 7.1 Introduction

As stated in the earlier chapters of this thesis, the life time of most thermal junctions between the electronic heat source and the cooling block is determined by the loss of adhesion between the thermal interface material (TIM) junction connecting both. Hence the use of (particulate filled) self-healing polymers, capable of autonomously restoring the interfacial adhesion up the unavoidable temperature rise upon loss of adhesion may lead to a significant life time extension. In the present work we explore the potential of a new physical material characterization technique, Laser Speckle Imaging (LSI) to directly image the collective molecular motion required to restore the contact between the TIM and a planar glass substrate. As the anticipated motions are very small and at or below the resolution of the technique we first study the change in molecular mobility during the curing of the self-healing polymer (containing < 1% nanosized TiO<sub>2</sub> particles).

Laser Speckle Imaging (LSI) is a non-contact and non-destructive optical testing method for measuring the relative displacements of inert scattering features on the surface of non-transparent materials or in the bulk of transparent or translucent materials. The basic theory of LSI was developed in the 1970s[1]. Since then extensive studies have been made relating speckle temporal dynamics to various forms of particle dynamics in dilute single-scattering suspensions [2-4]. The method was further developed in the 1990s with the availability of faster digital image acquisition and processing technologies. Nowadays LSI is successfully applied in biomedical optics (especially in the studies on blood flow within arteries), observation of thermally activated processes (such as the drying of paint) and tracking crack progress in polymers and bulk ceramics under mechanical load [5-9]. Recent research done by Van der Kooij et al. showed that LSI is an effective method to follow heterogeneous dynamics in drying and aging of paints [10].

The spatial and temporal resolution of the LSI technique depends on the stability and power of the laser light source, the quality of the optical components and the detector and finally the software used to deconvolute the scattering patterns into displacement fields [11]. For systems comparable to the one to be used in this work the lateral spatial resolution can be as fine as 1 micrometer while the time resolution can be from 10 milliseconds to weeks.

Over the past few decades, intrinsic self-healing materials which are capable of restoring their original properties after damage due to the occurrence of reversible

processes have attracted many researchers' attention as such material can heal local damage several times in succession [12-16]. Understanding the healing dynamics is essential to both designing and applying self-healing materials. Van der Kooij et al. have applied LSI to the study of healing of a polyetherimide polymer after cutting and showed its potential in tracking of local dynamic motions at different locations in the vicinity of the crack and linking that to damage recovery [17]. In that study a clear correlation was found between the time constant of the dominant collective molecular reorganization process as determined with LSI and the dominant time constant as determined using conventional rheology.

In this chapter we first demonstrate the potential of the LSI technique in monitoring the change in molecular mobility during curing of four highly comparable hybrid sol-gel polymers (two of the self-healing type and two of the non-self-healing type), linking the LSI experiments to rheological data during obtained during of the same polymer. Subsequently the average molecular motion during bonding of fully cured sol-gel polymer films to a glass plate was studied as a function of time for a fixed temperature of 70°C. The LSI data are complimented by companion interfacial adhesion strength measurements. LSI studies on polymer curing and re-adhesion of a polymer to a glass substrate have not been reported in the literature yet.

## 7.2 Experimental

### 7.2.1 Material preparation

Epoxy resin Epikote™ 828 (184-190 g/eq) and curing agent Ancamine® 2500 (105-110 g/eq) were provided by Akzo Noble. (3-Aminopropyl)trimethoxysilane (purity 97%), Pentaerythritol tetrakis (3-mercaptopropionate) (purity>95%) and Triethylamine, from hereon called APS, tetrathiol and TEA respectively, were purchased from Sigma-Aldrich. Bis[3-(triethoxysilyl)propyl]tetrasulfide and Bis[3-(triethoxysilyl)propyl]disulfide, from hereon called BTS and BDS respectively, were purchased from SiSiB Silanes. All chemicals were used as in their as-received well-packaged condition.

The polymers for this study were prepared in a multi-step process. At first, Epoxy resin and APS were mixed using a magnetic stirrer at 100 rpm for 5 min at room temperature. Then BTS or BDS were added while continuously stirring at 300 rpm for 3 h at room temperature. Then, the curing agent Ancamine® 2500 was mixed

into the mixture with a high speed mixer operating at 2500 rpm for 5 min. Because the polymers in this study are transparent to the laser applied, 0.5 wt% TiO<sub>2</sub> nano-particles (about 21 nm particle size, purchased from Sigma–Aldrich) was also added in this step to ensure local laser light reflection and high LSI contrast. Finally tetrathiol and the catalyst TEA were added and mixed at 2500 rpm for 0.5 min. The weight ratio of all components is shown in Table 7.1. As introduced in chapter 4, BTS-An polymer and BDS-An-TEA polymer have a good self-healing ability while the REF polymer and the BDS-An polymer are non-healing polymer variants.

**Table 7.1** Compositions of polymers studied in this work

Components	Polymers			
	REF	BTS-An	BDS-An	BDS-An-TEA
Epikote™ 828	1g	1g	1g	1g
Ancamine® 2500	0.579g	0.579g	0.579g	0.579g
APS	0	0.076g	0.076g	0.076g
BTS	0	0.733g	0	0
BDS	0	0	0.646g	0.646g
Tetrathiol	0.566g	0.566g	0.566g	0.566g
TEA	0	0	0	0.014g
TiO <sub>2</sub> nano-particles	0.011g	0.015g	0.014g	0.014g

## 7.2.2 LSI test geometry

### 7.2.2.1 Setup for monitoring the polymer curing

The LSI setup for monitoring the polymer curing process is shown in Figure 7.1. Immediately after mixing the polymer was cast on a glass substrate. Prior to this a frame with a thickness of 1 mm was built onto the glass substrate to prevent the polymer from flowing out and to prevent macroscopic flow of the material due to gravitational effects. Then the glass substrate was placed on a hot plate to heat up from room temperature to curing temperature 70°C and keep at 70°C. The heating up took about 2 min. A laser beam (220mW,  $\lambda=473\text{nm}$ ) was projected onto the sample and the raw speckle images were recorded by a camera at a frame rate of 60 fps and an exposure time 1200  $\mu\text{s}$ . The LSI recording included the heating up and holding period. The system as used was a modified copy of the system as described in the publications by van der Kooij [10, 17].

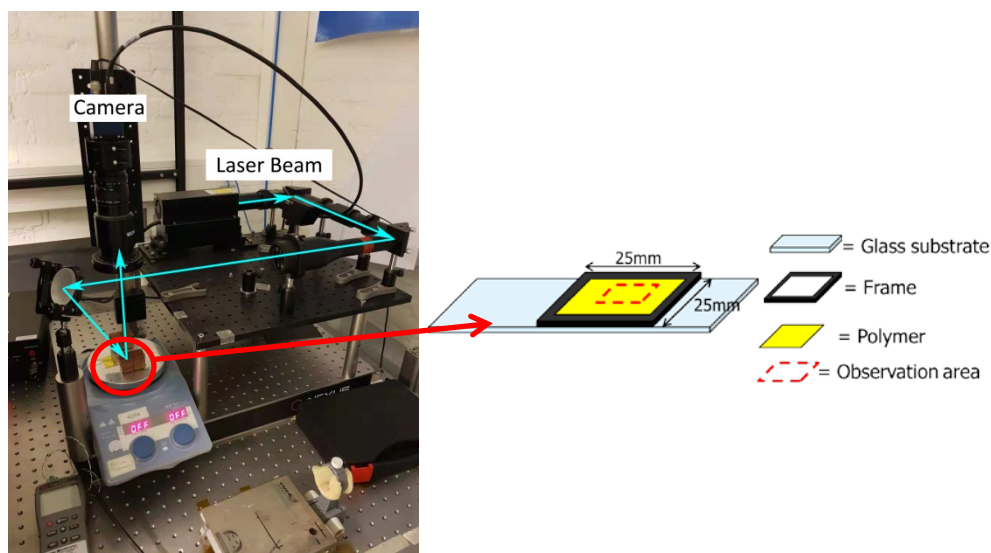
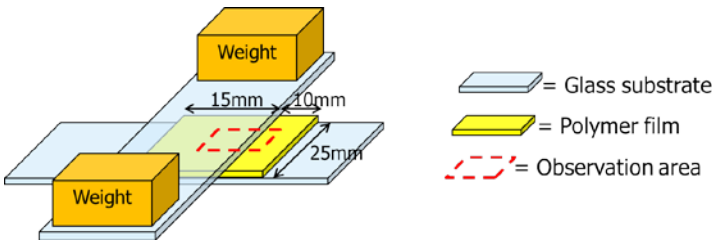


**Figure 7.1** LSI setup and polymer curing process observation geometry.



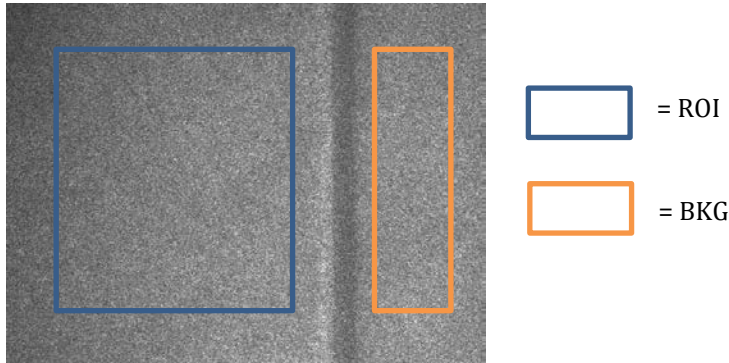
### 7.2.2.2 LSI setup for re-adhesion monitoring

Figure 7.2 shows the set up for monitoring the re-adhesion of the polymer. A cured polymer film (curing at 70°C for 48h) with a thickness of 1 mm was placed between two glass substrates. Two pieces of copper were applied on the top of glass substrate to provide a pressure of 7 kPa. The whole test setup was first kept at room temperature for polymer relaxing for 2h, then heated up from room temperature to 70°C using a hot plate (this heating up period took about 2 min), and then keeping the set-up at 70°C for 1h. The LSI recording started as soon as heating up process began (so includes the heating up period). The area imaged by the LSI (marked by a dashed red line in Figure 7.2) contains both the top area of the polymer film in contact with the glass plate and a small area outside the contact zone. The free-surface area in the field of observation serves as the internal reference frame and allows the spontaneous thermal behaviour to be subtracted from the thermal re-adhesion processes taking place at the polymer-glass plate interface.



**Figure 7.2** Polymer re-adhesion process observation geometry.

One of the raw speckle images of polymer adhesion process observation is shown in Figure 7.3. The left side of the image corresponds to the part of polymer film under glass substrate under pressure, which is expected to show the information of adhesion process and from hereon called ROI (region of interest). The right side of the image corresponds to the part of polymer film contact with air and from hereon called BKG (background).



**Figure 7.3** Raw speckle image of polymer adhesion process observation.

### 7.2.3 LSI principle, data acquisition and data processing

When monochromatic (single wavelength) and coherent (constant phase difference) incident light interact with 'scattering centers' (in this chapter  $\text{TiO}_2$  nano-particles) in a bulk material, it will generate pattern composed of randomly distributed light and dark spots, called speckles. When scattering centers move due to Brownian motion, fluid flow or any other source of material structure rearrangements, the speckle pattern changes. In order to quantify the temporal changes in the speckle pattern, a parameter  $d_2$  was introduced, defined as:

$$d_2(t, \tau) = \frac{\langle (I(t) - I(t + \tau))^2 \rangle}{\langle I(t) \rangle \langle I(t + \tau) \rangle} \quad (7.1)$$

where  $I$  is the intensity level for each pixel (measured by grey value ranging from 0 to 255) and the symbol  $\langle \dots \rangle$  means temporal and/or spatial averaging. A high value of  $d_2$  indicates a high variation of intensity between two frames and therefore greater activity, while a low  $d_2$  represents less detectable variations and therefore a lower level of activity.

$\tau$  is called 'correlation time' which defines the temporal distance between the frames to be compared. It acts as a tuning factor for the type of dynamics we aim to probe: small values of  $\tau$  bring to fast, high frequency dynamics, while large values of  $\tau$  correspond to slow, low frequency dynamics.

Averaging is broadly practiced in LSI to decrease statistical noise due to camera noise and/or laser power fluctuations [18-20]. Features of interest might be buried under statistical noise, while averaging can increase the contrast. So a parameter 'averaging window' ( $AW$ , in the unit of frames) is introduced. Then equation 7.1 can be expressed as:

$$\langle d_2(t, \tau) \rangle_{AW} = \frac{1}{AW} \sum_{i=1}^{AW} \frac{\langle (I(t)_i - I(t + \tau)_i)^2 \rangle}{\langle I(t)_i \rangle \langle I(t + \tau)_i \rangle} \quad (7.2)$$

The data processing scheme is shown in Figure 7.4. It needs to be pointed out that if  $AW$  is too long the signal of fast processes will be lost, while for too short  $AW$  values a greater effect of noise can be observed. An intermediate value of  $AW$  is therefore required. In the LSI measurements as reported here, a constant  $AW$  (60 frames) is applied to all LSI data processing.

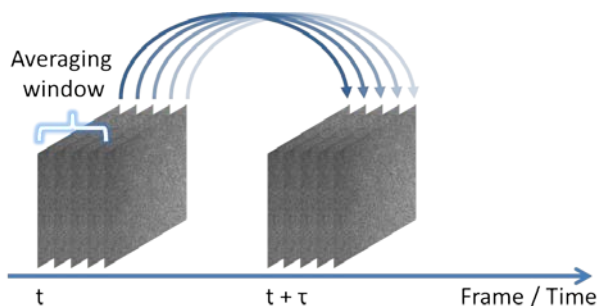


**Figure 7.4** Scheme of LSI data processing parameters

The actual software to analyze the LSI data has been made available by J. Sprakel (Wageningen University, Wageningen, the Netherlands). Due to its set-up the software allows the monitoring of an arbitrary number of processes each with a specific (selected) time constant during the entire measurement cycle. The volume over which the (vertically) averaged collective molecular mobility is determined is about  $5 \times 5$  mm in the rheology set-up and about  $5 \times 5$  mm for ROI and  $1.5 \times 5$  mm for BKG in the adhesion set-up. While the laser penetration depth of REF polymer and BTS-An polymer is about 0.5 mm and that of BDS-An polymer and BDS-An-TEA

polymer is about 0.1mm (BDS-An polymer and BDS-An-TEA polymer are less transparent than REF polymer and BTS-An polymer).

#### **7.2.4 Rheology measurement**

The rheological measurements on three of the four polymers specified in section 7.2.1, (the non-healing REF polymer and the self-healing polymers BTS-An and BDS-An-TEA), were performed using a Thermo Scientific™ HAAKE MARS 3 rheometer in oscillatory shear mode with plate/plate geometry (diameter 20mm). A shear strain of 0.05% was applied and the oscillating frequency was 1 Hz. The oven of rheometer was first heated up and kept at 70°C for 15min. Then the polymer was loaded on the test plate (already at 70°C) immediately after mixing to perform the isothermal measurements. A maximum curing time of 60 minutes was imposed.

#### **7.2.5 Adhesion strength measurement**

A cured polymer film (curing at 70°C for 48h) of each of the four polymers specified in section 7.2.1 with a thickness of 1 mm was placed between two glass substrates. The same pressure (7 kPa) and the same thermal treatment (heating up from room temperature to 70°C in 2 minutes followed by keeping at 70°C using a hot plate) as in the LSI testing was applied. Various isothermal holding temperatures of 10min, 20min, 30min, 40min, 50min and 60min were imposed. After annealing the samples were taken away from the hot plate and allowed to cool to room temperature for 30min. Then the adhesion strength was measured by single lap shear test using an Instron 3365 tensile testing machine with a 1 kN load cell and a cross-head speed of 1 mm/min.

### **7.3 Results and discussion**

#### **7.3.1 The polymer curing process**

Figure 7.5 shows the rheological time sweep curves of the curing process of the REF polymer, the BTS-An polymer and the BDS-An-TEA polymer. During the first 5-7

minutes the data are rather noisy as the induced shear forces are very small and close to the detection limit of the rheometer. Once the force level is above  $10^{-2}$  kPa the signal becomes stable and both  $G'$  and  $G''$  rise continuously until reaching a steady state value after 10-20 minutes. The rapid increase is due to the network formation as described in detail in chapter 4. The crossover of the  $G'$  and  $G''$  curves (the gel point) of the REF polymer, BTS-An polymer and BDS-An-TEA polymer can be found around 5 min, 7 min and 8 min, respectively.

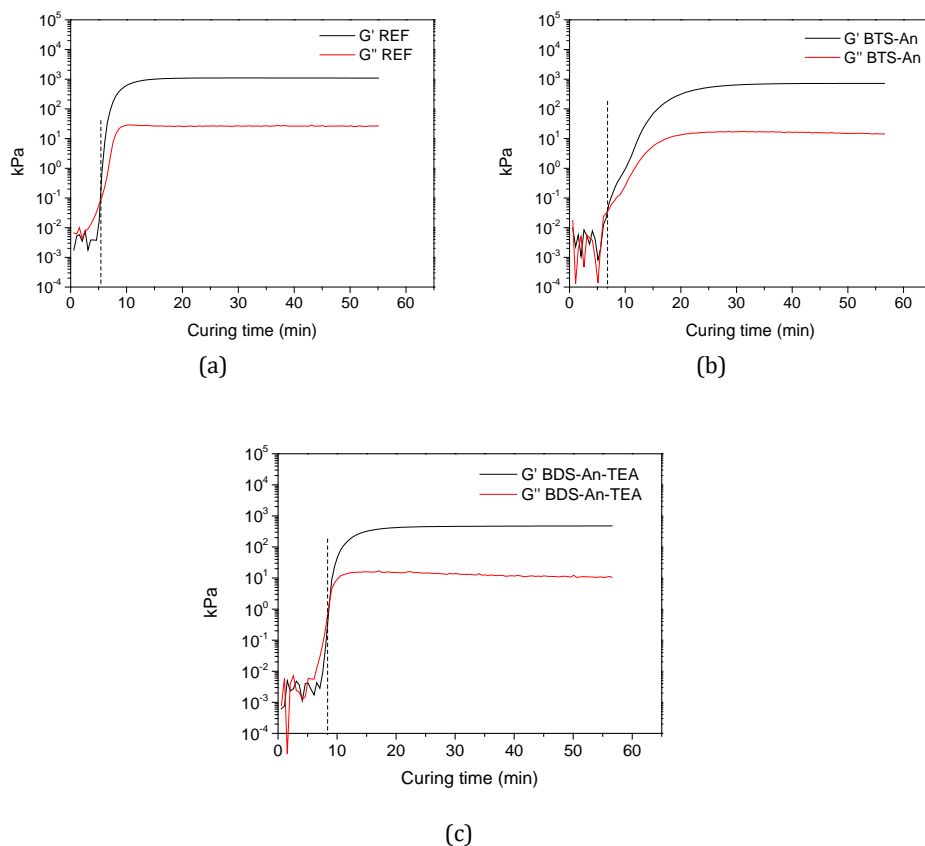


**Figure 7.5** The rheological time sweep of the curing process of (a) REF polymer, (b) BTS-An polymer and (c) BDS-An-TEA polymer. The dashed lines mark the time of the gel point. The measurements were carried out at 1 Hz frequency.

In order to allow direct comparison with the rheological data, the LSI data were processed at 1 Hz frequency (correlation time = 1s), and the results are shown in Figure 7.6. Higher  $d_2$  absolute values indicate higher molecular mobility. It is very clear that during the first few minutes molecular mobility of all polymers stays at a high level then suddenly decreases and stays at a low level as if the polymer networks are 'frozen'. The sharpest transition in molecular mobility transition occurs at 6 min, 11 min and 10 min for the REF polymer, the BTS-An polymer and the BDS-An-TEA polymer respectively. Those values are all a little bit later than the times at which the gel point was obtained during the rheology experiments (5 min, 7 min and 8 min, respectively), but this is due to the heating stage being shorter in the rheology experiments in which the polymer had to be dropped on the pre-heated plates. The times at which the equilibrium cured state is obtained correspond very well between both techniques with the REF polymer curing fastest and the BTS-An polymer curing slowest.

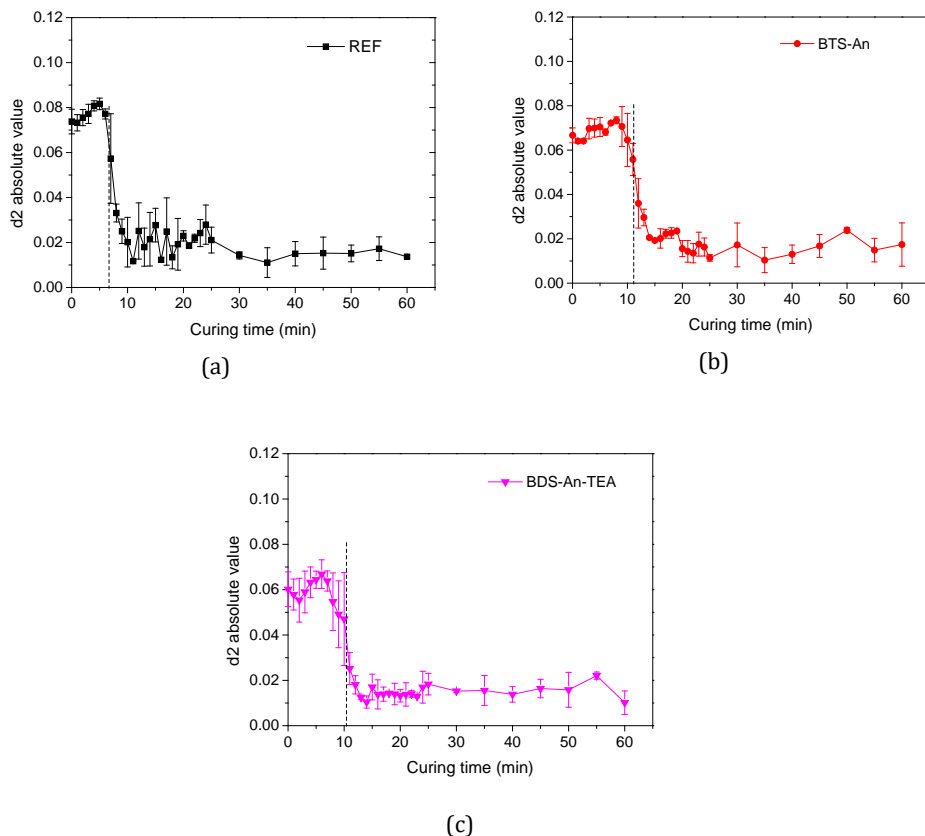


**Figure 7.6** LSI  $d_2$  values (processed at 1 Hz) of (a)REF polymer, (b)BTS-An polymer and (c) BDS-An-TEA polymer against curing time. Higher  $d_2$  values indicate higher collective molecular mobility.

The LSI data can also be processed at different frequencies (different correlation time) in order to understand how the spectrum of molecular mobilities changes during curing. Figure 7.7 shows LSI  $d_2$  values of the REF polymer, the BTS-An polymer and the BDS-An-TEA polymer against processing frequency for different curing times from 2 to 60 minutes. With increasing curing time, the LSI frequency sweep curves of all three polymers shift to the low frequency side. Clearly the most rapid molecular motions are stopped first by the curing process. Interestingly the curves become more noisy once the curing reaction is completed ( $t \geq 15$  minutes) but are very smooth up to that point. For the fully cured polymer only slow

molecular motions with a time constant  $>10$  seconds are observed. While the data in the low frequency domain and the long holding time are a bit noisy, they suggest that the frequency domain of active molecular motions of the only non-self-healing polymer, REF,  $< 0.02$  Hz is more restricted than that of the two self-healing polymer grades,  $< 0.2$  Hz. This may be due to the dynamic nature of the S-S bonds in the BTS-An and the BDS-An-TEA polymer.

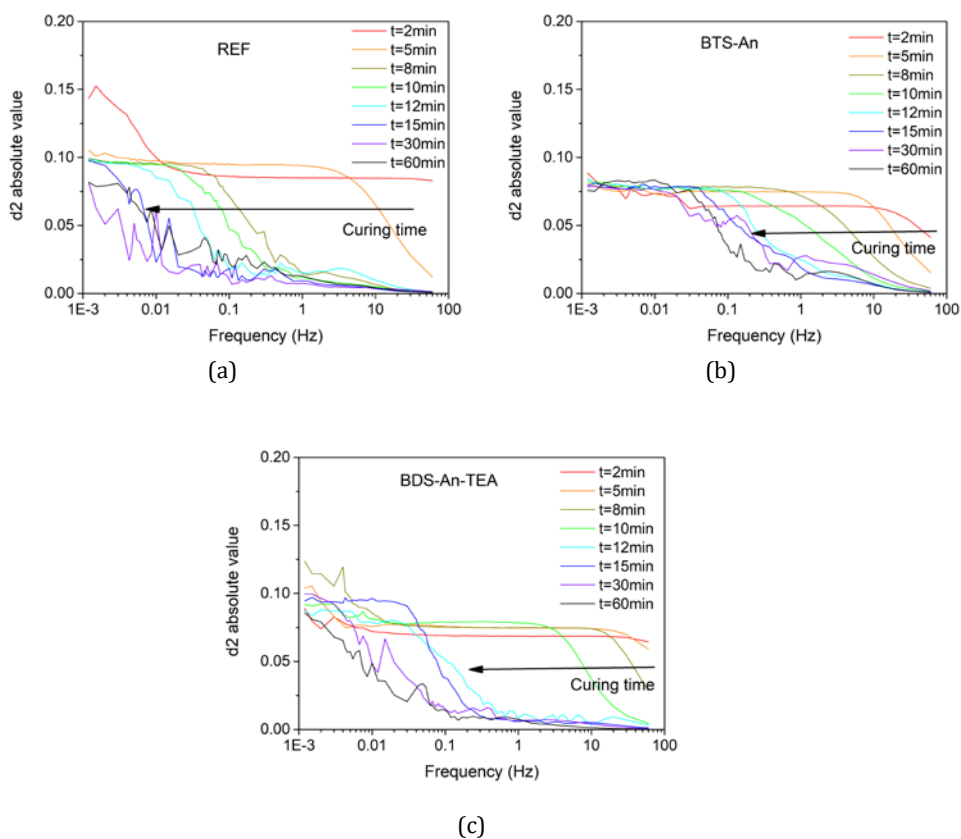


**Figure 7.7** LSI  $d_2$  values of (a) REF polymer, (b) BTS-An polymer and (c) BDS-An-TEA polymer against processing frequency at different curing times. Higher  $d_2$  values indicate higher collective molecular mobility.



### 7.3.2 The adhesive bonding process

The build-up of the room temperature lap shear adhesive strength with contact time at 70°C for the four polymers tested is shown in Figure 7.8. For BTS-An polymer, the lap shear strength increases with adhesion time and reaches a maximum value of 0.2 MPa after 50 min. BDS-An-TEA polymer shows similar behavior. The lap shear strength increases with adhesion time and reaches maximum value of 0.08 MPa after 40 min. It means that the self-healing dual network polymers are well bonded to the glass plate after 50 min treatment at 70°C under 7 kPa pressure. In contrast for both non-healing polymers (REF polymer and BDS-An polymer), no adhesion was observed under the same adhesion condition.

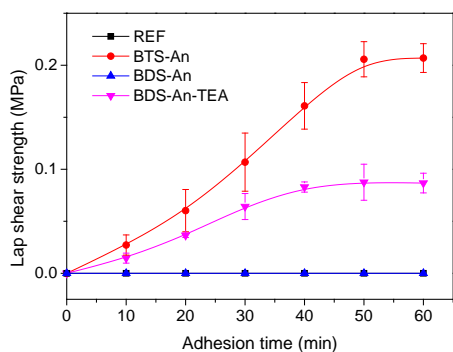


**Figure 7.8** Lap shear strength measurement against adhesion time. The applied pressure for adhesion is 7 kPa. Data for REF polymer and BDS-An polymer coincide in the plot and always show no adhesion.

Figure 7.9 shows LSI  $d_2$  values for the REF polymer, the BTS-An polymer, the BDS-An polymer and the BDS-An-TEA polymer against frequency for different contact times. As described in experimental section, in area ROI the polymers are in contact with the glass plate while in the area BKG the polymers are not in contact to the glass but are in contact with stagnant air. Then the comparison between BKG (solid lines) and ROI (dash lines) is expected to show the effect of local molecular rearrangements at the glass surface. It is obvious that in all polymers the most dynamic molecular behaviour was observed for the samples heated for only 5 minutes and in the free contact BKG region while the least dynamic behaviour was observed for the

polymers aged for 60 minutes in contact with the glass. However the data as plotted do not show obvious differences between BKG and ROI observations, no systematic differences between self-healing and non-self-healing polymers and no correlations to the observed adhesion behaviour. It can be noticed from Figure 7.10 that  $d_2$  curves of all samples are rather noisy when processing frequency is less than 1 Hz. Similar phenomenon was observed by Van der Kooij et al. [17] when they used LSI to measure the molecular activity of a self-healing polyetherimide at 100°C. According to their explanation those big ‘spikes’ correspond to reproducible intermittent molecular activities in the overall dynamics. Further discussion on these big fluctuations can be found in Appendix.

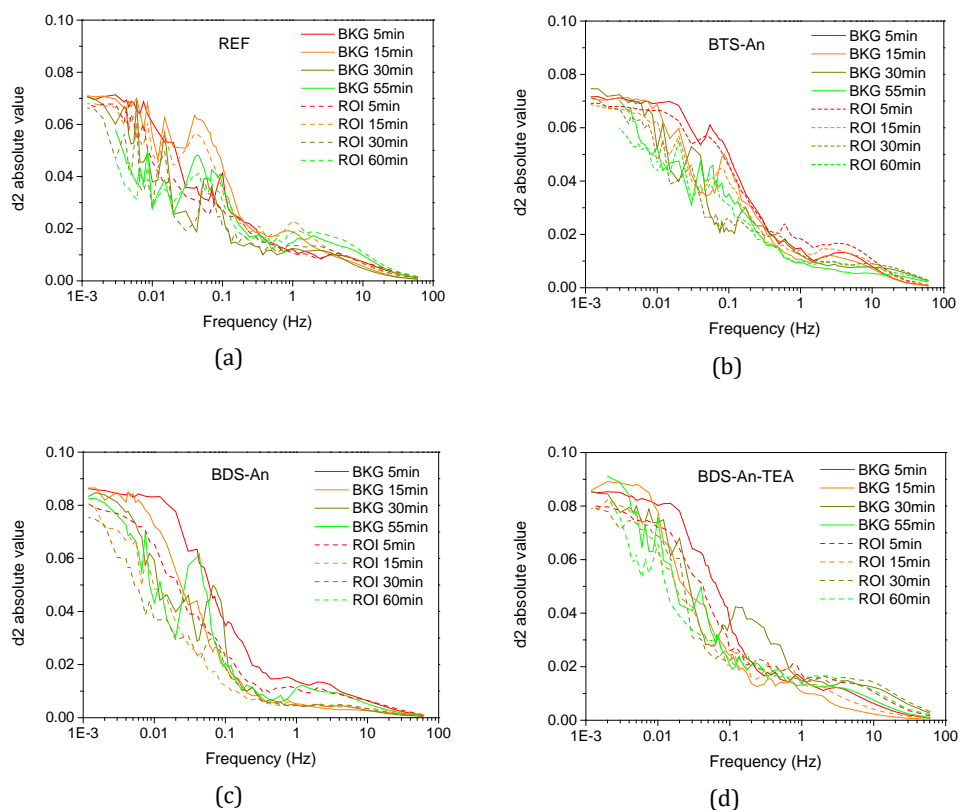


**Figure 7.9** LSI  $d_2$  values of (a) REF polymer, (b) BTS-An polymer, (c) BDS-An polymer and (d) BDS-An-TEA polymer against processing frequency at different adhesion times. Higher  $d_2$  values indicate higher collective molecular mobility.

To try and unravel the molecular motion effects from the thermal and instrumental noise five frequencies 10 Hz, 1 Hz, 0.1 Hz, 0.05 Hz and 0.01 Hz were chosen to perform further LSI data analysis. Figure 7.10 shows the polymer activity in the polymer-glass contact area with respect to background ( $\langle d_{2ROI} \rangle / \langle d_{2BKG} \rangle$ ). For the REF polymer and the BTS-An polymer,  $\langle d_{2ROI} \rangle / \langle d_{2BKG} \rangle$  is all around 1 irrespective of the observation frequency, which means that no difference in behavior between in the adhesion area and in background can be observed. The absence of a difference could be due to there being no difference in behaviour or because the penetration depth of the incident laser in the REF polymer and the BTS-An polymer is too large which leads to the LSI signal coming effectively from bulk material itself rather than from the polymer-glass interface. In contrast, the BDS-An polymer and the BDS-An-TEA polymer both being less transparent than the REF polymer and the BTS-An polymer and having a smaller penetration depth show a difference between the behaviour at the glass interface and that at the free surface. At higher mobility frequencies (10 Hz and 1 Hz) the normalized  $d_2$  activity of BDS-An-TEA polymer (which can adhere to the glass substrate) at adhesion area is higher than the background. While for BDS-An polymer (which shows no adhesion to glass)  $\langle d_{2ROI} \rangle / \langle d_{2BKG} \rangle$  is around 1. Those high frequency activities may be linked to the occurrence of the buildup of the adhesion. It is very interesting to note that at lower frequencies (0.1 Hz 0.05 Hz and 0.01 Hz) the activities of both the BDS-An polymer and BDS-An-TEA polymer in the adhesion area are lower than the background, which suggests that low frequency activities are somehow restricted by the (pressurized) contact with the rigid glass surface. However, the overall analysis of the LSI results and the comparison with the results of the adhesion test does force us to conclude that with the current LSI set-up and data analysis we were unable to extract new and relevant insights regarding the relation between the creation of polymer-glass adhesion and the required molecular motion near the interface.

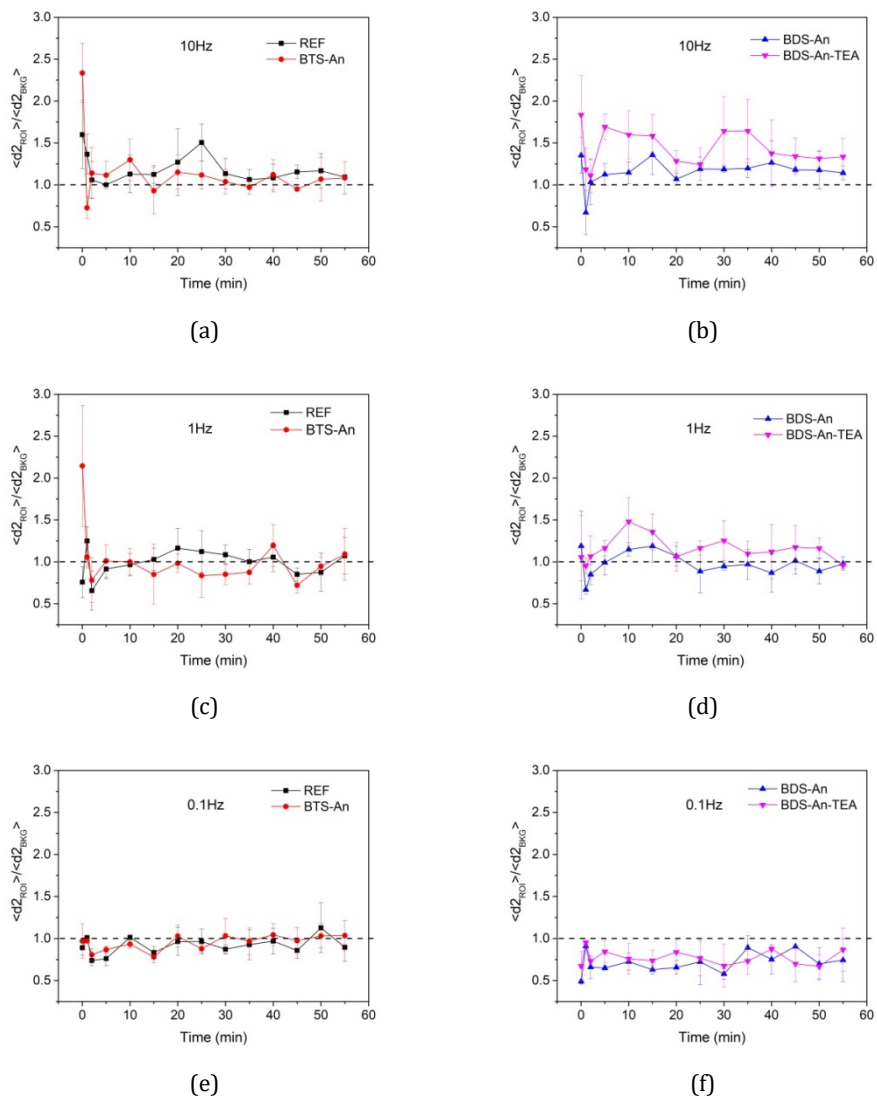


**Figure 7.10** Activity of the REF polymer, the BTS polymer, the BDS-An polymer and the BDS-An-TEA polymer in the glass contact area with respect to background ( $\langle d_{2ROI} \rangle / \langle d_{2BKG} \rangle$ ) at (a) (b) 10 Hz; (c) (d) 1 Hz; (e) (f) 0.1 Hz; (g) (h) 0.05 Hz and (i) (j) 0.01 Hz.

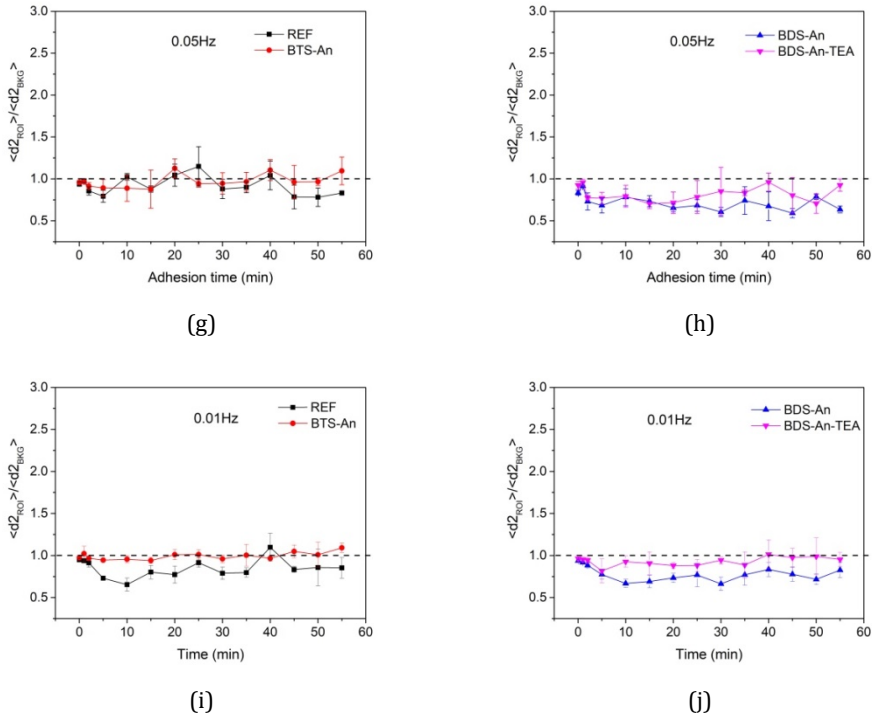


**Figure 7.10** Activity of the REF polymer, the BTS polymer, the BDS-An polymer and the BDS-An-TEA polymer in the glass contact area with respect to background ( $\langle d_{2ROI} \rangle / \langle d_{2BKG} \rangle$ ) at (a) (b) 10 Hz; (c) (d) 1 Hz; (e) (f) 0.1 Hz; (g) (h) 0.05 Hz and (i) (j) 0.01 Hz.

## 7

## 7.4 Conclusion

Laser Speckle Imaging (LSI) has a lot of potential applications due to its high spatial-temporal resolution. In this chapter, we report the first attempt to use LSI to monitor the molecular dynamics of the curing process in a sol-gel hybrid polymer and to link it to the results of conventional rheology measurement. The results show that LSI is a very effective non-destructive and non-contact method to follow polymer curing process and measure the polymer gel point as well as the end point of the curing process. The curing was shown to involve a transition from high frequency processes to low frequency processes. We found a weak indication that the natural mobility of fully cured self-healing polymer variants is higher than that of the non-self-healing variants.

We also applied LSI to observe the adhesion process of self-healing polymers to a glass substrate in order to figure out the dynamics of interfacial healing (or re-bonding) which plays an important role in self-healing thermal interface materials. The result shows that the method requires that the penetration depth of the incident laser in the polymer is small enough so that the activity at the interface can show up and does not disappear in the signal coming from below the surface. The observation of an increase of high frequency (10 Hz and 1Hz) activities near the glass-polymer interface may correspond to the buildup of the adhesion process. Similarly the observations on the low frequency (0.1 Hz, 0.05 Hz and 0.01 Hz) activities are restricted by contacting the glass under pressure.

## References

1. Goodman JW. Statistical properties of laser speckle patterns. Laser speckle and related phenomena: Springer; 1975. p. 9-75.
2. RIVA C, ROSS B, BENEDEK GB. Laser Doppler Measurements of Blood Flow in Capillary Tubes and Retinal Arteries. *Investigative Ophthalmology & Visual Science*. 1972;11(11):936-944.
3. Stern M. In vivo evaluation of microcirculation by coherent light scattering. *Nature (London)*. 1975;254(5495):56.
4. Berne BJ, Pecora R. Dynamic light scattering: with applications to chemistry, biology, and physics: Courier Corporation; 2000.
5. Cheng H, Luo Q, Zeng S, Chen S, Cen J, Gong H. Modified laser speckle imaging method with improved spatial resolution. *Journal of biomedical optics*. 2003;8(3):559-565.
6. Boas DA, Dunn AK. Laser speckle contrast imaging in biomedical optics. *Journal of biomedical optics*. 2010;15(1):011109.
7. Briers D, Duncan DD, Hirst ER, Kirkpatrick SJ, Larsson M, Steenbergen W, et al. Laser speckle contrast imaging: theoretical and practical limitations. *Journal of biomedical optics*. 2013;18(6):066018.
8. Silva Ed, Silva ERTd, Muramatsu M, Lannes SCdS. c. Food Research International. 2010;43(5):1470-1475.
9. Chen L, Cikalova U, Bendjus B, editors. Laser speckle photometry: an advanced method for defect detection in ceramics. *Speckle 2018: VII International Conference on Speckle Metrology; 2018: International Society for Optics and Photonics*.
10. Van Der Kooij HM, Fokkink R, Van Der Gucht J, Sprakel J. Quantitative imaging of heterogeneous dynamics in drying and aging paints. *Scientific reports*. 2016;6:34383.
11. van der Kooij HM, Dussi S, van de Kerkhof GT, Frijns RA, van der Gucht J, Sprakel J. Laser Speckle Strain Imaging reveals the origin of delayed fracture in a soft solid. *Science advances*. 2018;4(5):eaar1926.
12. Wu DY, Meure S, Solomon D. Self-healing polymeric materials: a review of recent developments. *Progress in Polymer Science*. 2008;33(5):479-522.
13. Yuan Y, Yin T, Rong M, Zhang M. Self healing in polymers and polymer composites. Concepts, realization and outlook: A review. *Express Polymer Letters*. 2008;2(4):238-250.
14. Cho SH, White SR, Braun PV. Self-healing polymer coatings. *Advanced Materials*. 2009;21(6):645-649.
15. Hager MD, Greil P, Leyens C, van der Zwaag S, Schubert US. Self-healing materials. *Advanced Materials*. 2010;22(47):5424-5430.
16. Zhong N, Post W. Self-repair of structural and functional composites with intrinsically self-healing polymer matrices: A review. *Composites Part A: Applied Science and Manufacturing*. 2015;69:226-239.
17. van der Kooij HM, Susa A, García SJ, van der Zwaag S, Sprakel J. Imaging the Molecular Motions of Autonomous Repair in a Self-Healing Polymer. *Advanced Materials*. 2017;29(26):1701017.
18. Thompson O, Andrews M, Hirst E. Correction for spatial averaging in laser speckle contrast analysis. *Biomedical optics express*. 2011;2(4):1021-1029.

19. Zhao X, Gao Z. Surface roughness measurement using spatial-average analysis of objective speckle pattern in specular direction. *Optics and Lasers in Engineering*. 2009;47(11):1307-1316.
20. Draijer MJ. High speed perfusion imaging based on laser speckle fluctuations. 2010.



## Appendix

It can be noticed from Figure 7.9 that  $d_2$  curves of all samples are very noisy when processing frequency is less than 1 Hz. To figure out what is the reason to cause such big mobility variation at low frequency, two control experiments were performed. The first one is the LSI observation of a sand-blasted aluminum plate at 70°C. Because at 70°C the mobility of aluminum plate itself is very small, the LSI can show the macro motion of the whole setup if there is any. As show in Figure 7.a1 the  $d_2$  absolute value of aluminum plate is very small at all observation frequencies which indicates that there is no macro motion of the LSI setup and the big spikes of BTS-An polymer at 70°C at low frequency is coming from other source. Another control experiment is the LSI observation of BTS-An polymer at 35°C. It is very clear that the curve is much smoother than the one at 70°C. To sum up, the fluctuations in the high-temperature curves are not experimental noises but correspond to reproducible intermittent activities in the overall dynamics and those activities only occur at high temperature (higher than  $T_g$  of the polymer).

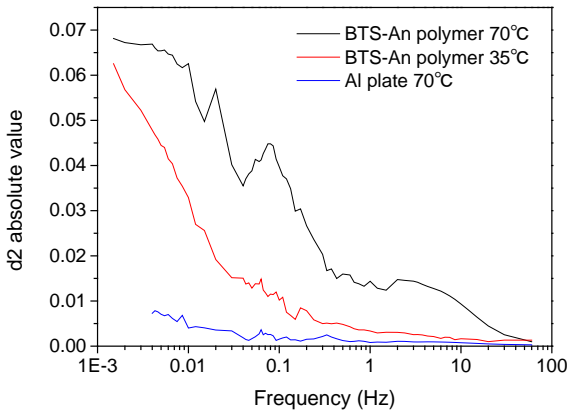


**Figure 7.a1** LSI  $d_2$  values of BTS-An polymer at 35°C and 70°C and sand-blasted aluminum plate at 70°C against processing frequency.

---

## Summary

---

Thermal interface materials (TIMs) are widely used as gap-filler materials between electronic devices such as LEDs and ICs and their heat sink and aim to control the heat dissipation and to provide mechanical anchoring. As the rated power densities of electronic devices are increasing rapidly, the TIMs are exposed to higher thermal and mechanical loads. The resulting aging of the TIMs may lead to delamination and internal crack formation causing loss of heat transfer as well as mechanical integrity leading to premature device failure. Therefore there is an increased demand for efficient and reliable TIM which can avoid, or even better, mitigate this thermomechanical damage. This thesis aims to contribute to the introduction of self-healing concepts into polymer-based TIMs to increase their reliability and service lifetime. As such, each chapter targets one of the scientific issues that are related to the development of commercial self-healing TIMs.

Chapter 2 gives a detailed overview of a variety of approaches to intrinsic structural and functional healing in polymer-based systems that have been reported in the literature in recent years. The intrinsic self-healing polymers are sorted based on external stimuli to trigger healing event (i.e. heat, UV light, electric current or moisture). Then the potential of healing structural or functional properties within polymer-based composites is evaluated. It is clear that in polymer-based composites mechanical damages in the matrix or debonding at the matrix-filler interface is responsible for the decrease in both structural and functional properties. The majority of recent studies regarding self-healing composite materials focus on the restoration of structural properties, such as stiffness and strength, while research into the self-healing of functional properties (electrical, electromagnetic, electromechanical, magnetic and thermal conduction) is still in its early stage development. Since the crucial factors for successful self-healing are similar for both structural and functional polymer-based composites, it is deemed promising to autonomously restore multiple properties using the same intrinsic self-healing mechanism.

Chapter 3 applies numerical simulations using COMSOL Multiphysics to investigate the effect of micro damage at the interface between the thermally conductive particle and the polymer matrix and that of macro delamination at a TIM-heat source interface on the thermal conductivity and mechanical properties of TIMs. Local interfacial debonding between matrix and filler particle is found to have a modest effect on overall thermal conductivity unless at higher filler volume fractions and for

very conductive filler materials. In contrast, the elastic modulus is found to drop already sharply at low debonding fractions. The thickness of the debonded region is found to have a modest effect on thermal conductivity but to have no noticeable effect on the overall material stiffness. Loss of thermal conduction as a result of macroscopic delamination at the interface between the TIM and the substrate is found to scale more or less linearly with the delaminated area fraction. Such macroscopic debonding leads to a rim of material near the edge of the delamination having a higher temperature and induced stresses. Both temperature levels and stresses increase with increasing delaminated area. The degree of temperature rise at the edge is important to guide the development of next generation TIMs based on intrinsic self-healing polymer matrices, as the healing kinetics are strongly temperature dependent

In Chapter 4, the development of healable organic-inorganic dual network polymers based on disulfide chemistry, which could serve as the polymer matrix in TIMs and other types of composites, is described. By tuning the reversible bond (disulfide bond) concentration and the irreversible crosslink density in the polymer structure, the mechanical properties and crack healing efficiency of polymer will change dramatically. In order to achieve efficient healing, the reversible bond concentration should be high enough to provide enough local network mobility for flow and damage repair. Meanwhile an increase in the irreversible crosslink density will lead to a decrease in fracture healing efficiency because the local network mobility is restricted. The application of disulfide cleavage catalyst TEA can promote self-healing in polymers with low disulfide bond concentration due to its ability to make disulfide bond easier to break.

In Chapter 5, a novel TIM system based on the healable organic-inorganic dual network polymers filled with spherical glass beads developed in chapter 4 is presented. The effect of particle volume concentration (PVC) and particle size on tensile strength and thermal conductivity healing behavior is investigated. The results show that a higher PVC increases the mechanical property of the composite but decreases the mechanical healing efficiency. For the same PVC, bigger particles lead to lower mechanical properties but higher thermal conductivity and higher mechanical healing efficiency. Unfortunately such healing efficiency is greatly reduced if the registry of the fracture surfaces brought in contact during healing is destroyed. Finally, the thermal conductivity restoration of TIMs can reach 100% even though the mechanical healing efficiency remains modest.

Chapter 6 presents some thermal cycling tests performed to investigate the long-term reliability of two self-healing TIMs and one commercial non-healing reference TIM. The chosen self-healing TIMs have a much better endurance during thermal cycling than the commercial non-healing TIMs when large shear stresses are applied, because their adhesive strength are higher at the peak cycle temperature (70°C), which is the optimal temperature of efficient and repetitive healing. Under moderate thermal cycling conditions (from 20°C to 70°C) both self-healing TIMs and the commercial non-healing TIM show good long-term reliability, as the testing conditions are too mild to induced damage. If thermal cycling condition becomes harsh (from -196°C to 70°C), self-healing TIMs are found to be more reliable than the reference commercial non-healing TIM because the damage caused by thermal cycling is healed autonomously when the samples periodically reach the healing temperature.

Chapter 7 explores the potential application of a recently developed optical material characterization technique, Laser Speckle Imaging (LSI) to monitor the adhesion process of a self-healing polymer to a glass substrate by monitoring the dynamics of interfacial healing (i.e. re-bonding). However the message derived from the observation is not very clear which indicates that this method requires that the penetration depth of the incident laser in the polymer should be small enough so that the activity at the interface can show up and does not disappear in the signal coming from below the surface. Prior to these measurements and in order to demonstrate the potential of the technique for the polymer system at hand, the molecular dynamics of the curing process in the sol-gel hybrid polymer has been measured and linked to the results of conventional rheology measurements. The results show that LSI is a very effective non-destructive and non-contact method to follow polymer curing process and measure the polymer gel point as well as the end point of the curing process.



---

## Samenvatting

---

Thermische Interface materialen (TIMs), zoals thermisch geleidende tapes, lijmen en pasta's, worden gebruikt om elektronische componenten zoals LEDs en IC te verbinden aan hun koelplaat om zo de warmte af te voeren en de componenten mechanisch te verankeren. Omdat het gedissipeerde vermogen van de componenten blijft toenemen, worden TIMs aan steeds hogere thermo-mechanische belastingen blootgesteld. Als gevolg hiervan treedt veroudering van de TIM op, hetgeen kan leiden tot onthechting en de vorming van inwendige microscheuren. Hierdoor wordt, de warmte niet langer goed afgevoerd en raakt de hechting verloren waardoor de componenten voortijdig bezwijken. Er is daarom een grote belangstelling voor voor efficiënte en betrouwbare TIMs die beter om kunnen gaan met de hoge belastingen en optredende schades. Dit proefschrift heeft als doel bij te dragen aan de ontwikkeling van zelf-herstellende TIMs met als uiteindelijk doel de betrouwbaarheid en de levensduur van de elektronische componenten te verhogen. Ieder hoofdstuk adresseert een andere wetenschappelijke vraag die beantwoord moet worden bij de ontwikkeling van commerciële zelf-herstellende TIM systemen.

Hoofdstuk 2 geeft een uitgebreid overzicht van de literatuur op het gebied van intrinsieke zelf-herstellende, polymeer-gebaseerde systemen voor zowel mechanische als functionele toepassingen. De polymeren worden eerst geclassificeerd naar de aard van de externe trigger (bijv. warmte, UV licht, elektrische stroom, luchtvochtigheid, etc. ) die nodig is om het herstelproces in werking te zetten. Daarna is gekeken in welke mate de gewenste functionaliteit hersteld kan worden. In polymeer-gebaseerde composieten is die schade vrijwel altijd in de vorm van inwendige microscheuren in de matrix of van inwendige of uitwendige delaminatie. De meerderheid van de studies aan zelf-herstellende composieten is gericht op het bepalen van het herstel van mechanische eigenschappen, en er zijn maar weinig studies uitgevoerd naar het herstel van andere, functionele, eigenschappen, zoals elektrische, elektromagnetische of thermische geleiding. Omdat het herstel van mechanische en functionele eigenschappen uiteindelijk van het gedrag van de polymere matrix afhangt, lijkt het zinvol om per herstelmechanisme te kijken naar het herstel van meerdere functionaliteiten.

Hoofdstuk 3 beschrijft numerieke simulaties met COMSOL Multiphysics software om het effect van micro-delaminatie aan het grensvlak tussen de thermisch geleidende deeltjes en de polymere matrix te berekenen alsmede de effecten van macro-

delaminaties op het grensvlak van de TIM en de elektronische componenten op de thermische geleidbaarheid en de mechanische eigenschappen te bepalen. Gebleken is dat lokale delaminaties maar een klein effect hebben op de thermische geleidbaarheid tenzij bij hoge vulgraden geleidende deeltjes en deeltjes met een zeer hoge geleidbaarheid. Daarentegen neemt de stijfheid van de TIM al bij lage delaminatiegraden snel af. De dikte van het onthechte gebied heeft een beperkt effect op de geleidbaarheid maar geen enkel effect op de stijfheid van het materiaal. Het verlies in thermische geleidbaarheid van de TIM schaaft min of meer met het percentage gedelamineerd grensvlak tussen TIM en de LED. De delaminatie leidt tot een lokale toename in temperatuur en inwendige spanningen nabij de grenslijn tussen gehecht en onthecht TIM. Beide nemen toe bij een relatief groter onthechtgebied. Omdat de kinetiek van het herstel proces sterk temperatuurafhankelijk is, is deze lokale temperatuur stijging van belang in de ontwikkeling van zelf-herstellende TIM systemen.

Hoofdstuk 4 beschrijft de ontwikkeling van een zelf-herstellend organisch-inorganisch netwerk polymeer gebaseerd op di-sulfide bindingen en met potentie voor toepassing als TIM. Door de hoeveelheid reversibele bindingen (de di-sulfides) en de hoeveelheid irreversibele crosslinks in het polymeer te variëren kunnen grote verschillen in mechanische eigenschappen en in zelf-herstellend gedrag gerealiseerd worden. Voor een goed zelf-herstellend gedrag is een hoge fractie reversibele bindingen wenselijk, maar voor goede mechanische eigenschappen wordt juist een hoog percentage irreversibele crosslinks gevraagd. Een hoog percentage crosslinks is juist weer slecht voor het zelfherstellende gedrag omdat het de mobiliteit van de polymeerketen verlaagt. De aanwezigheid van katalysatoren zoals TEA vergroot het zelf-herstellend vermogen in polymeersystemen met een laag di-sulfide gehalte omdat het breuk en (her-)vorming van de binding gemakkelijker maakt.

In Hoofdstuk 5 wordt een nieuw TIM, bestaande uit het polymeer van Hoofdstuk 4 maar nu gevuld met bolvormige glazen deeltjes, beschreven. Het effect van de volume fractie deeltjes en hun afmetingen op de treksterkte en de thermische geleiding is experimenteel bepaald. De resultaten laten zien dat een hogere volume fractie deeltjes de sterkte van de TIM doet toenemen, maar het zelf-herstellend vermogen doet afnemen. Bij een vaste volume fractie deeltjes zijn grotere glas deeltjes nadelig voor de sterkte maar gunstig voor het zelf-herstel, maar alleen als de gebroken grensvlakken perfect passend bij elkaar gebracht kunnen worden bij het begin van het herstelproces. De metingen laten zien dat de thermische geleiding van

de TIM bijna volledig hersteld kan worden, maar dat dat niet geldt voor de mechanische eigenschappen.

Hoofdstuk 6 beschrijft experimenten waarbij het lange-duur gedrag van twee zelf herstellende TIMs en één conventioneel TIM bij opgelegde thermische en thermo-mechanische cycli gemeten wordt. De twee nieuwe TIMs hebben een veel langere levensduur dan het referentie systeem maar dat zou ook kunnen komen omdat ze een hogere hechtsterkte hebben bij de hoogste temperatuur van de cyclus (70 °C). Deze hoogste temperatuur in de cyclus is gekozen dat die gelijk is aan de temperatuur voor efficiënt en meermalig zelf-herstel van de polymere matrix. Indien de temperatuur gevarieerd wordt tussen 20 °C en 70 °C hebben alle systemen een lange levensduur omdat de test condities te mild waren. Als de temperatuur tussen -196 °C en 70 °C gevarieerd wordt, treedt in alle drie systemen schade op, maar gedragen de zelf herstellende TIMs zich beter omdat ze de schade autonoom verhelpen elke keer dat de cyclustemperatuur de hersteltemperatuur bereikt.

In hoofdstuk 7 worden de mogelijkheden van een recent ontwikkelde optische materiaal -karakteriseringstechniek, Laser Speckle Imaging (LSI) verkend om de moleculaire dynamica tijdens het herstel van de hechting tussen het polymeer en een glasoppervlak te meten. Helaas waren de resultaten van deze experimenten niet heel duidelijk. Dit wordt toegeschreven aan het feit dat niet alleen moleculen aan het grensvlak maar ook moleculen dieper in het materiaal bijdroegen aan het te analyseren optische signaal. Alvorens deze metingen aan het herstel van hechting aan het grensvlak uit te voeren, zijn LSI experimenten uitgevoerd tijdens het crosslinken van het polymeer en zijn de resultaten gerelateerd aan die van conventionele reologische metingen. De resultaten laten zien dat LSI een zeer geschikte niet-destructieve contactloze methode is om het crosslink proces in de tijd te volgen en het gel-punt alsmede het einde van het proces te bepalen.





---

## Acknowledgements

---

Pursuing a PhD degree is such a unique journey that brings me interesting discoveries, numerous exciting moments and, of course, tough times. However it is never a lonely journey. I have met and collaborated with so many people who have contributed to this work in different ways.

First of all, I would like to express my gratitude to my promotor Sybrand van der Zwaag to give me the opportunity to work on such an interesting topic, self-healing thermal interface material. Your wisdom, excellent research guidance and commitment to the high scientific standards always keep me in the right direction. Without your great support, encouragement and critical feedback, especially during the final stage of my PhD, the completion of this dissertation would not have been possible.

I would also like to thank my other promotor Santiago Garcia. It is our detailed and fruitful weekly discussion that pushes this research forward and builds up this dissertation block by block. Your optimistic attitude, critical thinking and creative ideas inspire me a lot.

I would like to thank Michiel Hagenbeek to help me design the thermal cycling test system and kindly negotiate the heavily booked timetable of the climate chamber. I would like to thank Marlies Nijemeisland to help me operate the state-of-the-art LSI system and modify the MATLAB code to analyse the LSI data. Besides, there are many people in the Delft Aerospace Structures and Materials Laboratory such as Frans Oostrum, Lijing Xue, Johan Bijleveld and Berthil Grashof have helped me perform the chemical and physical experiments and have kept all experimental instruments in good condition. I really appreciate that.

During my PhD I also got involved in a MSc. project with master student Christian Floris. Together we have overcome a lot of difficulties and accomplished a nice work. Your willingness and courage to go to brand-new field not only brings your work to a higher level but also encourages me when my work runs into bottlenecks.

My special thanks go to Shanta Visser, our NovAM secretary. You are so warmhearted and always there to help me deal with all kinds of problems I have met in and outside the University. And you really put effort into making NovAM group feeling like a big family.

## Acknowledgements

---

I would like warmly acknowledge all present and former colleagues from NovAM group. Arijana and Wouter P, we joined NovAM group almost at the same time. So we usually faced and went through similar problems together. I am so grateful that I have you around me during my PhD. My officemates Wouter V, Antonio and Vincenzo, thank you for all the inspiring discussions we had and funny jokes we made. Furthermore I would like to thank Ugo, Ranjita, Hamideh, Michiel, Željka, Mina, Hongli, Paul, Nijesh, Maruti, Hari, Martino, Jimmy, Daniella, Qingbao, Jianwei, Qi, Xiaojun, Hao Chen, Hao Yu, Hussein, Marianella, Jibran, Mladen, Christian, Kevin, Vincent, Silvia, Nadine and all other NovAMers for the excellent academic atmosphere and comfortable social environment.

I would also like to thank my roommate Yaolin and Hongde and my friends Casper, Ann-Sophie, Maria, Yeli, Qingqing, Zhou, Zhaolong, and all other friends I have met in Delft for the nice beer and tasty food we have shared and making my life colorful and enjoyable.

Last but not least, I owe my deepest gratitude to my parents. I could not have come this far without your unconditional support and endless encouragement. You help me improve myself in different aspects through all steps of my life. Despite the physical distance, I can always feel your love and concern. Thanks for everything!

### Journal publications

Hernández M, Bernal MM, Grande AM, **Zhong N**, van der Zwaag S, García SJ  
*Effect of graphene content on the restoration of mechanical, electrical and thermal functionalities of a self-healing natural rubber*  
Smart Materials and Structures. 2017;26(8):085010.

**Zhong N**, Garcia SJ, van der Zwaag S  
*The effect of filler parameters on the healing of thermal conductivity and mechanical properties of a thermal interface material based on a self-healable organic-inorganic polymer matrix*  
Smart Materials and Structures. 2016;25(8):084016.

**Zhong N**, Post W  
*Self-repair of structural and functional composites with intrinsically self-healing polymer matrices: A review*  
Composites Part A: Applied Science and Manufacturing. 2015;69:226-239.

### Book chapter

**Zhong N**, Lafont U, Garcia SJ, van der Zwaag S  
*Self restoring thermal interface materials based on intrinsic healing polymer matrices*  
Self Healing Materials: Pioneering Research in the Netherlands. 2015:245.

### Selected conference contributions

**Zhong N**, van der Zwaag S, Garcia SJ  
*Role of di and tetra-sulfide containing silane on the network formation of a healable organic-inorganic hybrid dual-network*  
6<sup>th</sup> International Conference on Self-healing Materials, Friedrichshafen, Germany, June 2017

**Zhong N**, Garcia SJ, van der Zwaag S  
*Effect of filler particle parameters on thermal and mechanical healing of thermal interface materials*  
5<sup>th</sup> International Conference on Self-healing Materials, Durham, USA, June 2015

**Zhong N**, Garcia SJ, van der Zwaag S

*Thermal Interface Materials with Multiple Healing Functionalities*

Final IOP symposium on Self-Healing Materials, Utrecht, the Netherlands, October 2015

**Zhong N**, Garcia SJ, van der Zwaag S

*Conductive Composite Materials with Multiple Healing Functionalities*

The Eurotherm Seminar 103 "Nanoscale and Microscale Heat Transfer IV", Lyon, France, October 2014

**Zhong N**, Garcia SJ, van der Zwaag S

*Thermally Conductive Composites with Multiple Healing Functionalities*

Dutch Polymer Days, Lunteren, the Netherlands, March 2014

**Zhong N**, Lafont U, Garcia SJ, van der Zwaag S

*Study on Conductive Composite Materials with Multiple Healing Functionalities*

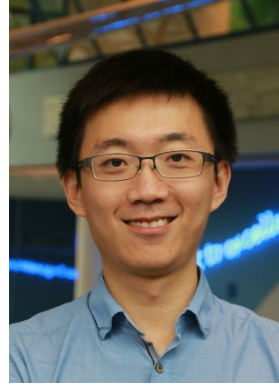
IOP-DFG Symposium on Self-Healing Materials, Gouda, the Netherlands, October 2013

---

## Curriculum Vitae

---

Nan ZHONG was born on 24<sup>th</sup> July 1987 in Chongqing, China. In 2006, he started to study Materials Science and Engineering in Tsinghua University. He obtained his Bachelor degree in 2010 working on “Sintering and Properties of Silicon Nitride Ceramic with LaF<sub>3</sub>/MgO Additives”.



In 2010, he joined a dual Master degree program from Tokyo Institute of Technology (Japan) and Tsinghua University (China). He majored in Organic and Polymeric Materials in Tokyo Institute of Technology and Materials Science and Engineering in Tsinghua University. He obtained his first Master degree in 2012 working on “Thermal Diffusivity and Thermal Conductivity Measurement of Silicon Nitride Particle Filled Silicone Rubber” and second Master degree in 2013 with a study on “Fabrication of Spherical Silicon Nitride Filler and Thermally Conductive Silicone Rubber”.

In August 2013, he joined the Novel Aerospace Materials group, Delft University of Technology to work on an IOP-SHM funded Ph.D. project on the development of self-healing thermal interface materials under the supervision of Prof. S. van der Zwaag and Dr. S.J. Garcia. As a part of his Ph.D. program he published multiple peer-reviewed papers and obtained the title of Accredited Polymer Scientist (RPK) from the National Dutch Graduate School of Polymer Science and Technology (PTN).